

Experimental Study of Local Heat Transfer during Quenching of Metals by Spray and Multiple Jets

Dissertation

zur Erlangung des akademischen Grades

Doktoringenieur

(Dr.-Ing.)

vorgelegt von

M.Sc. Umair Alam

geb. am 25.11.1978

in Karachi, Pakistan

genehmigt durch die

Fakultät für Verfahrens- und Systemtechnik
der Otto-von-Guericke-Universität Magdeburg

Gutachter:

Prof. Dr.-Ing. E. Specht,
Institute of Fluid Dynamics and Thermodynamics,
Universität Magdeburg.

Prof. Dr.-Ing. J. Schmidt,
Institute of Fluid Dynamics and Thermodynamics,
Universität Magdeburg.

Dr.-Ing. H.R. Müller,
Wieland-Werke AG, Ulm.

Eingereicht am: 05.04.2011

Promotionskolloquium am: 24.05.2011

Statement of Autonomy

I hereby declare that this submission is my own work and to the best of my knowledge it contains no materials previously published or written by another person, nor material which to a substantial extent has been accepted for the reward of any other degree or diploma at the University of Magdeburg or any other educational institution, except where due acknowledgement is made in the thesis. Any contribution made to the research by others, with whom I have worked at the University of Magdeburg or elsewhere, has been explicitly acknowledged in this thesis.

I also declare that the intellectual content of this thesis is the product of own work, except to the extent that assistance from others in the project's design and conception or in style, presentation, and linguistic expression is acknowledged.

Magdeburg, April 05, 2011

Umair Alam

Abstract

Spray quenching is widely used in industrial applications. In atomized spray quenching, liquid and air are supplied to the pneumatic atomizing nozzle at a certain flow rate and pressure to produce a full cone spray consisting of discrete droplets, while, in hydraulic spray quenching, only liquid is sprayed using hydraulic full cone nozzle. Impingement density of spray i.e. mass flow per unit area per unit time of liquid is considered to be the most influential parameter for heat transfer. Impingement density varies with radius and so as the heat flux. However, there are some other important factors of influence i.e. quality of water, velocity of droplets and their distribution, size distribution of droplets, initial surface temperature and surface roughness of the metal being quenched. Influence of water quality on local heat transfer in spray quenching has been analyzed by dissolving salts, polymer (surfactant), gases (CO_2 , O_2 , Air) in deionized water and the results are compared with those of deionized water. Water quality is altered by adding seven different salts i.e. NaCl , Na_2SO_4 , NaHCO_3 , Na_2CO_3 , MgSO_4 , Borax $\text{Na}_2\text{B}_4\text{O}_7 \cdot 10\text{H}_2\text{O}$ and CaCO_3 in de-ionized water with various concentrations. A surfactant ethoxylated ester, which is commonly added in cooling water in cast houses of metals, is also added to pure water in different concentrations i.e 50, 100, 200 and 500 ppm. A circular disc made of non-ferrous metals e.g. Nickel or AA6082 of thickness 2 - 3 mm and diameter 140 mm is heated to approximately 600 °C and sprayed on one side by atomized spray and the temperature distribution with respect to time and space is measured using Infrared camera on the other side of the disc. By this IR thermography, transient temperature measurement can be carried out within the window of 320×80 pixels with a minimum pixel real distance of 1 mm on the disc surface. Frequency of measurement is 150 Hz. Since the temperature measurement and cooling sides are opposite at 2 - 3 mm thickness apart, inverse heat conduction problem is solved by applying finite element method for calculating temperature and heat flux on the quenched side of metal sheet with respect to space and time. It has been observed that increasing the concentration of salts increases the leidenfrost point and critical heat flux and shortens the film boiling regime. MgSO_4 and Borax caused the strongest enhancement in this regard. While addition of surfactant decreases the leidenfrost point and critical heat flux and prolongs the film boiling regime. Maximum heat flux position is considered as the wetting front position. There is an abrupt variation of heat flux at wetting front position due to the change of boiling phenomenon from film boiling to transition boiling. Wetting front velocity has been compared for salt solutions, surfactant and deionized or pure water.

In direct chill casting of Aluminum ingots, the solidifying ingot is quenched by surrounding array of water jets striking the ingot surface at certain angle and jets' velocity which is called secondary cooling. Insufficient or excessive water supply changes the heat flux which is favorable for the growth of micro-cracks. The influence of jets' velocity on heat flux and wetting front velocity has been examined. An array of seven or eight water

jets striking the hot surface of rectangular sheets of Nickel, AA2024 and Inconel at an angle of 60° from horizontal plane are used at different jets' velocity. Initially, the heat flux and wetting front velocity increases with increasing jets' velocity until a threshold limit and beyond that the higher jets' velocity causes decline in wetting front velocity and heat flux. Similar phenomena is observed in visual examination of the same process by high speed camera.

Zusammenfassung

Die Sprühkühlung wird in industriellen Anwendungen weit verbreitet eingesetzt. Bei der Kühlung mit Sprühnebel wird eine Flüssigkeit und Luft, zur Erzeugung eines vollständigen Sprühkegels aus diskreten Tröpfchen, mit einem bestimmten Volumenstrom und Druck zur pneumatischen Zerstäuberdüse geführt. Während bei der hydraulischen Sprühkühlung nur Flüssigkeit, unter Verwendung einer hydraulischen Vollkegeldüse, versprüht wird. Die Beaufschlagungsdichte des Sprays d.h. der Massenstrom Flüssigkeit pro Flächeneinheit und pro Zeiteinheit wird als der einflussreichste Parameter für die Wärmeübertragung betrachtet. Die Beaufschlagungsdichte wie auch der Wärmestrom variieren mit dem Radius. Es gibt jedoch einige weitere wichtige Einflussfaktoren, wie z. B. die Qualität des Wassers, die Geschwindigkeit der Tropfen und ihre Verteilung, die Größenverteilung der Tröpfchen, Ausgangsoberflächentemperatur und Oberflächenrauigkeit des zu kühlenden Metalls. Der Einfluss der Wasserqualität auf den lokalen Wärmeübergang bei der Sprühkühlung wurde mit Salzlösungen, einem Polymer (Tensid) und Gasen (CO_2 , O_2 , Luft) in Wasser untersucht. Die Ergebnisse wurden mit denen von deionisiertem Wasser verglichen. Die Wasserqualität wurde durch Zugabe von sieben verschiedenen Salzen z.B. NaCl , Na_2SO_4 , NaHCO_3 , Na_2CO_3 , MgSO_4 , Borax $\text{Na}_2\text{B}_4\text{O}_7 \cdot 10\text{H}_2\text{O}$ und CaCO_3 in deionisiertem Wasser mit verschiedenen Konzentrationen verändert. Ebenso wurde ein Tensid (ethoxyliertes Ester), welches üblicherweise in Metallgießereien dem Kühlwasser beigelegt wird, mit unterschiedlichen Konzentrationen 50, 100, 200 und 500 ppm in dem Wasser zugesetzt. Eine kreisförmige Scheibe aus Nichteisenmetallen z. B. Nickel oder AA6082 mit einer Dicke von 2 - 3 mm und einem Durchmesser von 140 mm wurde auf ca. 600 °C erhitzt und auf der einen Seite besprüht. Die Temperaturverteilung in Bezug auf Zeit und Raum wurde mittels Infrarotkamera auf der anderen Seite der Scheibe gemessen. Mit dieser Infrarotthermographie können transiente Temperaturmessungen innerhalb eines Fensters von 320 x 80 Pixel durchgeführt werden, mit einem realen Mindestabstand von 1 mm zwischen den Pixel auf der Oberfläche der Scheibe. Die Frequenz der Messung betrug 150 Hz. Da die Temperaturmessung und die Kühlung auf verschiedenen Seiten mit einem Abstand von 2 - 3 mm Dicke erfolgte, musste das Inverse Wärmeleitproblem unter Anwendung der Finite-Elemente-Methode gelöst werden. Hierbei wurden die Temperatur und der Wärmestrom auf der gekühlten Seite des Bleches in Abhängigkeit von Raum und Zeit berechnet. Es wurde beobachtet, dass ein Anstieg der Konzentration der Salze den Leidenfrostpunkt und die kritische Wärmestromdichte erhöhte, während sich gleichzeitig der Bereich des Filmsiedens verkürzte. MgSO_4 und Borax verursachten die stärkste Veränderung. Bei der Zugabe von Tensiden sanken der Leidenfrostpunkt sowie die kritische Wärmestromdichte, und der Bereich des Filmsiedens verlängerte sich. Die Position der maximalen Wärmestromdichte wird als Position der Benetzungsfront betrachtet. Es kommt zu einer plötzlichen Veränderung des Wärmestromes an der Benetzungsfront durch den Übergang der Siedetemperatur vom Filmsieden zum Übergangsbereich. Die Geschwindigkeit der Benetzungsfront wurde für Salzlösungen, Tenside und für deionisiertes oder reines Wasser ver-

glichen.

Beim direkten Kokillenguss von Aluminiumbarren wird der erstarrende Barren durch eine Vielzahl von Wasserstrahlen gekühlt. Diese treffen mit einem bestimmten Winkel und Geschwindigkeit auf die Oberfläche der Barren. Dies wird als sekundäre Kühlung bezeichnet. Eine unzureichende oder übermäßige Wasserversorgung veränderte den Wärmestrom, wodurch das Wachstum von Mikrorissen begünstigt wurde. Der Einfluss der Geschwindigkeit der Wasserstrahlen auf den Wärmestrom und auf die Geschwindigkeit der Benetzungsfront wurde untersucht. Eine Anzahl von sieben oder acht Wasserstrahlen mit verschiedenen Wasserstrahlgeschwindigkeiten trifft auf die heiße Oberfläche eines rechteckigen Bleches aus Nickel, AA2024 und Inconel in einem Winkel von 60° zur horizontalen Ebene. Zu Beginn steigen der Wärmestrom und die Geschwindigkeit der Benetzungsfront mit zunehmender Wasserstrahlgeschwindigkeit bis zu einem Grenzwert an. Darüber hinaus bewirkte eine höhere Wasserstrahlgeschwindigkeit einen Rückgang in der Geschwindigkeit der Benetzungsfront und des Wärmestroms. Analoge Phänomene sind in der visuellen Untersuchung des gleichen Prozesses durch eine Hochgeschwindigkeitskamera beobachtet worden.

Acknowledgement

This dissertation would not have been possible without the guidance and the help of several individuals who in one way or another contributed and extended their valuable assistance in the preparation and completion of this study.

First and foremost I offer my heartiest gratitude to my supervisor, Prof. E. Specht, who has supported and guided me throughout my thesis with his patience and knowledge. Without his motivation and encouragement, this dissertation would not have been completed. Although, it has been a valuable learning process by numerous discussions with him, he also provided me and my colleagues opportunities to visit various high-tech industries in Germany which helped us to actually see the real processes. During my stay as Ph.D. student, I have visited more than twenty industrial plants. I found him a friendly, affectionate and extremely caring person who guided me on both educational and personal levels.

I am grateful to my second supervisor Prof. J. Schmidt for reviewing and examining my thesis. Besides that I also thank him for his administrative support and co-operation.

As this Ph.D. was experimental in nature, it is most important to thank those personnel who helped and guided me in successfully performing those experiments. Dr. H. Woche made it possible to procure the required equipment as soon as possible and helped in communicating with machine shop personnel for building experimental set up. I am extremely thankful to him for his technical guidance. I would like to thank my master thesis supervisor Mr. Jacek Krol who taught me the technical aspects of executing experimental work in the lab. I would also like to thank Mr. R. Süring, Mr. R. Timpe, Mr. D. Meinecke and Mr. P. Fischer for providing technical help in building experimental set up. In spite of my below-average technical German language, I am so impressed by the fact that they used to understand all what I meant to say. I also thank Dr. Al-karawi for providing the equipment for performing experiments.

I am indebted to the personnel with whom I have worked on industrial project. Their advices and feedback has helped me to acquire an insight of the practical problems faced by industry. I am extremely thankful to Dr. H.R. Müller for reviewing and examining my thesis and his valuable advices in every project meeting. I thank Dr. H. Böttcher who has been a mentor and provided the Aluminum plates for performing experiments. I am grateful to Mr. P. Meslage and Mr. O. Siemon for their encouragement and full support. I am also thankful to Dr. W. Droste, Dr. E. Schmid, Mr. J. Buuren, Mr. H. Siewert for their keen interest in this project.

I owe my deepest gratitude to higher education commission of Pakistan and DAAD for providing me scholarship for completing my Ph.D. degree. I am indebted to these two organization who gave me such a golden opportunity of studying in Germany and making my dream come true.

In my daily work I have been blessed with a friendly and cheerful group of fellow students. I am thankful to my friend and group mate K.H. M. Abdalrahman who helped me in performing experiments and also discussed on many important aspects of research. I

am thankful to my friendly colleagues in my group including Ashok Kumar Nallathambi, Mohammed Al-Fakheri, Ping Meng, Duc Hai do, Nadine Lorenz, Gourisankar Sandaka, Koteswara Rao Sunkara, Fabian Herz, Magda El-Fakharany, Hassanein Rafeey, Hassan Fauzy Elattar, Pavan Kumar and Zigua Xu. They were all so kind and co-operative friends. I thank Ms. Christin Hasemann for rendering her efficient services for carrying out official tasks.

During my stay as Ph.D. student, I shared so many precious joyful moments with my Pakistani friends. Dr. Ayaz Farooque, Haseeb Akram, Ahmed Shahzad and Rehan Anis are a few worth-mentioning among many sincere friends I found in wonderful city of Magdeburg.

I am thankful to my loving brothers M. Zaheer, M. Jahangeer and M. Azam for their moral support. I thank my Fiancee, Anum, from bottom of my heart for her patience and moral support specially during writing of this thesis.

Last but not least, I want to mention two people who are actually the reason of my existence. My parents supported and kept me motivated throughout my studies. Their selfless love and affection gave me the drive to negotiate through thick and thin of my life. I have no words to thank them.

Contents

1	Introduction	1
1.1	Motivation & scope	1
1.2	Overview of the subsequent chapters	3
2	Theory & Literature Review	5
2.1	Direct chill casting of non-ferrous metals	5
2.1.1	Primary cooling	6
2.1.2	Secondary cooling	7
2.2	Mechanism of heat transfer during secondary cooling	7
2.3	Quenching with array of water jets	9
2.4	Liquid sprays	14
2.4.1	Application of liquid sprays	14
2.5	Spray quenching	15
2.6	Influence of quality of water on quenching of metals	19
3	Materials & Methods	23
3.1	Introduction	23
3.2	Infrared thermography	23
3.2.1	Optical device Optris CT LT	24
3.3	Coating	25
3.3.1	Selection of coating	25
3.3.2	Measurement of emissivity	25
3.4	Cooling components	26
3.4.1	Pneumatic atomizing nozzle	26
3.4.2	Hydraulic full cone nozzle	27
3.4.3	Mold or array of jets	28
3.5	Metal samples	30
3.6	Measurement of impingement density distribution	30

3.7	Method	33
3.7.1	Preparation	33
3.7.2	Main procedure	33
3.7.3	Post process	34
3.8	Heat transfer analysis	36
3.8.1	One dimensional analysis	36
3.8.2	Two dimensional analysis	39
3.9	High speed photography	42
3.10	Composition of industrial casting water	43
4	Spray Quenching & Influence of Water Quality	45
4.1	Introduction	45
4.2	Comparison of pneumatic atomizing & hydraulic full cone nozzle	45
4.3	Influence of impingement density on heat transfer in atomized spray quenching	50
4.4	Influence of addition of chemicals in cooling water for spray quenching	53
4.4.1	Repeatability of hydraulic spray	55
4.4.2	Effect of salts & their solutions	55
4.4.3	Effect of surfactant	64
4.4.4	Effect of mixture of salts and surfactant	66
4.4.5	Effect of dissolved gases	70
4.5	Local control of atomized spray quenching	78
5	Influence of Water Velocity on Quenching by Array of Water Jets	83
5.1	Introduction	83
5.2	Mold with higher water flow	83
5.2.1	Calculated heat flux	85
5.2.2	Maximum heat flux propagation	86
5.2.3	Surface heat flux & temperature	87
5.2.4	Importance of IHCP	88
5.3	Mold with lower water flow	88
5.4	Measurement of wetting front velocity by high speed camera	92
5.5	Surface roughness & its influence	97
6	Conclusion	105
	List of Tables	109

List of Figures	111
Nomenclature	119
Bibliography	121

1 Introduction

1.1 Motivation & scope

Quenching or rapid cooling is an essential process in different technical applications. In many heat treatment processes, metallic products must be quenched in a specified way. The aim of these quenching processes is to control material properties such as strength, hardness, machinability and so on. At the same time the quenching process must be carried out with defined precision, as only then the necessary quality can be achieved. In addition, using defined quenching, warping of a work piece can be reduced. During hardening, for instance, steels are quenched quickly from 900 °C to 400 °C in order to achieve a certain degree of hardness. Similarly, non-ferrous metals are quenched during continuous casting process e.g. Direct chill casting of aluminum and its alloys. Quality of quenching process affects the resulting properties of metals. Different methods can be employed to carry out the quenching process. In bath or immersion quenching, metallic component is immersed in oil or water bath[1]. In impinging jet quenching, an array of continuous flowing liquid jets from a mould are doused at the hot metallic surface[1]. While, in spray quenching, water is atomized into small droplets with the help of a nozzle using compressed air or without air[1][2][3]. The distinct drop flow produced is sprayed on the hot surface. This research work deals with three methods of quenching:

1. Quenching by array of water jets
2. Atomized spray quenching (with pneumatic atomizing nozzle)
3. Spray quenching (with hydraulic full cone nozzle)

Different important operating parameters influence the local heat transfer during these quenching process which consequently have an impact on quality of the metallic products being quenched.

How does the impingement density of spray distributed in cases of pneumatic atomizing nozzle and hydraulic full cone nozzle? What is the effect of air pressure and water flow rate on impingement density in atomized sprays? How does the impingement density affects the resulting heat fluxes during spray cooling of metals? What is the influence of the initial surface temperature of hot metal during spray quenching? How does the addition of salts and organic matters like surfactant in cooling water alters the cooling rate during spray quenching? Does the increase in jet velocity always increases the wetting front velocity in quenching by array of jets? This research work is an effort to search the answers of these questions by experimental investigation.

It is a well known fact that heat transfer in quenching of metals primarily depends on the water flow rates. In case of atomized spray quenching, it is dependent on impingement density or mass flux of water per unit time while for water jet quenching, it depends on volume

flow rate of water. Experiments have been started by analyzing the effect of impingement density and water flow rates. For this purpose, two types of nozzles i.e. pneumatic atomizing nozzle and hydraulic full cone nozzle were installed. Former one generates spray of fine droplets (droplet diameter $10 - 20 \mu m$) by mixing internally air with liquid and other one generates spray of a bit coarser droplets (droplet diameter $0.1 - 0.2 mm$) with only single fluid i.e. liquid. The impingement densities were measured for the two kinds of nozzles by varying air pressure and water flow rates. Circular discs made up of non-ferrous metals like AA2024, AA6082, pure nickel etc. were quenched by these sprays. The surface temperature distribution along with the radial direction of the discs were measured and compared for two nozzles and materials as well. Likewise, the heat transfer coefficients were calculated for the same cases. The values of Leidenfrost temperature and its variation for the two cases of sprays were also analyzed.

It is water which mostly used as coolant during casting of non-ferrous metals. This water is not pure distilled water in most of the cases. It contains some impurities or additives e.g. mineral salts, surfactant, lubricants, and other biological ingredients. Film boiling appears to be very sensitive to water conditions, but we have very few instances when a known water change coincides with a known change in final product. So, changes in the water quality are not understood or predictable. It is required to investigate experimentally how the addition of different Salts, Surfactant and Polymers in cooling water affects the heat transfer in quenching. S. Chandra et al. [4] performed experiments with spray cooling and analyzed the effect of dissolving salts, surfactants[5] in cooling water on boiling regimes. They also studied the effect of addition of gases or solids in water droplet boiling on hot metal surface [6]. Similarly Cheng et al. [7] focused on analyzing the effects of dissolved salts on Leidenfrost point. These described studies and some other studies will be discussed in detail in second chapter under literature review. Since our study was focusing on the process of casting for non-ferrous metals and specially direct chill casting of Aluminum and its alloys, experiments for water quality analysis were initiated with mold producing seven water jets. However, the results were not satisfactory because of the lack of reproducibility of results. This is why, this analysis went through an evolution process of experimentation. After using mold, a series of experiments performed with atomized spray of pneumatic atomizing nozzle using salts like NaCl, NaHCO₃, Na₂CO₃, MgSO₄ and Na₂SO₄ and also carbonated water as solute in different concentrations. After that it was decided to use hydraulic sprays for this analysis in order to exclude the air cooling effect in case of pneumatic atomizer. So, finally solutions of MgSO₄, borax (which is used as a lubricant and cover on the melt level in the mold for casting of copper alloys, then washed from the strand surface and dissolved in the water of the secondary cooling zone) and also some other samples of industrial water were analyzed for their influence on local heat transfer during metal cooling process. Influence of gases such as air, pure O₂, pure CO₂ dissolved in cooling water was also a subject of study.

Mold is the name of devices which were utilized for producing array of jets. Two molds; one having larger water throughput with eight orifices of 4.75 mm diameter each and other having smaller water throughput with seven orifices of 2.5 mm diameter each were installed to quench rectangular sheets of different metals. The effect of water velocity on heat flux and wetting front movement are the focus of investigation in these cases. The wetting front propagation has also been examined by high speed photography for spray cooling and for cooling by array of jets and the results were compared with calculated results. For

this purpose, a sophisticated high speed camera HighSpeedStar 6 made by *La Vision* was used. Similarly, the surface condition of metal also influences the local heat transfer during quenching. Previous research shows that surface roughness affects the value of Leidenfrost temperature. Therefore it is required to investigate the influence of surface roughness on Leidenfrost temperature. With the help of sand paper different surfaces were produced and resulting rates of local heat transfer and respective Leidenfrost points were examined. Alloys of copper i.e. L49 (CuNi9Sn2), K12 (SE-Cu), K75 (CuCrTiSi), B14 (CuSn4), Inconel 600 were also used in those experiment in addition to AA2024.

The temperature of the surface of the metal was measured with the help of infrared thermography. It is a technique of non-contact temperature measurement of the surface. Infrared camera SC 3000 made by FLIR systems was used for temperature measurement in all the experiments. The rare side of quenched sheet was painted with black graphite paint to develop an emissivity of 0.94 approximately because the accuracy and uniformity of thermal images depends on the correct and uniform value of emissivity over the surface being examined.

1.2 Overview of the subsequent chapters

- **Chapter 2**

Chapter 2 is entitled as *Theory & Literature Review*. This chapter is started with the literature review comprising of the discussion regarding the research work already done in the past. Main focus is drawn on the research work done in the area of water quality influence on quenching of metals, wetting front propagation phenomenon, cooling process related to DC casting and continuous casting of steel. Calculation for finding values of heat transfer coefficient using energy balance equation, in case of one dimensional analysis and also two dimensional analysis, are formulated and explained. Non-iterative finite element method is explained to solve the inverse heat conduction problem. This method is significant considering the fact that the quenched side and temperature measured side are 2 – 3 mm apart that is the thickness of the sheet being quenched. That is why, it is required to measure the heat flux and temperature on the quenched side of the sheet using the temperature data of the measured side.

- **Chapter 3**

Chapter 3 is captioned as *Materials & Methods*. It comprises of every information related to experiments. Experimental set up is explained in detail. The specification of measuring equipment e.g. infrared camera, high speed camera, optical instrument, patternator etc. and their functions relating to performing experiments are described. The properties of materials and dimensions of the rectangular sheets and circular discs samples are explained with figures and tables. Description of cooling components i.e. pneumatic atomizing nozzle, hydraulic full cone nozzle and molds is thoroughly written.

- **Chapter 4**

Chapter 4 is entitled as *Spray Quenching & Influence of Water Quality*. It starts with the comparative study of hydraulic and pneumatic sprays. Their impingement

density distribution along the radial direction, temperature profiles, and heat transfer coefficients are presented and compared. After that the results regarding influence of water quality on spray quenching are discussed. This part is published in two publications in conferences [8][9]. Local regulation of atomized spray quenching with single and multiple nozzle is also discussed and these results are also published in research paper in a Journal [10].

- **Chapter 5**

Chapter 5 is named as *Influence of water velocity on quenching by array of water jets*. It is comprised of the results addressing the effect of water jets' velocity on the cooling of rectangular sheets and the wetting front propagation velocity are discussed in detail which are published in three publications in conferences [11] [12] [13]. Wetting front velocity for the case of three metals i.e. AA2024, Inconel and nickel is measured by high speed camera and results are presented. A short discussion on surface roughness and its influence on Leidenfrost temperature is presented in the form of table.

- **Chapter 6**

Chapter 6 is *Conclusion*. Results are concluded in this chapter and a short note regarding the scope for future research work in this area is suggested.

2 Theory & Literature Review

2.1 Direct chill casting of non-ferrous metals

Continuous casting processes for aluminum alloys were developed several decades ago to produce shapes for subsequent semi fabrication processes such as extrusion or rolling. As-cast product shapes include thick slabs/ingots (wide rectangular cross-section with thickness between 500 to 750 mm), strips (thickness between 1 and 12 mm), and rounds/extrusion billets (100 to 500 mm diameter). The productivity of casting process is controlled by the casting speed, so higher speeds are always sought. However, the casting speed cannot be increased arbitrarily for several reasons. First, the resulting increase in depth of the liquid pool and surface temperature of the strand prolongs the solidification process and increases the cooling requirements. In extreme cases, the structurally weak solid shell may rupture, leading to a "breakout" of liquid metal below the mold, or to excessive bulging if containment is exceeded for larger sections. Second, higher casting speeds often lead to cracks, caused by the higher thermal stresses. The practical range of operating speeds depends on alloy composition and product geometry. Owing to cracking difficulties during startup, aluminum alloy ingots and billets are cast at much lower speeds, increasing from 0.00075 to 0.001 m/s to steady speeds ranging from 0.001 to 0.003 m/s. The continuous casting machinery is comprised of the mold and secondary water-cooling systems. These are designed to extract superheat from the incoming liquid metal (5 % of the total heat content in the metal), latent heat of fusion at the solidification front (20 % of total heat content), and heat of phase transformation and sensible heat (75 % of the total heat content) from the solidified metal [14].

The direct chill (DC) casting process for aluminum alloys is shown schematically in Figure 2.1 (a). DC casting is a semi continuous process; as the strand is withdrawn vertically for a short length (~ 10 m) until the process must be stopped and restarted when the cast ingot reaches the bottom of the casting pit. Thus, considerable attention must focus on the initial start-up stage, when defects are most likely to be initiated. To start the process, a bottom block is partially inserted into an open rectangular mold (usually ~ 100 to 150 mm in length). Superheated liquid aluminum flows through a launder, down the nozzle spout, through a distribution bag, and into the mold, at a predetermined, time-varying filling rate. Once the molten metal fills the bottom block to a prescribed height, the bottom block and cast ingot are lowered into a casting pit. The aluminum ingot is subjected to cooling by the transfer of heat to the water-cooled aluminum mold over a very short length (~ 70 to 90 mm), and to cooling through the contact of chill water with the solid shell after it emerges from the mold cavity. This water emerges from a series of holes, which surround the mold at its base. The defining character of the DC casting process is the extraction of heat due to this direct impingement of water on the ingot surface; typically, more than 80 % of the total heat is removed by this method under steady-state conditions. Finally at the end of casting,

the bottom block stops and the ingot is removed from the casting pit to cool. The various

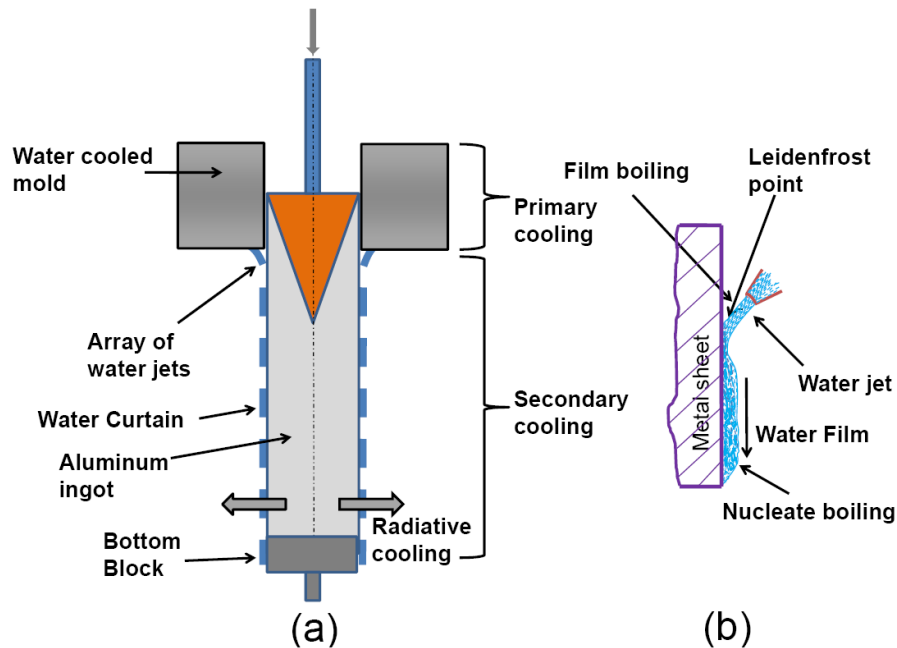


Figure 2.1: (a) Secondary cooling regime during DC casting of aluminum (b) detail of boiling regimes during water film cooling process

heat-transfer phenomena acting on the surface of the strand during the DC casting of aluminum alloys is schematically shown in Figures 2.1(a). This process involves a complex interplay of several heat-transfer mechanisms, which include convection of superheat in the liquid pool due to the momentum of the incoming metal, axial advection, and conduction through the moving solid shell; heat conduction from the solidification front to the colder outside surface of the metal; and heat transfer by convection to the mold (referred to as primary cooling), to the cooling water below the mold (referred to as secondary cooling), and to the bottom block. Change in the temperature gradient across the solid shell due to an abrupt increase or decrease in the heat extraction rate causes differential thermal expansion in the solidifying metal and the generation of high thermal stress and strain. This can ultimately lead to internal or surface defects, which can severely compromise the quality of the cast product. The heat extraction process during DC casting of Aluminum and its alloys can be divided into two stages:

1. Primary cooling or mold cooling
2. Secondary cooling or water jets' cooling

2.1.1 Primary cooling

Heat transfer at the metal/mold interface in continuous casting is referred to as mold or primary cooling. It varies with time, or distance down the mold, and can be subdivided into two regions of behavior (1) mold/metal direct contact and (2) air gap cooling. In the beginning at the meniscus, the solidifying metal is in close contact with the mold, and

the heat-transfer rate is very high. Peak heat flux can exceed 1 MW/m^2 in aluminum DC casting. In DC casting, however, the duration of this initial contact stage is quite brief, ending within 80 mm (depending upon the casting speed, alloy composition, and ingot geometry) of mold-metal contact. Stage 1 ends with the formation of a significant air gap between the metal and mold as soon as the solid shell is strong enough to contract away from the mold faces. Shrinkage of the thick shell away from the untapered mold produces gap formation around the entire perimeter. Once the gap has formed, the heat-transfer rate is greatly reduced, resulting in a reheating effect within the solid shell. Within stage 2, heat is conducted away from the shell via a series of thermal resistances: (1) air gap, (2) mold wall, and (3) mold/ cooling water interface. Primary cooling in the mold accounts for only about 20 % of the total heat extracted from the solidifying ingot during the DC casting of aluminum alloys. The heat extracted by primary cooling determines the surface temperature of the ingot at the point of exit from the mold. This subsequently influences the mode of boiling water heat transfer (film/nucleate boiling) below the mold. The peak heat-transfer coefficient reported for aluminum contacting a chilled mold ranges from 2000 to $4000 \text{ W/m}^2/\text{K}$. By comparison, in the air gap, the heat transfer coefficient may be as low as $150 \text{ W/m}^2/\text{K}$.

The impact of mold cooling water on primary cooling during the DC casting of aluminum has not been explored, perhaps because the mold cooling water also has an even more important role below the mold. Research has mostly focused on the secondary heat extraction process of direct impingement of water on the hot metal surface exiting the mold.

2.1.2 Secondary cooling

The continuous-cast strand is cooled by direct contact of water with the hot metal surface after emerging from the mold as shown in Figure 2.1 (a). This is referred to as secondary cooling. For aluminum casting, water jets emerge from holes located below the water-cooled mold and directly contact the metal surface. These jets form a continuous film, which wets the vertical ingot surfaces and rolls downward. Two distinct sub-zones can be distinguished on the ingot surface: (a) the water impingement zone, where abrupt cooling occurs due to the direct contact with water, and (b) the streaming zone located below (a), where the heat flux diminishes as the water film loses momentum with increasing distance from the impingement point. The length of the water impingement zone is usually ~ 10 to 15 mm, depending on the diameter of water holes at the base of the mold and angle of impingement. This heat-transfer process is critical in DC casting as the chill water extracts about 80 % of the total heat content during the steady-state regime below the mold.

2.2 Mechanism of heat transfer during secondary cooling

The extraction of heat by cooling water is quite complex because it is governed by the water boiling water phenomena, which depends greatly on temperature. As shown in Figure 2.2, four mechanisms of heat transfer can be distinguished when cooling water comes in contact with a hot metal surface. In order of decreasing surface temperature, they are as follows:

1. Film boiling at high temperatures (>Leidenfrost temperature)

Leidenfrost point (LFP) can be defined as "It is the temperature of a hot surface at which the evaporation time of the liquid in contact with the metal surface is the longest, and the extracted heat amount per time interval in dependence on the surface temperature is at a minimum"[15]. At temperatures above the LFP, heat is transferred by conduction through the stable vapor film. The heat transfer coefficient does not change much with temperature and is very low compared to that at the burnout point. Theories based on hydrodynamic instability, homogeneous and heterogeneous nucleation, thermo-mechanical effect were utilized to construct models to predict the LFP. Bernardin and Mudawar [16] described the existing theoretical models for LFP. Although some models are unable to predict the Leidenfrost temperature, they give an idea about the parameters affecting the transition. Baumeister et al. [17] presented the most common Leidenfrost temperature correlation as given in equation 2.1:

$$T_{Leid} = T_1 + \frac{0.844T_c \left\{ 1 - \exp \left[-0.016 \left[\frac{(\rho_s/At)^{1.33}}{\sigma_f} \right]^{0.5} \right] \right\} - T_1}{\exp(3.066 \times 10^6 \beta) \operatorname{erfc}(1758\sqrt{\beta})} \quad (2.1)$$

A model for minimum film boiling temperature T_{MFB} based on Taylor instability was presented by Berenson [18] by the following relation:

$$T_{MFB} = T_{sat} + 0.127 \frac{\rho_v h_{1v}}{\lambda_v} \left(\frac{g(\rho_1 - \rho_v)}{\rho_1 + \rho_v} \right)^{2/3} \times \left(\frac{\sigma}{g(\rho_1 - \rho_v)} \right)^{1/2} \left(\frac{\mu_v}{g(\rho_1 - \rho_v)} \right)^{1/3} \quad (2.2)$$

Another model for calculating T_{MFB} was suggested by Henry [19] considering the wall effect. This correlation was given as follows:

$$T_{MFB} = T_{MFB,B} + 0.42 (T_{MFB,B} - T_1) \times \sqrt{\frac{\lambda_1 \rho_1 c_{p1}}{\lambda_w \rho_w c_{pw}}} \left[\left(\frac{h_{1v}}{c_{pw} (T_{MFB,B} - T_{sat})} \right) \right]^{0.6} \quad (2.3)$$

where $T_{MFB,B}$ is the T_{MFB} calculated using the correlation of Berenson. The correlations mentioned above depict that Leidenfrost temperature is a function of the thermo-physical properties i.e. thermal conductivity, specific heat capacity and density of both wall and vapors. In addition it also depends on the surface tension, viscosity and latent heat of vaporization of the cooling fluid. This experimental study also shows that Leidenfrost temperature also depends on the method of quenching. When nickel disc was quenched by hydraulic spray and pneumatic spray, the Leidenfrost point was found to lie at ≈ 360 °C for pneumatic spray and at ≈ 240 °C for hydraulic spray. In near past, Bernardin and Mudawar [20][21] propounded a LFP correlation based on growth of bubble for the prediction of LFP for water drops and floro carbon FC-72.

2. Transition boiling between CHF and Leidenfrost temperatures

Beyond the critical heat flux (CHF) point, the bubbles start sticking to the metal surface and a layer of vapor begins to form, which cuts down the circulation of heat. The heat-transfer coefficient decreases sharply with increasing temperature, as the vapor film continues to cover more of the metal surface, with ever decreasing amounts of

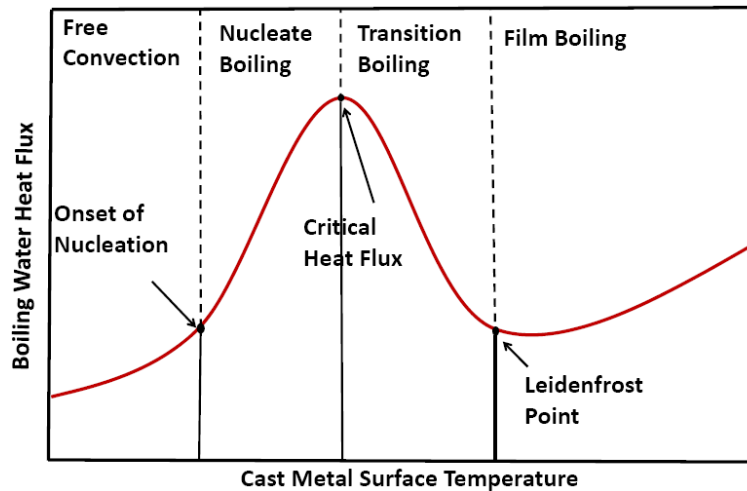


Figure 2.2: Boiling curve for water cooling indicating the different heat transfer regimes

metal surface exposed directly to water. When the metal surface is fully covered by a stable vapor film, the heat-transfer coefficient associated with the boiling curve reaches a minimum, which is referred to as the leidenfrost point.

3. Nucleate boiling between 100 °C and CHF point

As the surface temperature increases, bubbles of water vapor form on the metal surface, break off, and flow in the water film, eventually escaping from the free surface. The intensity of bubble formation and breakaway continues to increase as the surface temperature rises. This effect encourages good circulation in the water film causing the heat-transfer coefficient to increase rapidly until it reaches a maximum (referred to as the burnout point). The critical heat flux temperature is about 200 °C for aluminum, and increases with increasing water flow rate.

4. Free convection at temperatures lower than 100 °C

In this regime, heat transfer occurs via natural convection currents in the water film adhering to the metal surface, and the heat-transfer coefficient is very low.

2.3 Quenching with array of water jets

Mould is a metallic object which is used to produce water jets in order to quench the metal during casting process. This quenching technique is different from atomized spray quenching. In this process, only water jets without the addition of air are used. It is made of metal with as many orifices or holes as the number of water jets are required. These water jets are spread over the complete width of the metal object to be quenched. We have machined two different molds in our laboratory. One has seven orifices with a diameter of 2.5 mm each and other has eight orifices with a diameter of 4.78 mm. These molds are provided by two different metal manufacturers of Aluminum ingots. Rates of heat transfer are much higher in case quenching by mold as compared to that by sprays. Water is pumped to the mould with different volume flow rates of water and effect on heat transfer is measured. A comparison between spray cooling and film flowing cooling during the rewetting of a

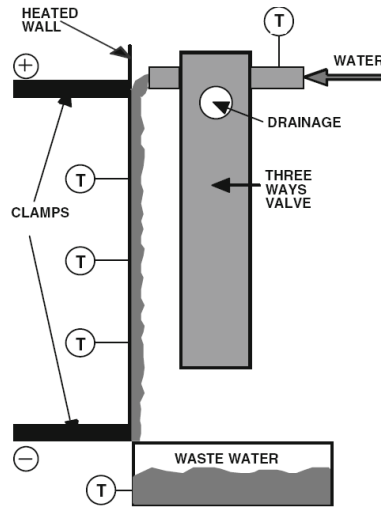


Figure 2.3: Film flow device [Celata et al. [22]]

hot surface was investigated experimentally by Celata et al. [22]. In their work, previous results with spray cooling are compared with experimental runs in which the spray injection is replaced with a falling film all along the test section. They measured the wetting front velocity during quenching of steel plate by falling water film of a single jet by using three thermocouple embedded into a stainless steel sheet and also by using a digital images system based on the video image registered during runs as shown in following figure 2.3. Temperature profiles with respect to real time for spray quenching and film quenching have been compared along with heat fluxes. In addition, the influence of initial temperature on re-wetting velocity or wetting front velocity and influence of jet exit velocity on wetting front velocity have been analyzed for the two modes of quenching. They found that the wetting front velocity decreases with increasing initial surface temperature and this result is validated by performing experiments for two jet velocities i.e. 3 and 5 m/s as shown in figure 2.4 . It was noteworthy that when re-wetting velocity for film quenching was lower for lower initial surface temperature (300 °C) than that for spray quenching, it becomes higher at higher initial surface temperature (500 °C). Referring to figure 2.5, the wetting front velocity was always more for spray quenching than for film quenching at a given initial surface temperature and jet exit velocity, however, the volume flow rate for different nozzle diameter has not been mentioned for spray quenching. Maximum heat flux peaks also possess considerably higher values for spray quenching as compared to film quenching as shown in figure 2.6. Nevertheless, they did not consider the influence of impingement density of spray quenching and also the method of finding the wetting front velocity was not specifically defined in that research. The effect of advanced cooling front (ACF) phenomena on film boiling and transition boiling regimes in the secondary cooling zone during the direct chill casting of aluminum alloys was investigated experimentally by Caron and Wells [23]. They used a rectangular block made up of Aluminum alloy AA5182 of dimensions $250 \times 150 \times 100$ mm and heated it up to initial temperature of 475 °C. The thermocouple of type E were used for temperature measurement and the block is moved up and down with a casting speed of 10 to 20 mm/s for simulating the actually DC casting process as shown in figure 2.7. Inverse heat conduction model was developed to calculate

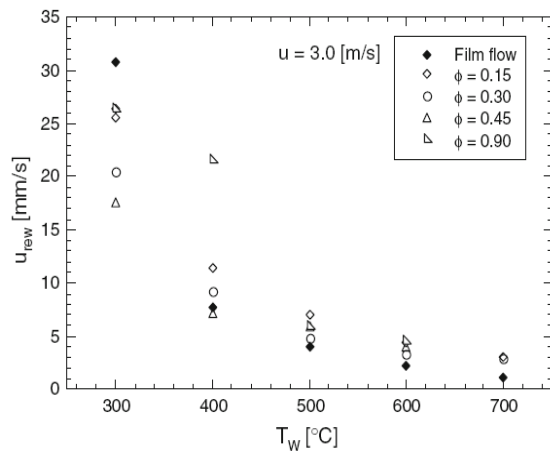


Figure 2.4: Wetting front velocity vs temperature [Celata et al. [22]]

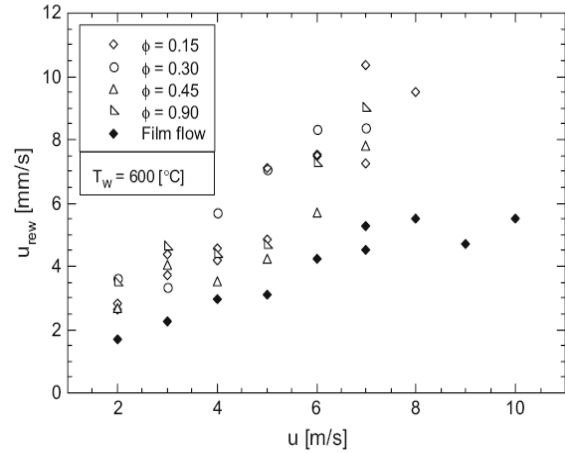


Figure 2.5: Wetting front velocity vs jet velocity [Celata et al. [22]]

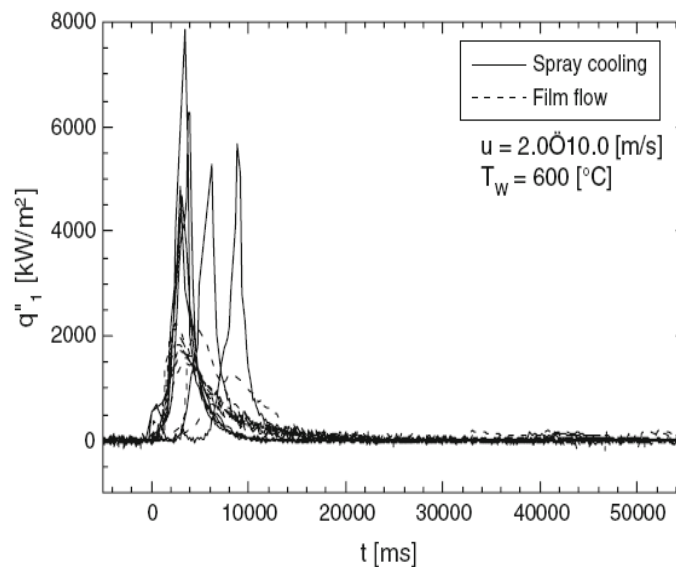


Figure 2.6: Heat flux vs time [Celata et al. [22]]

the second derivative of temperature with respect to time to identify the progression of the wetting front along the sample surface. They found that the cooling water flow rate influences the Leidenfrost point and re-wetting temperature as well as the critical heat flux at the impingement point; its importance thus depends on the other factors (initial temperature and casting speed). They have drawn the curves for heat flux with respect to surface temperature; however, the results show the considerable fluctuation especially in nucleate boiling regime. They assumed that the position of the wetting front and corresponding moving boundary is identified by evaluating the second derivative of the temperature with respect to time. Chang et al. [7] studied cooling by array of liquid jets for attaining high heat fluxes. Cooling was provided by an array of small-diameter water jets operating at considerably higher speeds of 47 m/s. These jets impinged on the rear side of a 2 to 4 mm-thick metallic faceplate from which the heat load is absorbed at the rate of 17 MW/m² and they also claimed to reach a heat flux of 20 MW/m², although difficulties with the heating

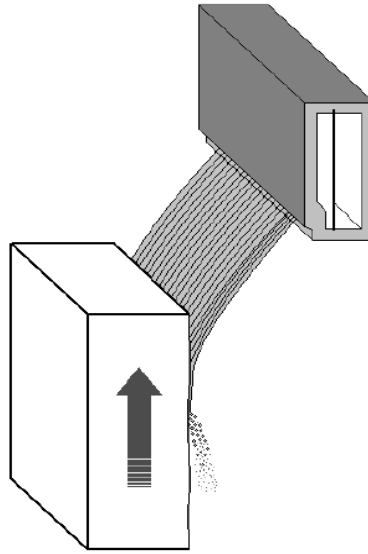


Figure 2.7: Moving aluminum sample quenched by array of water jets [Caron and Wells [23]]

element prevented this level from being reached.

Masanori Monde and Coworkers [24] researched extensively the boiling phenomena related to quenching of metals by single water jet. They started with quenching a metallic cylindrical block by water jet at atmospheric pressure for studying the characteristics of heat transfer and wetting front. For temperature measurement, 16 CA-type thermocouple embedded in cylindrical block made of three metals i.e. steel, brass and copper were used and meanwhile a high speed camera recorded the wetting front over the heated block surface. They observed that the maximum heat flux occurs neither in the wetting front, nor in the transition boiling region but in the fully wetted region and that the maximum heat flux is not achieved at the same time when the jet strikes the heated block, but it is achieved when the surface temperature decreases to a value less than 170 °C. They worked further in the same field of research and analyzed the delay of wetting propagation during jet impingement quenching. They enunciated that when the jet strikes the hot surface, the wetting front becomes stagnant for a certain period of time in a small central region before wetting the entire surface. This wetting delay may be described as *resident time* which is a strong function of block material and jet sub-cooling and also a function of initial block temperature and jet velocity. They proposed a correlation for the resident time and the surface temperature at the resident time at the wetting front [25]. They also observed that when the surface temperature at the wetting front drops to 120 from 200 °C, the surface heat flux reaches its maximum value due to forced convection nucleate boiling. They introduced a new correlation for maximum heat flux which shows that the maximum heat flux is a strong function of the position on the hot surface, jet velocity, block material properties and jet sub-cooling [26] [27]. The temperature profile and heat flux with respect to the radial position is shown in figure 2.8 showing the calculated heat flux and temperature and also the one image from high speed camera. It can be observed from the figure that maximum heat flux position (approx. 2 MW/m²) lies at the inner layer of wetting front and wetting front succeeds or precedes this point. In their subsequent work, the cooling curves at the center of the impinging surface for different experimental conditions were also explained in rela-

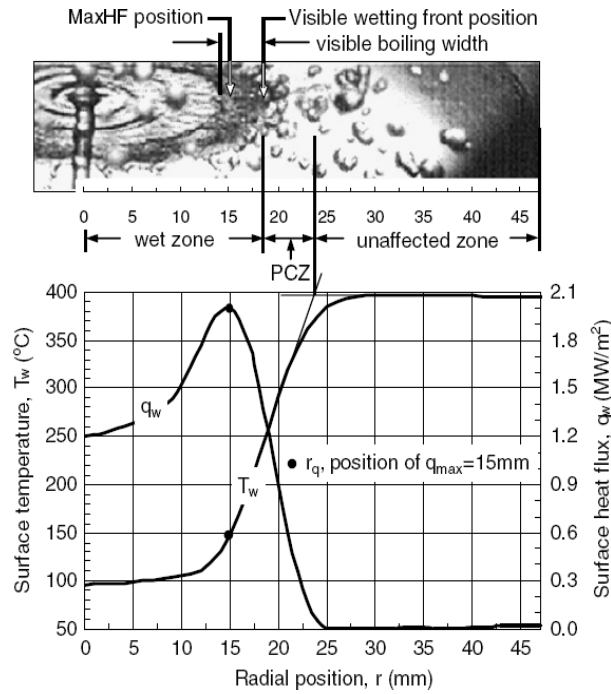


Figure 2.8: Hydrodynamic phenomena on the surface together with cooling curve and heat flux at $t = 4.8$ s [Monde et al. [24]]

tion with the limiting temperature and three characteristic regions having different types of flow patterns were also identified [28]. The jet impingement quenching came up with different types of flow patterns depending on the surface temperature and material properties. They divided the flow in six different patterns A, B, C, D, E and F. Each of flow patterns has distinct hydrodynamic and boiling character and it is shown in the form of high speed camera images. The flow patterns for steel and brass have also been compared [29]. They also analyzed the coupling between high heat transfer rates and observed boiling pattern for estimating the width of boiling region [30] and proposed that boiling width increases with the material conductivity and decreases with jet sub-cooling and velocity because increasing the jet velocity increases the sub-cooling and brings about the enhancement of cooling potential of the jet which results in steep radial temperature gradient and narrow boiling region. Boiling width also increases with increasing radial distance from center of the jet. It is also influenced by the initial surface temperature, however, this influence is not as strong as that of liquid sub-cooling and jet velocity. Material properties have a large effect on quenching phenomena. for the same parameters and radial distance, the boiling width for copper is 20 mm which is about 10 times that of steel. The reason could be that the heat flux transferred from a semi-infinite solid is proportional to $\sqrt{\lambda\rho c}$. *There is also an inverse relation between boiling width and radial temperature gradient [31].*

Meyer et al. [32] worked on the single-phase and two-phase cooling with an array of rectangular jets. The performed experiments to explore the effect of jet width, impingement velocity and inlet sub-cooling on the cooling performance of an array of three confined rectangular FC-72 and ethanol jets impacting a 3 cm \times 3 cm heated surface. They observed that single-phase heat transfer increased with increasing water jet velocity and/or jet width. Increases in jet velocity, jet width and/or sub-cooling broadens the single-phase

region preceding the commencement of boiling and enhanced critical heat flux (CHF). In this study, rectangular sheets of Nickel, Aluminum alloy AA2024 and Nickel Alloy Inconel 600 of thickness 2 - 3 mm were subjected to quenching by the array of seven or eight jets impinging on the surface at an angle of 60 degree. These jets are generated with help of molds which are a small section of actual mold for DC casting. It must be clear to the reader that these experiments are not intended to mimic the actual casting process, but it is an effort to analyze the effect of array of water jets' parameters, impinging on the metal surface, on local heat transfer. The influence of jet velocity, varying from 0.9 to 1.8 m/s for seven jets flow and 1.0 to 1.5 m/s for eight jets, on heat flux and wetting front velocity was investigated. Later, the wetting front velocity for the case of seven jets were also examined by high speed camera. The wetting front velocity measured by visual measurement of high speed camera and that calculated by solving inverse heat conduction problem were found in agreement to each other.

2.4 Liquid sprays

A dispersion of small liquid drops in a continuous gaseous phase is called liquid spray. Different researchers have assigned various nomenclature according to the dimensions of the droplets produced. Some researchers e.g. Fortier [33] differentiated between mist and cloud. A mist is dispersion including drops smaller than $10^{-1} \mu\text{m}$, whereas; a cloud refers to a dispersion of larger drops. Some other researchers called an aerosol a dispersion of sub-micrometer particles and a mist much larger drops e.g. drops of a diameter of $150 \mu\text{m}$. In this research, two kinds of sprays have been employed i.e. atomized spray (pneumatic) and hydraulic spray. Normally, in case of atomized spray the droplet size is 10 to $20 \mu\text{m}$ while in case of hydraulic spray, it is ten times higher.

2.4.1 Application of liquid sprays

A process of disintegration of the liquid phase results in an increase in the interfacial surface area between the liquid and the medium into which it penetrates. This increase can be quite important: in some instances, the initial interfacial surface area can be come several hundred times larger. Atomization can thus intensify the physical or chemical processes occurring at the interface i.e. mass, momentum and energy transfers. This advantage is use in various industrial applications.

Liquid spraying is common in various fields: air conditioning and ventilation, gas absorption, washing and cleaning, fire protection, coating of surfaces, spray drying, combustion, cooling of hot gases, cooling of hot surfaces etc. The last application is actually the focus of our research i.e. cooling of hot metal surfaces by liquid spray. It is in the steel and metal works industry that one finds the most numerous uses of atomization in order to quench the hot walls e.g. cooling of slabs, rolled products and cylinders in classical mills and quenching of molten metal immediately after its exit from the mould in continuous casting units. From a metallurgical point of view, the rate with which the heat is extracted from the metal during water cooling is very important in order to obtain a good quality product. It has been proved that for low alloy steel, high strength can be achieved without reducing ductility or weldability provided that the size of grains can be reduced. One of the best ways to

reach this goal is to regulate the cooling during austenite-ferrite transformation [34][35]. For rolled wire rods, a drastic cooling without quenching is desirable. Furthermore, when spraying, the surface temperature could be considerably lower than that at the center of rod which is undesirable. Therefore, in order to avoid superficially quenched structures, one has to divide the spray cooling zone into several parts separated by air cooling zones. This arrangement bring about uniformity of the temperature distribution inside the rod. Furthermore, it is necessary to take into account a variation of the surface heat transfer coefficient α with the temperature of the rod in the design calculations [36]. If one uses an average heat transfer coefficient, large discrepancies can appear e.g. one notices a difference of about 100°C in the rod surface temperature when using constant and temperature varying coefficients. This ensures the importance of studies focusing on to determine the parameters influencing heat transfer in such applications. In nuclear power plants, spray cooling is one of the safety system employed in case of loss of cooling accident. Schematically two techniques exist: top spraying i.e. liquid spray on to the core from above; and bottom reflooding i.e. immersion from below. In the latter case, drops can sputter from the upper liquid level and impinge on hot walls. Many related publications-both theoretical and experimental- have described the phenomena occurring in various core configurations and possible incidents. Besides the steel and nuclear industries, the chemical industry also uses liquid sprays in order to cool hot surfaces, for example, in the cooling of hot vessels and tanks. Liquid sprays are also used in the extrusion process of plastic insulated telephone wires.

2.5 Spray quenching

Spray quenching is used as secondary quenching technique in continuous casting of metals e.g. steel [37][14]. Strand of hot solidifying metal, coming out of mold after losing heat from primary quenching, is subjected to secondary quenching with the help of an array of nozzles as depicted in figure 2.9. Water being the coolant, the quenching phenomenon is divided into four stages i.e. Film boiling, nucleate boiling, transition boiling and free convection. Leidenfrost point LFP defines the end point of film boiling region. At LFP, the film collapses and water gets in direct contact with the surface which results in sharp increase in heat flux. Location of LFP depends on many parameters such as flow of water [38][39][40][10], body geometry, surface roughness, the properties of material to be cooled, method of quenching and last but not least the water quality.

Atomized spray quenching is a process in which water is atomized with the help of compressed air by a pneumatic atomizing nozzle on a hot surface in order to cool it rapidly. In this process, very high heat flux can be achieved as compared to other modes of quenching processes. Sprays are also generated by hydraulic nozzle, where atomization takes place without air. This kind of spray is referred here as *hydraulic spray*. In case of immersion quenching, coolants have a disadvantage i.e. the non-uniform break down of the vapor film which leads to different quenching speeds at different places of component because film boiling and nucleate boiling occur at same time at different location of the component to be cooled. As a result, non-uniform hardness warping or cracking occurs. The vapor film breaks down faster at corners, edges, pits as compared to the smooth plane surfaces which lead to the nucleate boiling at corners or edges at earlier stage. In spray quenching, uniform

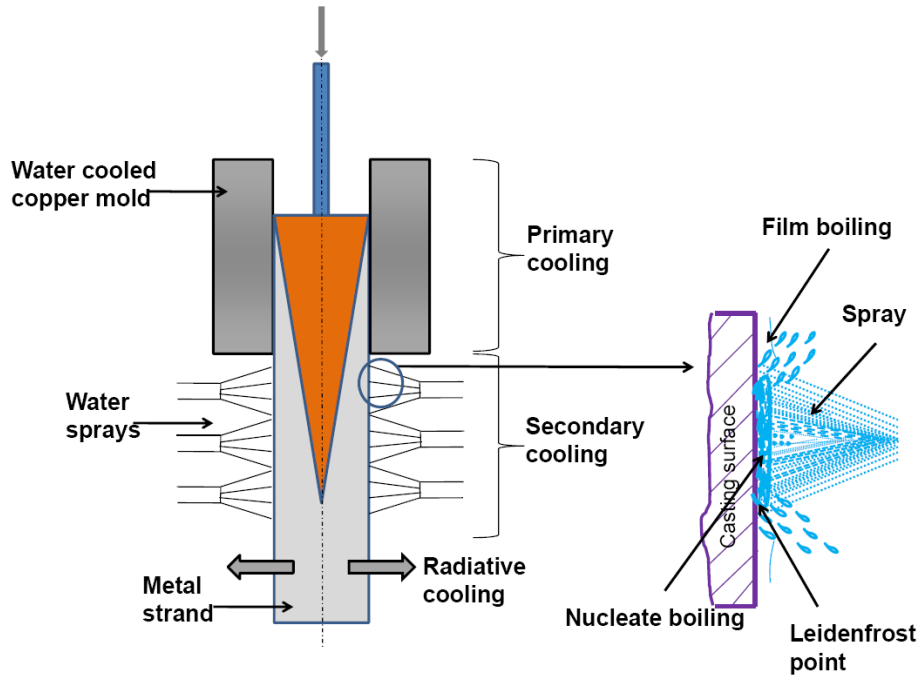


Figure 2.9: Schematic of cooling process in continuous casting

vapor film forms on the hot surface above Leidenfrost temperature and the heat transfer coefficient in film boiling regime is almost independent of the change in temperature therefore more defined and uniform quenching is possible which results in uniform properties of the product. Another advantage with spray quenching compared to bath quenching (when the whole part is submerged into a liquid bath) is that different areas of the component can be individually cooled. This allows control of the surface heat flux at thicker and thinner sections and therefore gives the opportunity to get a uniform cooling of the whole component which reduces residual stresses in the material. Depending on the shape of the component, different types of spray nozzles are used at different areas to get the correct heat flux, that a certain type of spray nozzle can generate.

However, while spray cooling shows promising results in both present and emerging technologies, much research is still needed to broaden the understanding of droplet impact and heat transfer mechanism of sprays. Quenching of heat treatable metallic parts has received considerable attention in the past decade from steel and aluminium producers for the automotive, aerospace industries, respectively. During a quench, the part experiences a relatively large and rapid temperature drop intended to suppress the precipitation of the alloying elements (solutes), enabling superior mechanical properties to be realized through subsequent aging. Accurate prediction of cooling rate and resulting material properties is highly desirable in order to reduce scrap and minimize costly trial and error production practices. The rate of quenching process is influenced by operating parameters of atomized spray. These parameters are:

- water impingement density
- size distribution of drop diameter

- distribution of drop velocity
- surface temperature of metal
- surface properties of metal (Roughness, thermo-physical properties)
- quality of water

Many researchers have done extensive work on the influence of above mentioned parameters on leidenfrost temperature, critical heat flux, nucleate boiling and transition boiling heat flux. Bernardin and Mudawar [41] studied the heat transfer regimes of water drops impinging on polished surface. They used high speed photography to record the impact behavior of water droplets on a hot aluminum surface. Effect of droplet velocity and surface temperature on impact behavior and ensuing heat transfer were studied. Three Weber numbers ($\rho_f v^2 d / \sigma$) of impacting droplets i.e. 20, 60 and 220 and surface temperature ranging from 280 to 100 °C were used. Temperature corresponding to critical heat flux and Leidenfrost point showed little sensitivity to both droplet velocity and impact frequency. A theoretical study of droplet impingement on a solid surface below the Leidenfrost temperature was done by Fukai et al.[42]. They suggested that meniscus profile plays an important role in the spreading behavior of a liquid droplet impinging on hot surfaces. Bernardin and Mudawar also investigated the changes in surface roughness associated with spray quenching [43]. They used samples of Aluminum alloys i.e. AA1100 and AA2024 with three types of surfaces i.e. polished, particle blasted and extruded finished surfaces. The purpose of investigation was to assess the influence of small scale roughness features on cooling rate by increasing the number of bubble nucleation sites during transition and nucleate boiling and more importantly the influence on the impact and spreading of spray droplets as well the leidenfrost temperature for spray quenching and how the spray quenching changes the surface properties of metals. Surface roughness features up to about 25 μm increase the bubble nucleation density during transition and nucleate boiling regimes, while large roughness feature of about 25 to 1 mm influence the impact and spreading of spray droplets and consequently leidenfrost temperature. However, surface temperature corresponding to critical heat flux was fairly independent of surface roughness [44]. Ciofalo and Brucato studied experimentally the effect of impingement densities (8 to 80 $\text{kg}/\text{m}^2/\text{sec}$), mean droplet velocities (13 to 28 m/sec) and mean droplet diameters (0.4 to 2.2 mm). A slab of beryllium copper alloy of dimensions $4 \times 5 \times 1.1$ mm was electrically heated to about 300 °C and cooled by two nozzles. The temperature was measured by thermocouple. The inverse heat conduction problem was solved by an approximation of Stefan solution. The heat transfer coefficient α and critical heat flux CHF were found to depend on impingement density and mean drop velocity while droplet size had a negligible influence [45]. A correlation of Sauter mean diameter d_{32} and critical heat flux for spray cooling was proposed by Estes et al. for three kinds of liquids i.e. FC-72, FC-87 and water [46]. This correlation shows a strong dependence of CHF on volume flow rate and Sauter mean diameter. On the other hand, Chen and coworkers [47][48] also performed experiments for analyzing the effect of three very important characteristics of spray i.e. Impingement density, Sauter mean diameter of droplets d_{32} and droplet velocity on CHF. They propounded that CHF varies with impingement density and droplet velocity and is relatively independent of d_{32} . They also suggested that to achieve the maximum possible CHF while using the minimum

quantity of water, it is desirable to select nozzles that a small a droplet diameter with as high a velocity as possible. Pautsch and Shed [49] performed experiments for analyzing the array of spraying nozzle. Their designs of array of nozzles were ranging from 1 to 16 hydraulic spray nozzles and they arranged them in the sets of 1, 2 3, 4, 5, 9 and 16 nozzles with different orientations and nozzle-nozzle spacing and tried to find the effect of these different patterns of nozzle arrangements on cooling effectiveness and critical heat flux. It was concluded that there is significant sensitivity of heat transfer performance to nozzle spacing and geometry. Jon and Mudawar [50] used three upward oriented nozzles and compared the results with three downward oriented nozzles with three different fluids i.e. water, FC-72 and FC-87 and proved that nozzle orientation has virtually no effect on spray cooling performance, provided the cooling system doesn't promote coolant accumulation over the test surface. The effect of spray inclination angle (the angle between the surface normal and the axis of symmetry of spray) on heat transfer during spray cooling was investigated experimentally by Silk et al. [51]. They changed the nozzle angle from 0° to 45° as shown in figure 2.10. Contrary to the past research, they observed that inclination of the spray axis between 0° and 45° relative to the heater surface normal created a noticeable increase in heat flux compared to the normal positions i.e. 0° . As possible reason of this effect, they proposed that the inclined sprays promoted better liquid drainage from the heated surface through elimination of stagnation zone which may cause the increased heat flux.

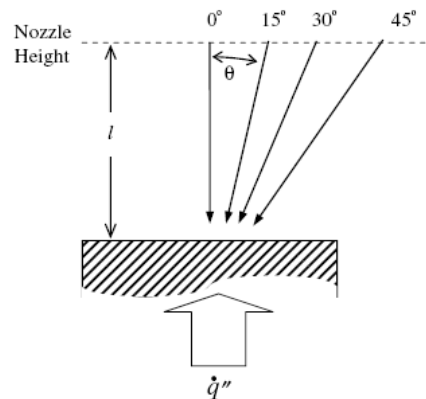


Figure 2.10: Orientation of spray inclination angle [Silk et al. [51]]

The purpose of this study is to measure the impingement density distribution of Hydraulic full cone nozzle and Pneumatic atomizing nozzle, to compare their radial temperature distribution with respect to nozzle type and material, to compare the heat transfer coefficient within film boiling zone for the two types of nozzles for varying impingement densities and analyze the effect of initial surface temperature of the metal during spray quenching. Circular disc (of dimensions Dia = 140 mm and thickness = 2 - 3 mm) made up of aluminum alloys AA2024, AA6082, pure nickel and inconel 600 are used as samples and quenched by spray. The temperature is measured by infrared thermography which is rarely used in past research. The impingement density distribution of multiple nozzles and the maximum heat transfer coefficient achieved within film boiling by atomized spray is also a subject of discussion. The influence of addition of salts and surfactant in cooling water of spray on

heat transfer is discussed in detail in the subsequent section and the results are presented in chapter 4.

2.6 Influence of quality of water on quenching of metals

One method of improving spray cooling efficiencies, into which little research has been done, is by dissolving additives (such as salts, surfactant) in the water. Gottfried et al. [52] used organic liquids as coolant on stainless steel and found that exact value of Leidenfrost point (LFP) appears to depend on surface properties of metal and method of depositing the droplets. It has been researched that even a slight variation in the water quality affects the heat treatment results [53]. Earlier investigations researched the water quality effect on quenching phenomena specially in immersed quenching. The subject of quenching of metals by immersion has been extensively researched in the past. Jeschar et al. executed experiments by submerging hot nickel sphere in solutions in order to determine the Leidenfrost point for dissolved salts, gases and polymers and they found that salts lead to increase the Leidenfrost point whereas gases and polymers tend to decrease the LFP. The effects of dissolved salts and gases on droplet boiling were investigated by Cui et al. [6][54] in detail. Dissolved carbon dioxide had little effect on droplet boiling because the gas comes out of solution and escaped almost immediately after droplets contact the hot surface. They also found that addition of salts prolongs the evaporation time but the droplet lifetime is decreased within nucleate boiling region. Due to the faster rate of vaporization during the initial contact, it is expected that some salt molecules do not diffuse fast enough and deposit on the surface. Moreover, the salt particles precipitating from the evaporating droplet act as nuclei to initiate bubble formation and promote the nucleate boiling heat transfer. The deposition of salts enhances the surface roughness and upgrade the LFP. Qiau and Chandra [4] used spray quenching technique to analyze this effect. They observed experimentally that the addition of salts i.e. NaCl, Na₂SO₄ and MgSO₄ decrease the quenching time and increase the Leidenfrost temperature. Figure 2.11 depicts that the three salts enhanced the heat flux specially in nucleate and transition boiling regions. MgSO₄ solution caused the largest increase in nucleate boiling heat transfer and also caused a similar effect in transition boiling regime as shown in figure 2.12. 0.4 molar solution of MgSO₄ enhanced the critical heat flux from 1.5 MW/m² to 3 MW/m². Foaming in the liquid film generated by the dissolved salts contributes to the enhancement of nucleate boiling. During transition boiling particles of salt adhered to the heated surface, raising surface roughness and increasing heat transfer. Moreover, the dissolved salt alters some physical properties in the liquid-vapor system such as surface tension, saturation temperature and liquid density. For most salts, the solution surface tension increases with increasing concentration and surface tension influence the LFP. It is also a known fact that salt solutions have higher density and boiling point as compared to de-ionized water. Change of boiling temperature with respect to salt concentration is explained by Roul't's law which states as follows:

$$\Delta T_b = i \times k_b \times m_{ml} \quad (2.4)$$

where ΔT_b is the change of boiling temperature, i is the dissociation constant which depends on the kind of salt, k_b is the boiling point elevation constant and m_{ml} is the solution concentration in molality [55].

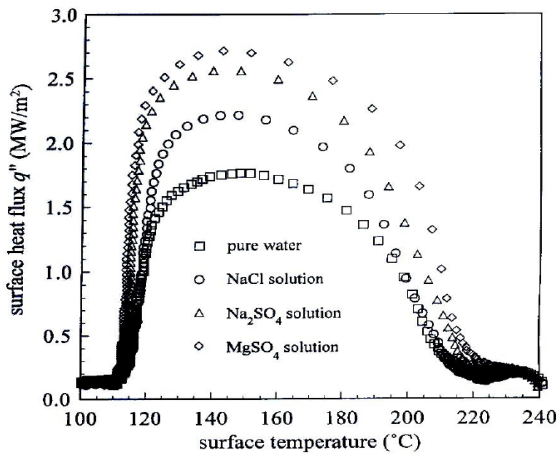


Figure 2.11: The effect of dissolved salts on heat transfer during spray cooling with 0.06 mol/l concentration salt solutions with impingement density of $3.0 \text{ kg/m}^2 \cdot \text{s}$ [Cui et al. [6]]

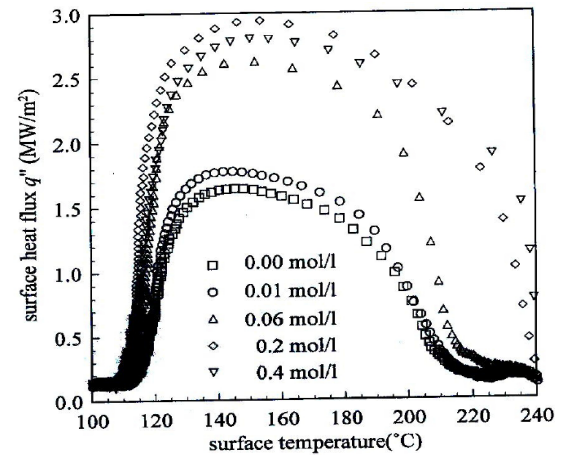


Figure 2.12: The effect of varying salt concentration on heat flux during spray cooling with MgSO_4 solution with with impingement density of $3.0 \text{ kg/m}^2 \cdot \text{s}$ [Cui et al. [6]]

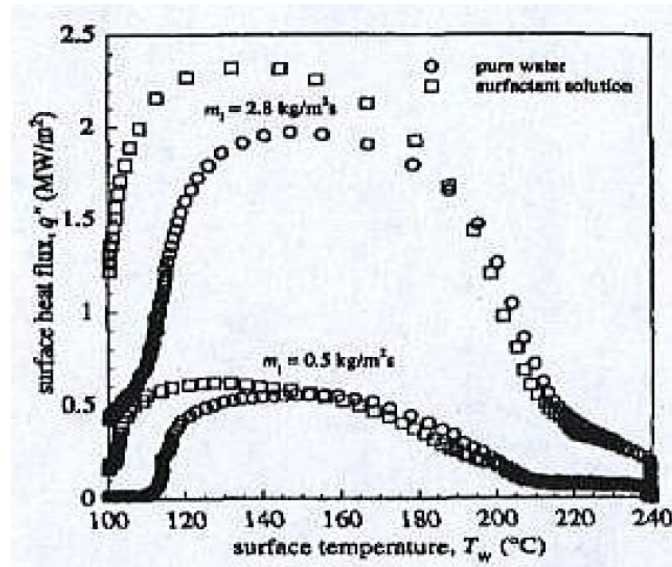


Figure 2.13: The effect of surfactant on spray cooling heat transfer at two different impingement densities [Chandra et al. [5]]

In this work, inorganic additives i.e. NaCl , Na_2SO_4 , MgSO_4 , Na_2CO_3 , NaHCO_3 , CaCO_3 and $\text{Na}_2\text{B}_4\text{O}_7 \cdot 10\text{H}_2\text{O}$ (Borax) were dissolved in the cooling water sprays. Borax is a chemical which is usually added to the cooling solution in the cast house of copper. The first five salts were added to the water in concentrations of 0.05, 0.1 and 0.5 Molar and the solution is used to quench Nickel disc with pneumatic spray. Among five salts MgSO_4 and Na_2SO_4 showed considerable enhancement of quenching. After that it was decided to exclude the influence of air by using hydraulic sprays. Solutions of MgSO_4 , Borax and CaCO_3 were

used as coolant with hydraulic sprays keeping the operating parameters constant and then the results were compared with those of deionized water. In order to assess the influence of dissolved CO_2 in water, pressurized pure CO_2 is injected to the deionized water at pressure of 2 bar for 10 minutes and immediately this Saturated carbonated water is used for spray quenching. Similarly, pure Oxygen O_2 and pressurized air are dissolved in deionized water and their influence was analyzed. In addition, drinkable carbonated water, which contains 190 mg/l of bicarbonate HCO_3^{-1} along with other ions, was also used as coolant.

Surfactants are the chemicals which are added to the water for decreasing its surface tension and enhancing the wettability of fluid so that it can have a better contact with the solid surface. Addition of surfactant e.g. Ethoxylated ester in cooling water at cast house of Aluminium casting is a normal practice. Earlier investigations were based on the hypothesis that this reduction of surface tension influences the nucleate boiling heat transfer [56]. later studies showed that additives which don't change the surface tension also influence the pool boiling in similar way [57][58]. Shah et al. found the values of heat transfer coefficient for different surfactant concentrations and concluded that enhancement of heat transfer with increasing surfactant concentration may not be caused by surface tension but by foaming and could be explained in the light of foaming [59]. Contrary to this, Shibayama et al. [60] found, by experiments of cooling a heated surface with a flowing liquid film with a small circular jet of liquid impinging at the center of heated surface, that the boiling heat transfer coefficient is proportional to the minus 0.4 powers of surface tension of liquid. Kotchaphakdee and Williams [61] investigated the heat transfer in nucleate boiling of dilute aqueous polymer solutions and compared the results with that for pure water. Hydroxyethyl cellulose, polyacrylamide and monomer acrylamide were dissolved in a pure water in a concentration ranging from 62 to 500 ppm and then boiled on a horizontal steam heated chrome-plated surface. Heat transfer in each polymeric solution exceeded that for water except one acrylamide monomer. They proposed that effect on heat transfer is better correlated with the viscosity of the solution caused by the addition of these polymers rather than with the surface tension of the solution. Few researchers also proposed that heat transfer enhancement by addition of surfactant could be caused by change in *dynamic surface tension* because of surfactant concentration variation at surface of expanding vapors [62][63][64] and increased convection at hot surface [65][66]. Furthermore, Qiau and Chandra [5] also carried out experimental study on the effect of dissolving a surfactant (sodium dodecyl sulphate SDS) in water sprays with a concentration of 100 ppm to cool a hot surface of copper. They analyzed the influence of addition of surfactant on boiling curve under the surface temperature of 240°C . So, their main areas of examination were nucleate boiling and transition boiling. It was found that addition of surfactant enhances the nucleate boiling heat flux by up to 300 % as shown in figure 2.13. This effect was correlated with the surfactant promoting bubble nucleation and foaming in spray droplets. On the other hand, this addition slightly reduced the transition boiling.

In this study, a surfactant known as Ethoxylated ester ($\text{RCOO-CH}_2\text{-CH}_2\text{-OH}$) is dissolved into deionized water in concentrations of 50 ppm, 100 ppm, 200 ppm and 500 ppm. This chemical is added to the cooling water in DC casting of aluminum and its alloys. The solutions are used to cool metallic discs by hydraulic sprays and the results were compared with that of deionized water. Addition of surfactant to cooling water seems to decrease the heat transfer coefficient values specially with film boiling region and thereby; prolongs the cooling time. Since salts and surfactant exhibited opposite results, mixture of MgSO_4 and

borax with ethoxylated ester were also utilized as coolant for spray quenching experiments. The combination of salts and surfactant showed the results similar to that of individual salts solutions.

3 Materials & Methods

3.1 Introduction

In order to analyze the influence of significant parameters on heat transfer during the process of atomized spray quenching, hydraulic spray quenching and quenching by array of jets, an experimental set-up is required. In addition, some supplementary set-ups were built for the purpose of calibration and measurements of parameters related to important components of main experimental set-up e.g. the measurement of distribution of impingement density with respect to the radius of atomized spray and hydraulic spray or the calibration of emissivity coefficient of the surface of graphite paint at various temperatures. Primary components of the main experimental set-up are infra-red Camera, electrically heated furnace, cooling devices e.g. pneumatic atomizing nozzle, hydraulic full cone nozzle and molds, metal sheets of various materials, centrifugal pump for water circulation and also high speed camera.

3.2 Infrared thermography

Temperature of the surface of an object can be measured by many ways. Thermocouple is the devices which is mostly used for this purpose in experimentation. However, considering the high heat fluxes, rapid cooling during quenching process and difficulties in attaching thermocouple at specific locations on moving metallic sheets, a sophisticated method of temperature measurement is required which can record the temperature values with higher frequencies and at various positions in real time. Infrared Thermography is a technique for non-contact temperature measurement. Any object which is kept at temperature higher than zero absolute radiates energy in the form of electromagnetic radiations also called heat waves. The amount of radiations or intensity of radiations increases with temperature of the object. IR Thermography is a method, which detects energy emitted from an object in the infrared range of the electromagnetic spectrum e.g. 8-9 μm , converts it to temperature, and displays images of temperature distribution. It is the function of infrared camera to make this correlation and show the distribution of temperature on the surface of object in the form of thermograph or thermal image. The accuracy of measurement depends on certain physical parameters i.e. emissivity coefficient of the measured surface, distance between lens and surface, relative humidity of atmosphere, ambient temperature etc. Emissivity ϵ is one of the most important influencing parameters and its value must be calibrated before measurement. In order to avoid the reflection of light and having a constant surface emissivity, the measured side is painted with black paint which has an emissivity coefficient of about 0.9. Few researchers in the past have used IR thermography for the measurement of surface temperature and heat flux. Freund and coworkers [67] measured the local heat transfer coefficients in spray cooling with the help of IR thermography. Schmidt and Boye



Figure 3.1: *Infra-red camera [Courtesy:FLIR systems]*

[68] and Puschman et al. [39] also used the same technique for analyzing heat transfer in spray cooling.

ThermaCAM SC 3000 Infrared camera, made by FLIR systems Inc., was used for temperature measurement during experiments. It is equipped with high speed QWIP (Quantum well infrared photo-detector) thermal imaging system for advanced thermal analysis. It has extremely high sensitivity of less than 20 mK at 20 °C. This system has a provision of setting different measuring frequencies and temperature measurement ranges. Measurements can be made with frequencies, 50, 150, 250 until 750 Hz and within three temperature ranges -20 to +80 °C, 10 to 150 °C, 100 to 500 °C, 350 to 1500 °C. The size of measuring window varies with the frequency. 50 Hz frequency provides a larger measuring window of 320×240 pixels, while 150 Hz provides a smaller window of size 80×320 pixels. The axis of IR camera can be adjusted in order to achieve an optimum measuring area with desired frequency. Temperature values can be recorded at every pixel. In this way, this measuring technique has the capability of recording 25600 readings of temperature in one second with a frequency of 150 Hz. Distance of 1 mm between two measuring points on the real surface was kept during the experiments. ThermaCAM researcher 2001 is the software which is used to monitor the camera and analyze the data later. Every trial or experiment is recorded as a number of thermographic images in one data file like an IR movie. After the recording, the sequence can be replayed and temperature profiles can be drawn for different selected shapes like point or spot, line, circle, rectangle etc. In case of line and two dimensional shapes, provisions of measuring average, maximum and minimum temperature are also possible.

3.2.1 Optical device Optris CT LT

An optical device known as Optris CT LT infrared sensor was also used for knowing the starting temperature of the metal sheet. As soon as the surface temperature of the hot metallic sheet reaches the desired starting temperature, main IR camera is commanded to start data acquisition. This starting temperature is alarmed by Optris CT by change of color from yellow to blue. The principle of working of Optris is same as that of infrared camera; however, the measurement is more tentative instead of very accurate as in case of IR camera. It can measure the temperature from -50 °C to 975 °C. The spectral IR range for that device is 8-14 μm .



Figure 3.2: Optical device for measuring starting surface temperature [Courtesy:optris]

3.3 Coating

3.3.1 Selection of coating

It is very significant to know at the initial stage that what is the stability of four available coatings KS 81, KS 82, KS 83 and Graphite coating at higher temperature of up to 600 °C. After the confirmation of stability, the tests for emissivity were supposed to be performed. For this purpose, Nickel sheet is coated by these paints. After drying these painted sheets, they are heated to 600 °C in a furnace. After heating, it was found that the surface of KS 81, KS 82 and KS 83 were not smooth as shown in figures 3.3 & 3.4. They become very brittle and detach from the metal surface when touched even with bare hands. Therefore, it is concluded that these three coatings can not be used for measurement of temperature by IR camera because the surface must be smooth after heating which is an essential requirement of Infrared Thermography. However, the graphite coating was found to be stable at a temperature of 700 °C and the surface was also very smooth before and after heating. Having confirmed the stability of graphite coating, next step was to know exactly the emissivity of this graphite coating and the dependence of Emissivity of this graphite coating upon surface temperature.



Figure 3.3: Surface of KS 83 coating after heating into furnace at 600 °C



Figure 3.4: Surface of KS 82 coating after heating into furnace at 600 °C

3.3.2 Measurement of emissivity

Emissivity of a surface can be defined as, "It is a ratio of energy radiated by a surface to the energy radiated by a black body kept at the same temperature". One side of the metal sheet which is in front of the IR camera is painted with graphite coating. Accuracy

of surface temperature measurement is influenced by the accurate measurement of emissivity of this coating. For this purpose, a higher value of emissivity is required because higher value leads to higher emission of radiations at the given temperature; furthermore, graphite coating avoids reflection of other incident radiations. The experimental set up used for measurement of emissivity is shown in figure 3.5. A small copper cylinder is machined with an inside bore. A thermocouple is inserted inside the bore for temperature measurement. This cylinder is painted with graphite coating and placed inside a horizontal cylindrical furnace. IR camera is positioned in front of the outlet of this furnace and the coated surface is zoomed in by camera. The temperature of the furnace is increased in steps of 50 °C from 50 to 700 °C and the temperature of the cylinder measured by thermocouple and that of IR camera are matched with each other by adjusting the emissivity value in the settings of the camera. In this way, emissivity is recorded versus temperature of the surface of cylinder. It was found that emissivity of coating changed from 0.92 to 0.94 with mode value of 0.92. Hence, it can be inferred that a constant value of emissivity of 0.92 should be used for accurate measurement of surface temperature.

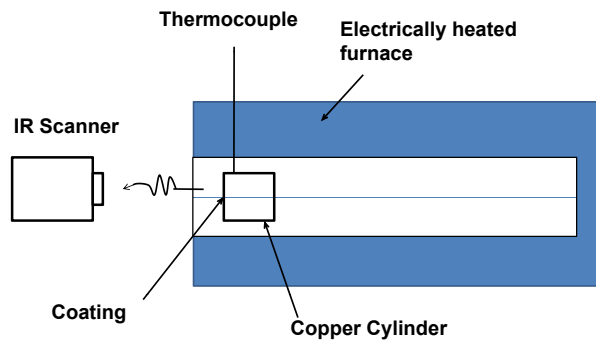


Figure 3.5: Set-up for calibration IR camera for emissivity

3.4 Cooling components

Selection of cooling component primarily depends on the method of quenching to be employed. In this work, three methods of quenching i.e. atomized spray quenching (ASQ), spray quenching (SQ) and array of jets were used. Therefore, pneumatic atomizing nozzle, hydraulic full cone nozzle and two kind of Molds of different flow rates have been installed according to the required method. Spray nozzles are generally used in secondary cooling unit in continuous casting of steel while molds or array of jets are commonly used in direct chill (DC) casting of non-ferrous metals e.g. Aluminum and its Alloys.

3.4.1 Pneumatic atomizing nozzle

As the name suggests, Pneumatic Atomizing Nozzle combines two fluids i.e. air and water to generate a full conical spray of discrete droplets. There are two kinds of such nozzle

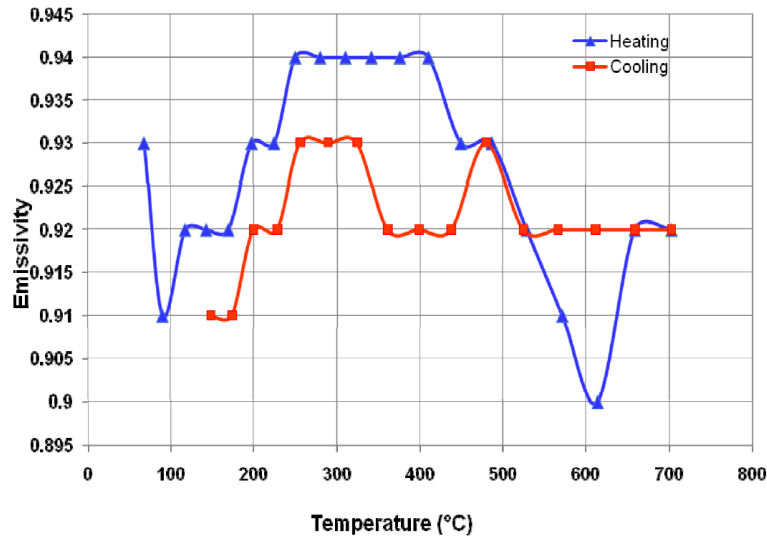


Figure 3.6: Relation between emissivity & temperature

Inside mixing and Outside mixing. Inside mixing should be preferred, when water, low viscosity liquids or liquids without solid matters are to be atomized. Outside mixing is particularly suited for atomizing viscous liquids which are prone to impurities and therefore tend to cause clogging of the nozzle. Low liquid pressures are used with this type of nozzle due to its design. The advantage of atomized spray quenching over water spray quenching is that due to discrete droplets moving at high speed caused by superimposed air flow, the water film does not form on the metal surface and breakage of this film which causes high heat flux at corners or sharp edges is avoided. The droplet size of water was measured to be 10 to 20 μm which is considered to be very fine. A pneumatic atomizing nozzle made by Lechler GmbH (Lechler-156.103.35.13) is used for this purpose as shown in figure 3.7. Water at a flow rate of 20 to 40 l/h and air at pressure of 2 to 4 bar with flow of 8 Nm^3/h is supplied to nozzle to generate an atomized spray of different impingement densities depending on the water and air flow. The sample to be quenched is cut in circular disc for symmetrical analysis because the cone of atomized spray is also circular having a cone angle of 20° and distance of 150 mm between nozzle and surface of the metal. The impingement density of the spray produced by pneumatic atomizing nozzle is normally distributed having symmetry around the nozzle axis as illustrated in figure 3.8. The heat flux, in case of pneumatic atomizing nozzle, are approximately 8 to 10 times higher as compared to hydraulic full cone nozzle.

3.4.2 Hydraulic full cone nozzle

Water or liquid solutions are the only cooling media that this nozzle sprays to the hot surface. There are two different style of full cone nozzles:

1. Axial full cone nozzle
2. Tangential full cone nozzle

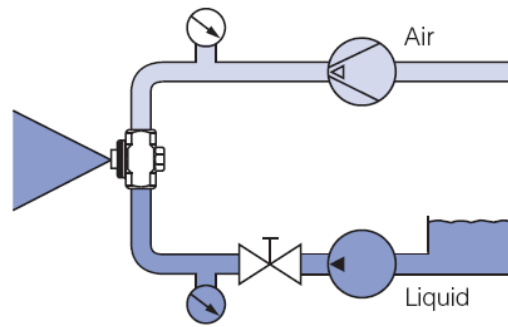


Figure 3.7: Flow diagram of pneumatic atomizing nozzle

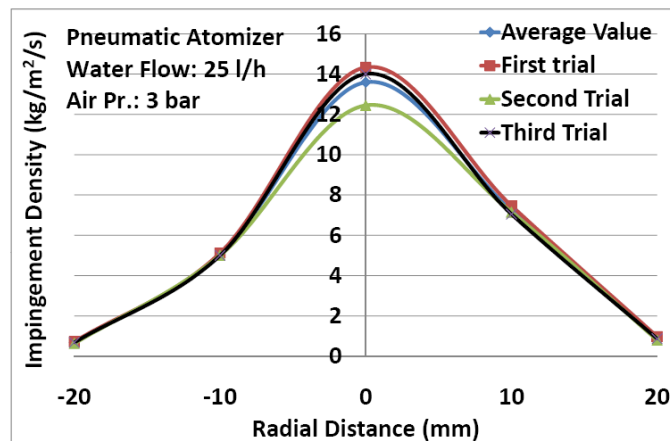


Figure 3.8: Impingement density distribution of pneumatic atomizer

The type of hydraulic full cone nozzle employed for the experiments was Axial full cone nozzle. Axial flow nozzle sprays on the same axis as the inlet fluid as shown in figure 3.9. Water or solution are supplied to this kind of nozzle through a single long metallic pipe of length 50 cm. Variation of the cooling capacity is only possible by changing the water pressure. The droplets of produced spray are larger in diameter and the velocity is also lower as compared to pneumatic atomizing nozzle. It was particularly used to analyze the influence of water quality on heat transfer in spray quenching process. Since the water flow rate is lower in this case (20 l/h) which result in lower heat flux, effect of water quality on quenching can be better analyzed by using this kind of nozzle as compared to pneumatic atomizing nozzle or mold. A nozzle made by spraying system having a cone angle of 45° is used with a water flow of 20 l/h. Impingement density of this kind of nozzle is symmetrically distributed around the nozzle axis, sinusoidally increasing and decreasing as shown in figure 3.10.

3.4.3 Mold or array of jets

Metallic devices called molds have been used for quenching experiments for analyzing the phenomenon of heat transfer during quenching of metal by an array of water jets as shown in figures 3.11 & 3.12. They represent a small section or part of a real mould for direct chill

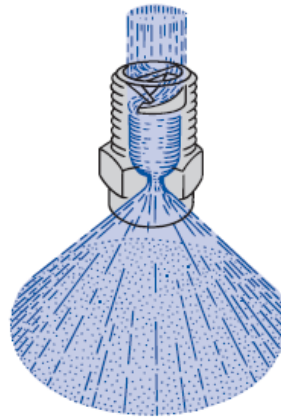


Figure 3.9: Flow diagram of hydraulic full cone nozzle

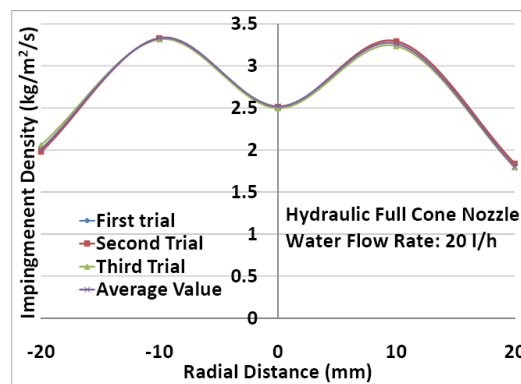


Figure 3.10: Impingement density distribution of hydraulic full cone nozzle

casting plant. Two molds were installed. One has 8 orifices of diameter 4.78 mm each. It is designed for the average flow rate of 500 l/h with an outlet velocity of 1 m/s. Another has 7 orifices of diameter 2.5 mm each which is designed for an average flow of 150 l/h with an outlet velocity of 1.5 m/s.

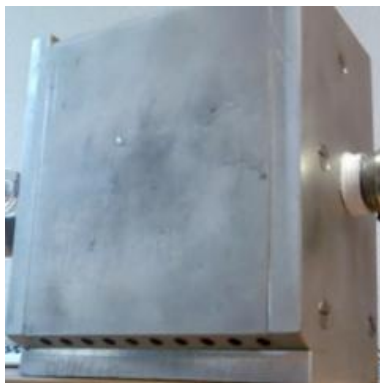


Figure 3.11: Mold with eight orifices



Figure 3.12: Mold with seven orifices

3.5 Metal samples

Metallic sheet is one of the main components of experimental set up which is used to calculate the heat transfer coefficient in water spray, atomized spray and mould quenching for different kinds of metals and to investigate cooling phenomena in each case. We used nickel, aluminium alloy, copper alloys and nickel inconel 600. The thickness of sheets varies from 4 to 2 mm. Sheet is heated by electrical furnace then it is cooled from one side by any selected mode of quenching. The opposite side is painted by a commercial furnace paint that possesses an emissivity of 0.9 approximately. The temperature is measured on this opposite black side. Thermal conductivity, specific heat capacity and density are the thermal-physical properties of the material which must be known in order to calculate the heat transfer coefficient. The metals are cut in two shapes depending upon the method of quenching i.e. rectangular shapes are machined for quenching by array of jets while circular disc shapes are formed for quenching by water spray or atomized spray. These specifications of materials are given in table 3.1. The width of the rectangular sheets depends on the size of the mold. 110 mm and 70 mm wide sheets were used for the small and big mold respectively as shown in figures 3.13 and 3.14. The sheets should have such width that it stops the water flow and it should not wet the rare side of the sheet to err the measurements by camera. The metal samples are cut by laser cutting. In case of copper, they are cut by water jet cutting because laser cutting does not work precisely when the conductivity of material is too high. After cutting, the sheets are painted with black graphite paint and heated to 250 °C for 30 minutes for the proper fixation of the paint. The front and back sides of circular and rectangular sheets are shown pictorially in figures 3.15, 3.16, 3.17 and 3.18.

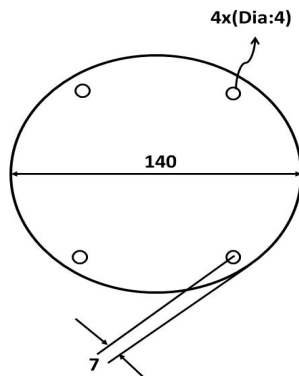


Figure 3.13: Circular disc

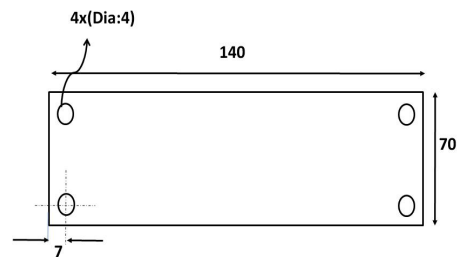


Figure 3.14: Rectangular sheet

3.6 Measurement of impingement density distribution

Impingement density or mass flux can be defined as "mass flow of water droplets of the spray passing through a unit area in unit time" and the unit of impingement density is



Figure 3.15: Front side of nickel sheet for mold quenching



Figure 3.16: Back side of nickel sheet for mold quenching

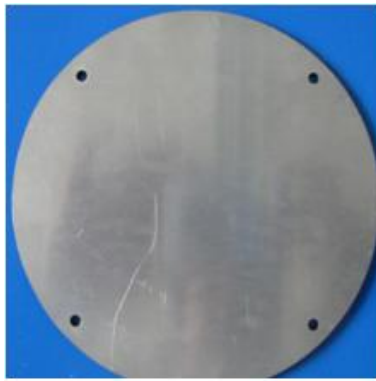


Figure 3.17: Front side of aluminium sheet for spray quenching



Figure 3.18: Back side of aluminium sheet for spray quenching

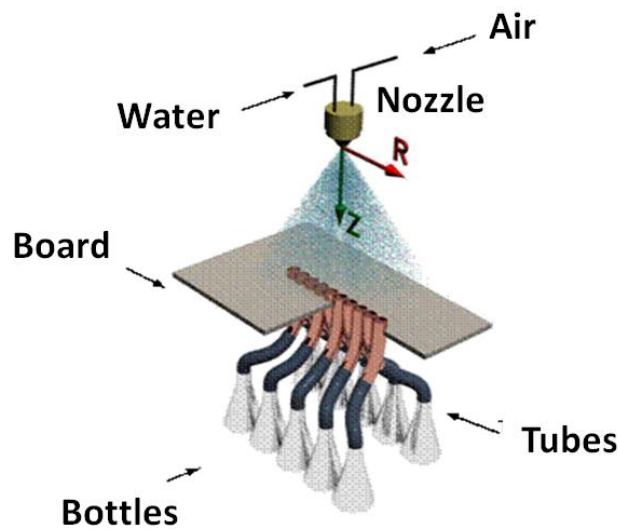
$kg/m^2/sec$. The heat flux during spray quenching depends directly on the impingement density. Higher the impingement density, higher will be the heat flux. Impingement density varies with the radius of the cone. For example, in atomized spray quenching, it is highest at the center and lowest at the circumference of the spray cone. For pneumatic atomizing nozzle, it is found to be the function of both water flow rate and air pressure while for hydraulic full cone nozzle it depends on only water flow. It is important to know the impingement density distribution at different operating conditions. A device known as patternator is indigenously designed and installed for this purpose as shown in figure 3.19. It consists of brass tubes of diameter 10 mm each fixed in a linear fashion adjacent to each other. From bottom, each tube is bent and terminates to a flask for water collection. Water droplets are sprayed over the patternator tubes. The mass of water droplets M_w is collected by the tubes in a period of time Δt . The impingement density is calculated by the equation 3.1. The impingement density distribution is graphically represented in figure 9.

$$\dot{m} = \frac{4 \times M_{water}}{\pi \times d^2 \times \Delta t} \quad (3.1)$$

where \dot{m} is the impingement density in $kg/m^2/sec$, M_{water} is the mass of water collected by the individual tube in Δt seconds and d is the diameter of the tube.

Table 3.1: Specification of different materials of metal samples

Kind of Metal	Composition	Thermal Conductivity (W/m/K)	Specific Heat Capacity (J/kg/K)	Density (kg/m ³)	Thickness (mm)
Pure Nickel	Ni: 98 %	91	444	8908	2
AA2024	Al: 92.4-97.8 %, Cu:2.0-4.9 %, Mg:0.15-1.8 %	177	875	2770	3
AA6082	Al: 97.4 %,Si: 1 % Mg: 0.9 %,Mn: 0.7 %	150	900	2720	3
Inconel 600	Ni: 78 %,Cr: 14 % Fe: 6 %,Mn: 1 %	14.8	460	8450	3
Copper Alloy K75	CuCr0,3Ti0,15Si0,002	300	400	7900	3
Copper Alloy B14	CuSn4	96	400	7900	4
Copper Alloy L49	CuNi9Sn2	48	400	7900	4
Copper Alloy K12	SE-Cu	385	400	7900	2.7

**Figure 3.19:** Patternator: A device for measuring impingement density distribution

3.7 Method

3.7.1 Preparation

Before performing experiments, a preparatory work has to be done. The first step of preparation for performing experiments for metal cooling by nozzle or mold is to prepare the metal samples which are to be heated and then cooled. Mold quenching requires rectangular metal sheets while spray quenching requires circular discs of 2 or 3 mm thickness. These shapes are cut with precision by laser cutting. Normally aluminium alloys and nickel are cut by these methods. On the other hand, copper alloys are cut by water jet cutting because of their high conductivity values they are not cut by laser. After cutting, these samples are painted from one side by black furnace paint and then these samples are kept in the furnace for 30 minutes so that the paint is adhered to the metal surface. After fixing of paint, the samples are ready to be used in experiments. The cooling components i.e. hydraulic full cone nozzle, pneumatic atomizing nozzle or mold are installed in such way that nozzle center coincides with the center of circular disc sample and the nozzle axis remains perpendicular to the disc surface and similarly, mould orifices level coincides with the top of the rectangular sample and water does not splash on the other side (painted side) of the sample. Then, the electrical furnace is set for heating which takes two to three hours to raise the temperature of the furnace from ambient to 600 °C. The next step is the setting of infrared camera. The important parameters include the distance between camera lens and metal surface, the emissivity of the surface, the temperature range for measurement, ambient conditions i.e. relative humidity and ambient temperature and the frequency of infrared imaging. Once the metallic samples are prepared and IR Camera is ready, the main procedure of actually executing the experiments for metal quenching can be started.

3.7.2 Main procedure

Experimental set up is shown schematically in figure 3.20. It consists of a furnace, a cooling component e.g. a pneumatic atomizing nozzle (Lechler-156.35.13) or a hydraulic full cone nozzle or a mould with 7 or 8 orifices, infrared camera FLIR SC3000, metallic sheet samples of 2 or 3 mm thickness. At first, the metal sample is heated up by electrically heated furnace to a temperature of 600 °C. This temperature can be adjusted according to the requirement. For example, if the sample is nickel, it can be heated to 800 °C, while, in case of Aluminum and its alloys, the set temperature is not more than 520 °C. After that the sample is shifted by relay to the cooling unit where it is sprayed on by an atomized spray or hydraulic spray or array of jets depending on the method of quenching. The water flow rate, pressure and air pressure are also adjusted according to current objective of the experiments. Front side of the sheet which is sprayed on by spray is polished while the rear side is painted with black graphite paint in order to achieve an emissivity of 0.9. The surface temperature of the rear side is measured with the help of infrared camera. This technique of contactless temperature measurement is regarded as infrared thermography. This IR camera has capability of measuring the temperature with a frequency of 150 Hz within a window of 240 x 80 pixels. Temperature at every pixel can be measured. The real distance between the two consecutive pixels is approximately 1 mm. The experiments are repeated with different concentrations of salts solutions, surfactant solution, de-ionized

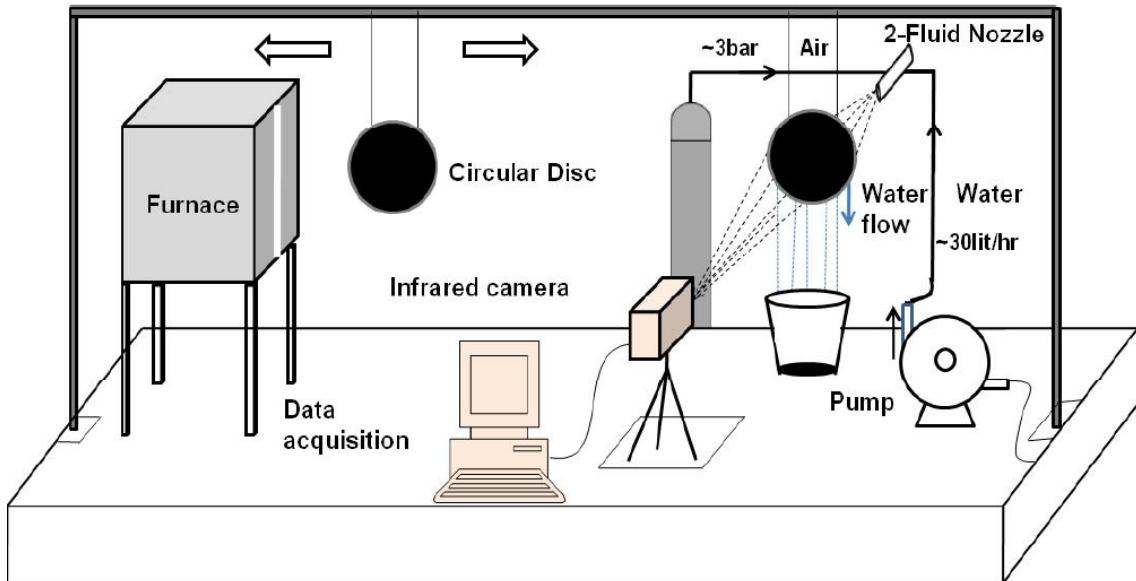


Figure 3.20: *Experimental set-up*

water, impingement densities and jet velocities. The data is saved in the computer connected to the infrared camera. The parameters which influence the IR thermography are emissivity of the surface, ambient temperature, relative humidity and the distance between the lens and measured surface.

3.7.3 Post process

After the execution of sequences of experiments, infrared sequences are saved using a software named ThermaCAM researcher version 2001. It is used to operate the IR camera and using the saved data for analysis. Every sequence consists of many infrared images captured in the real time. Different shapes e.g. single point, circular area, rectangular area, single line etc can be selected on the object surface being examined and the temperature profiles for actual temperature, average temperature, minimum and maximum temperature for the specific shape can be achieved with respect to real time. The infrared images of rectangular and circular sheets are shown in figures 3.21 and 3.22 respectively. Figure 3.21 shows a horizontal image which actually vertical from left to right. The water film travels from left to right (top to bottom) on the surface the rectangular metal sheet. The camera is rotated to 90 degree angle so that the complete sheet can be captured because at higher frequency of 150 Hz, the measuring window of IR camera shrinks to 240×80 pixels while in case of measuring frequency of 50 Hz, the measuring window is 240×320 . The points or spots are selected on the surface and then the sequences are run or played to obtain the temperature profile for each spot in real time. This temperature-time data is used later to perform the heat transfer analysis. A run time IR image of a circular disc being quenched by full cone spray is shown in figure 3.22 where the IR image, analysis table and temperature-time curve are shown in real time. The temperature profiles can be drawn for every pixel selected at the same time or for every shape selected e.g. triangle, rectangle, circle or line as shown in figure 3.22. After drawing the curves, temperature

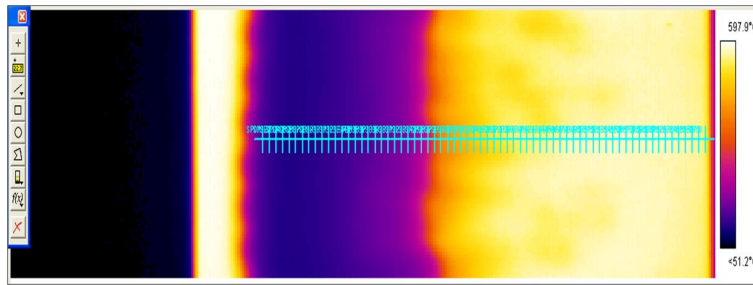


Figure 3.21: Infrared image of rectangular sheet quenched by array of jets

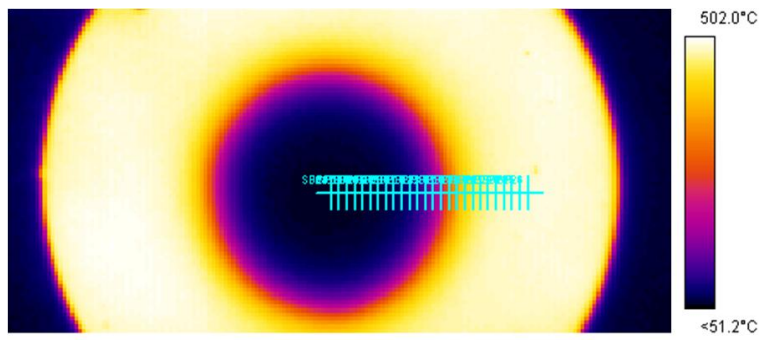


Figure 3.22: Infrared image of circular sheet quenched by full cone spray

data are saved for every pixel in the form of excel files. These temperature data are then processed by using MATLAB and inverse heat conduction problem is solved to calculate the temperature and heat flux on the quenched side by using non-iterative finite element method.

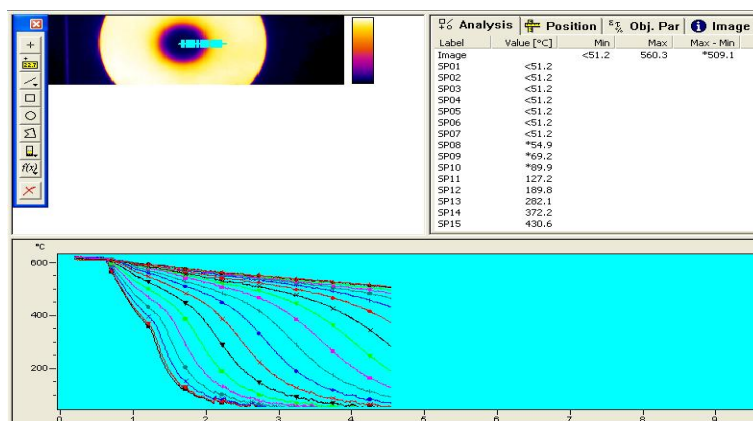


Figure 3.23: A run time temperature profiles image for quenching circular disc by full cone spray

3.8 Heat transfer analysis

3.8.1 One dimensional analysis

3.8.1.1 Energy balance

Heat transfer during quenching of circular disc by spray can be calculated by using the first law of thermodynamics or law of conservation of energy. Let us consider a small circular element at the center of the disc of radius r . The total energy of this element changes at a rate heat is transferred from its surface to the spraying fluid. This energy balance can be written as under:

$$\frac{dh}{dt} = -\alpha A_s(T_s - T_{sp}) \quad (3.2)$$

$$\frac{d}{dt}(\rho c_s s T_s \pi r^2) = -\alpha A_s(T_s - T_{sp}) \quad (3.3)$$

where T_s , ρ , s and c_s are the temperature, density, thickness and specific heat capacity of the metal respectively, T_{sp} is the temperature of the spray, α is the heat transfer coefficient and A_s is the surface area (πr^2). Equation 3.3 assumes that the surface temperature is uniform (T_s) through the entire time of cooling.

$$A_s = \pi r^2$$

Therefore,

$$\rho c_s s \frac{dT_s}{dt} = -\alpha (T_s - T_{sp})$$

$$\frac{dT_s}{(T_s - T_{sp})} = -\frac{\alpha}{\rho c_s s} dt$$

Integrating on both sides

$$\int \frac{dT_s}{(T_s - T_{sp})} = -\int \frac{\alpha}{\rho c_s s} dt$$

$$\ln |T_s - T_{sp}| + C = -\int \frac{\alpha}{\rho c_s s} t \quad (3.4)$$

Applying the initial conditions i.e. $T_s = T_o$ at $t = 0$. So, the constant of integrations will be

$$C = \ln |T_o - T_{sp}|$$

Substituting C from the initial condition into equation 3.4 yields:

$$\ln \left| \frac{T_s - T_{sp}}{T_o - T_{sp}} \right| = \frac{\alpha t}{\rho c_s s}$$

$$\alpha = \ln \left| \frac{T_s - T_{sp}}{T_o - T_{sp}} \right| \cdot \frac{\rho c_s s}{t} \quad (3.5)$$

Hence, Substituting the values of T_o , T_{sp} , ρ , c_s and s , a measure of T_s with respect to time by Infrared camera will yield α . Using equation 3.5 heat transfer coefficient α is plotted against surface temperature of the disc in film boiling region during spray quenching. The curves are found to be independent of surface temperature within film boiling region. This correlation based on the assumption that the surface-convection resistance is large compared to the internal-conduction resistance. Such an analysis may be expected to yield reasonable estimates within 5 percent when the following condition is met:

$$\frac{\alpha(V/A)}{\lambda} < 0.1$$

where λ is the thermal conductivity of the disc material. If we consider $V/A = s$ i.e. thickness as characteristic dimension of disc the dimensionless group is called Biot number:

$$\frac{\alpha s}{\lambda} = \text{Biot number} = Bi$$

In case of spray quenching with hydraulic nozzle, heat transfer coefficient varies from 400 to 600 $W/m^2/K$ within film boiling region. Therefore, the equation 3.5 is used for plotting heat transfer coefficient with respect to surface temperature.

3.8.1.2 Energy balance with conduction

To calculate the heat transfer coefficient for a position regarded on the test sheet, an energy balance is performed for this position. The energy balance is based on the following statement which is the formulation of the first law of thermodynamics on the basis of time:

The rate at which thermal and mechanical energy enters a control volume, plus the rate at which the thermal energy is generated within the control volume, minus the rate at which thermal and mechanical energy leaves the control volume must equal the rate of increase of energy stored within the control volume.

The energy balance in our case can be written as:

$$\frac{dh}{dt} = -\dot{q}_{sp} - \dot{q}_{\lambda} - \dot{q}_{\alpha} - \dot{q}_R \quad (3.6)$$

The change of enthalpy in the volume element regarded is calculated by

$$\frac{dh}{dt} = \rho c_s s \frac{dT}{dt} \quad (3.7)$$

Convection and radiation are considered for heat loss. Heat loss leads away heat from the volume element regarded. Radiation is considered on both sides of the metal sheet surface. Convection is only considered on the side where surface temperature is measured. Radiative heat loss can be calculated as follows:

$$\dot{q}_R = (\epsilon_1 + \epsilon_2) \cdot \sigma \cdot (T_s^4 - T_{\infty}^4) \quad (3.8)$$

where ϵ_1 and ϵ_2 are the emissivities of the front and rear side of the sheets. Since the front side is polished, its emissivity is 0.3 and the rear side is painted black therefore its emissivity is 0.9 approximately. Convective heat loss can be calculated as:

$$\dot{q}_{\infty} = \alpha \cdot (T_s - T_{\infty}) \quad (3.9)$$

Due to radial temperature distribution with the minimum temperature in the center of the spray, heat is conducted within the metal sheet plane from outer regions of the sheet to its center. This heat flux is calculated using Fourier differential equation for cylindrical coordinates

$$\dot{q}_\lambda = -s \cdot \lambda \cdot \frac{1}{r} \frac{\partial}{\partial r} \left(r \cdot \frac{\partial T}{\partial r} \right) \quad (3.10)$$

In order to calculate the factor $\frac{1}{r} \frac{\partial}{\partial r} \left(r \cdot \frac{\partial T}{\partial r} \right)$, we have to follow a step wise calculation procedure using the software Therma Cam 2001 Researchers. Seven spot measurements of temperature are carried out at the center of the spray jet on metal sheet in such a way that spot 4 is at the center and spot 1 and spot 7 are at the corners. Distance between two consecutive spot is equal to 10/11 mm which is regarded as pixel size. The steps which are to be followed to calculate the factor $\frac{1}{r} \frac{\partial}{\partial r} \left(r \cdot \frac{\partial T}{\partial r} \right)$ are explained by table 3.2:

Table 3.2: Algorithm for the calculation of heat of conduction

(1) Pixel (spot):	1	2	3	4	5	6	7
(2) Co-ord.r:	-2.73	-1.82	-0.91	0	0.91	1.82	2.73
(3) Temp. T:	9	4	1	0	1	4	9
(4) Co-Ord. r:		-2.275	-1.365	-0.455	0.455	1.365	2.275
(5) $\frac{\partial T}{\partial r}$:		-5.494	-3.296	-1.099	1.099	3.296	5.494
(6) $r \frac{\partial T}{\partial r}$:		12.49	4.49	0.5	0.5	4.49	12.49
(7) Co-Ord. r:		-1.82	-0.91	0	0.91	1.82	
(8) $\frac{\partial}{\partial r} \left(r \cdot \frac{\partial T}{\partial r} \right)$		8.79	4.38	undefn	4.38	8.79	
(9) $\frac{1}{r} \frac{\partial}{\partial r} \left(r \cdot \frac{\partial T}{\partial r} \right)$		4.829	4.817	4.817	4.817	4.829	

The final value of $\frac{1}{r} \frac{\partial}{\partial r} \left(r \cdot \frac{\partial T}{\partial r} \right)$ is by averaging two middle values in step (9) which is then used to calculate the heat flux due to conduction. The water spray also causes a heat flow outside the volume element regarded. This heat flux q_{sp} is determined by energy balance equation. The heat transfer coefficient of the water spray α_{sp} is defined with the water spray temperature T_{sp} by the equation

$$\dot{q}_{sp} = \alpha_{sp}(T_s - T_{sp}) \quad (3.11)$$

As radiative and convective heat flows are very small (5% of the total heat loss) as compared to conductive heat flow and heat transfer due to spray, they can be neglected. So, Equation 3.6 can be written as:

$$\rho c_s s \frac{dT}{dt} = s \lambda \frac{1}{r} \frac{\partial}{\partial r} \left(r \frac{\partial T}{\partial r} \right) - \alpha_{sp}(T_s - T_{sp}) \quad (3.12)$$

$$\alpha_{sp} = \frac{s \lambda \frac{1}{r} \frac{\partial}{\partial r} \left(r \frac{\partial T}{\partial r} \right) - \rho c_s s \frac{dT}{dt}}{(T_s - T_{sp})} \quad (3.13)$$

3.8.2 Two dimensional analysis

The estimation of heat flux (HF) demands the solution of the IHCP. Using Laplace transform, Monde [69] solved the inverse heat conduction problem analytically for a one-dimensional (1D) heat conductor. Ijaz et al. [70] have presented an adaptive state estimator for the estimation of input heat flux and measurement sensor bias in two-dimensional (2D) inverse heat conduction problems. Continuous-time analogue Hopfield neural network based inverse solution algorithm has been proposed by Deng and Hwang [71]. Conjugate gradient method for the estimation of surface heat flux has been used by Huang and Wu [72] and Xue and Hang [73]. A non-iterative least square minimization technique along with FEM proposed by Ling et al. [74] simplifies the inverse problem computation and produces consistent results.

In case of direct heat conduction problem (DHCP), the boundary conditions are known and interior domain solution is to be solved by using governing differential equation (GDE). In inverse heat conduction problem (IHCP), the boundary conditions are unknown and interior domain solution is known by experimental temperature data. The boundary conditions are estimated by solving GDE using this experimental data. Finite element method (FEM) is used to solve IHCP using experimental data and DHCP temperature solution.

3.8.2.1 Direct heat conduction problem

Let an open bounded domain $\Omega \in \mathbb{R}^{n_d}$ ($n_d = 1, 2, 3$) be the configuration of a non-linear heat conductor with particles defined by $\vec{X} \in \vec{\Omega}$, $\Gamma = \partial\Omega$ its smooth boundary and the time interval analysis $t \in \Upsilon$ ($\Upsilon \subset \mathbb{R}^+$). As usual, $\vec{\Omega} = \Omega \cup \Gamma$ and $\Gamma = \Gamma_\theta \cup \Gamma_q$, the metal quenching problem consists of finding the absolute temperature field $\theta : \Omega \times \Upsilon \rightarrow \mathbb{R}^+$ such that [75].

$$\nabla \cdot k \nabla \theta = \rho c_p \dot{\theta} \text{ in } \Omega \times \Upsilon \quad (3.14)$$

subject to the boundary conditions

$$\theta = \theta_s \text{ in } \Gamma \times \Upsilon \quad (3.15)$$

$$k \nabla \theta \cdot \mathbf{n} = q \text{ in } \Gamma \times \Upsilon \quad (3.16)$$

the initial condition is

$$\theta(\vec{X}, t)_{t=0} = \theta_0(\vec{X}) \text{ in } \Omega \quad (3.17)$$

Equation 3.14 represents the energy balance obtained from the first law of thermodynamics and Fourier's law of heat conduction. Where ρ is the density, c_p is the specific heat capacity and k is the thermal conductivity and q is the temperature and space dependent normal heat flux due to the convection radiation heat transfer. Applying the variational principle and Euler backward time difference method, the final form of FEM equation at the current time step $n+1$ is given as [76]

$$(\mathbf{M} + \Delta t \mathbf{K}) \Theta^{n+1} = \mathbf{M} \Theta^n + \Delta t \mathbf{f}^{n+1} \quad (3.18)$$

where the capacitance matrix (\mathbf{M}), the conductance matrix (\mathbf{K}) and the force vector (\mathbf{f}) are given in the element form as

$$\begin{aligned}\mathbf{M}^e &= \int_{\Omega_e} \rho c_p \mathbf{N} \mathbf{N}^T d\Omega \\ \mathbf{K}^e &= \int_{\Omega_e} k (\nabla \mathbf{N}) (\nabla \mathbf{N})^T d\Omega \\ \mathbf{f}^e &= \int_{\Gamma_e} \mathbf{N} q d\Gamma\end{aligned}\quad (3.19)$$

3.8.2.2 Inverse heat conduction problem

Let an interior of the domain Ω bounded by the curve $\Gamma = \Gamma_\theta \cup \Gamma_q$, where Γ_θ is the temperature described boundary and Γ_q is the unknown heat flux boundary due to water cooling. Using the standard finite element discretization technique, convective heat flux vector $\tilde{\mathbf{q}}^{n+1}$ at the current time step on the boundary Γ_q is represented as

$$\tilde{\mathbf{q}}^{n+1} = \left[\tilde{q}_1^{n+1}, \tilde{q}_2^{n+1}, \dots, \tilde{q}_J^{n+1} \right]^T \quad (3.20)$$

where J is the total number of nodes on Γ_q . In order to determine the vector $\tilde{\mathbf{q}}^{n+1}$, we assume that instantaneous time-varying temperature measurement, $\tilde{\mathbf{Y}}^{n+1}$, are available at I measurement sites nodes

$$\tilde{\mathbf{Y}}^{n+1} = \left[\tilde{Y}_1^{n+1}, \tilde{Y}_2^{n+1}, \dots, \tilde{Y}_I^{n+1} \right]^T \quad (3.21)$$

where I is the total number of nodes on the measurement site. The objective of the IHCP is to estimate the surface heat flux at the quenched site using the measurement site temperature data. Assume that $\tilde{\Theta}^{n+1}$ is the calculated temperature vector using inverse FEM at the I measurement site nodes. Therefore the instantaneous error norm is defined by Ling et al. [74] as

$$S = (\tilde{\mathbf{Y}}^{n+1} - \tilde{\Theta}^{n+1})^T (\tilde{\mathbf{Y}}^{n+1} - \tilde{\Theta}^{n+1}) \quad (3.22)$$

Using a non-iterative technique proposed by Linge et al. [74] while minimizing the error norm with respect to the surface heat flux ($\partial S / \partial \tilde{\mathbf{q}} = 0$, called a *matrix normal equation*), yields the *sensitivity coefficient matrix* $\tilde{\mathbf{X}}$ as in Ling et al. [74]

$$\tilde{\mathbf{X}}_{ij} = \frac{\partial \tilde{\theta}_i^{n+1}}{\partial \tilde{q}_j^{n+1}} \quad (3.23)$$

where superscript on $\tilde{\mathbf{X}}_{ij}$ is suppressed. Exploiting the advantage of FEM, the force vector as mentioned in equations 3.18 and 3.19 is modified as in Ling et al. [74]

$$\mathbf{f}^{n+1} = \tilde{\mathbf{D}} \tilde{\mathbf{q}}^{n+1} + \mathbf{c} \quad (3.24)$$

where \mathbf{c} is determined by the known temperature distribution on Γ_θ and $\tilde{D}_{Pj} = \partial f_p^{n+1} / \partial \tilde{q}_j^{n+1}$, is a constant matrix of dimension $N \times J \cdot N$ is the total number of nodes

on $\tilde{\Omega}$, P is the global node number. From the DHCP (Eq.(3.18)), the temperature vector is rewritten as in Ling et al. [74]

$$\Theta^{n+1} = \psi^n + \Delta t \mathbf{U} \mathbf{f}^{n+1} \quad (3.25)$$

ψ^n and \mathbf{U} in eq.3.25 are given in Ling et al.[74] as

$$\mathbf{U} = (\mathbf{M} + \Delta t \mathbf{K})^{-1} \quad (3.26)$$

$$\psi^n = \mathbf{U} \mathbf{M} \Theta^n$$

Substituting Eq.(3.24) in Eq.(3.25), the measurement site calculated temperature vector $\tilde{\Theta}^{n+1}$ is given as in Ling et al. [74]

$$\tilde{\Theta}^{n+1} = \tilde{\psi}^n + \Delta t \tilde{\mathbf{U}} [\tilde{\mathbf{D}} \tilde{\mathbf{q}}^{n+1} + \mathbf{c}] \quad (3.27)$$

where $\tilde{U}_{iP} = U_{GP}$ and $\tilde{\psi}_i^n = \psi_G^n$ are mapped from the global nodes to the nodes on the quenched boundary Γ_q . The sensitivity coefficient matrix is explicitly rewritten from Eq.(3.23) and Eq.(3.27) as,

$$\tilde{\mathbf{X}}^{n+1} = \Delta t \tilde{\mathbf{U}} \tilde{\mathbf{D}} \quad (3.28)$$

Finally, from minimization of error norm, the unknown surface heat flux is given as

$$\tilde{\mathbf{q}}^{n+1} = (\tilde{\mathbf{X}}^T \tilde{\mathbf{X}})^{-1} \tilde{\mathbf{X}}^T (\tilde{\mathbf{Y}}^{n+1} - \tilde{\psi}^n - \Delta t \tilde{\mathbf{U}} \mathbf{c}) \quad (3.29)$$

The inverse solution algorithm is summarized as follows:(i) Θ^n , \mathbf{M} , \mathbf{K} , \mathbf{c} are known from previous time step. $\tilde{\mathbf{Y}}^{n+1}$ is the known current experimental temperature vector. Using these quantities, $\tilde{\mathbf{q}}^{n+1}$ can be determined from Eq. (3.29). (ii) Force vector \mathbf{f}^{n+1} has to be determined using the current $\tilde{\mathbf{q}}^{n+1}$ according to the relation given in Eq.(3.24). (iii) Global temperature vector Θ^{n+1} can be determined by substituting \mathbf{f}^{n+1} in Eq. (3.25).

3.9 High speed photography

Wetting front velocity is a physical quantity which gives us idea about the propagation of maximum heat flux position. Two methodologies were worked out to calculate or to measure the wetting front velocity i.e.

1. by calculating the propagation of maximum heat flux using two dimensional analysis of solving inverse heat conduction problem
2. by measuring the wetting front velocity using real images at different times with accurate scaling using high speed camera

High speed camera is a device used for recording fast moving objects as a photographic image(s) onto a storage media. After recording, the images stored on the media can be played back in slow motion. A normal motion picture camera is filmed and played back at 24 frames per second, while television uses 25 frames/s. High speed cameras can film up to a quarter of million frames a second by running the film over rotating prism or mirror instead using shutter, thus reducing the need for stopping and starting the film behind a shutter which would tear the film stock at such speeds. The fastest camera are generally in use in scientific research, military test and evaluation, and industry. An example of an industrial application is crash testing to better document the crash and what happens to the automobile and passengers during a crash. A problem for high speed cameras is the needed exposure for the film, so one needs very bright light to be able to film at forty thousands frames per second sometimes leading to the subject of examination being destroyed because of the heat of the lighting.

The camera which was used for the visualization of wetting front phenomena was High-SpeedStar 6 made by *La Vision* as shown in figure 3.24. Nickel, inconel 600 and AA2024 sheets and discs were quenched by atomized spray and water jets with different flow parameters and visualized by high speed camera. This camera has different options of size of screen and frequency. Images can be captured at maximum frequency of 5400 frames/sec, when the screen resolution is selected as 1024×1024 pixels. Similarly, for the screen size of 512×512 pixels, the maximum frequency would be 16000 frames/sec. However, the maximum frequency for this camera is 150 kHz. As the frequency of measurement increases, more intense lighting is required for illuminating the subject properly. Minimum inter-frame time is $4.8 \mu\text{s}$ and pixel size is $20 \mu\text{m} \times 20 \mu\text{m}$. A software is used for data acquisition and visualization of captured or saved images named as *DaVis 7*. This arrangement is equipped with scaling the subject being analyzed to the real dimensional coordinates. Using this provision, first the disc or rectangular sheet is scaled on the screen to the actual dimensions and then the high speed movie is made with a selected frequency of frames/sec, exposure time and exposure time in the presence of high intensity lights. Once the images are saved, the position of wetting front is related to real dimensions and its change is noted with respect to time which is wetting front velocity. The results from these experiments are shown in chapter 4.

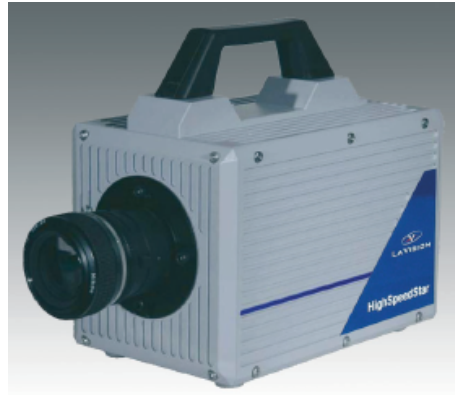


Figure 3.24: High speed camera [Courtesy: La Vision]

3.10 Composition of industrial casting water

Water quality of cooling water used for quenching during solidification of non-ferrous metals is a subject of research interest. During this work, different salts e.g. NaCl , Na_2SO_4 , MgSO_4 , NaHCO_3 , Na_2CO_3 , $\text{Na}_2\text{B}_4\text{O}_7 \cdot 10\text{H}_2\text{O}$ (Borax), CaCO_3 etc are dissolved in cooling water in different concentrations and the effect was analyzed during spray quenching. Similarly, the influence of surfactant and dissolved CO_2 is examined. However, it is very important to know the real typical composition of cooling water that actually used in cast houses of non-ferrous metals. Typical compositions of such water are given in table 3.3. It is noteworthy that concentration of ingredients are relatively lower in real cooling water as compared to that used in our experiments. The primary purpose of this experimental work is to show the influence of individual ingredient separately by keeping a relatively higher concentration and also to investigate that which ingredient influence the rate of heat transfer most. If the ingredients are dissolved in the same lower concentrations in experiment's cooling water solutions as that in actual industrial water, the results would be difficult to compare and even then the results would not close to the reality because in real water, ingredients are present in combination not individual.

Table 3.3: Example composition of cooling water in cast-house of copper and aluminum

Ingredient (concentration)	Cu-cast water		Al-cast water	
	Sample A	Sample B	Sample A	Sample B
pH	8.6	8.5	7.6	7.93
Total alkalinity (mmol/lit)	1.81	2.55	1.6	–
PO ₄ ⁻³ (mg/lit)	0.4	0.6	<0.2	0.12
P Total (mg/lit)	2.2	0.8	–	–
Cl ⁻¹ (mg/lit)	69	97	6.3	145.33
SO ₄ ⁻² (mg/lit)	31	47	8.5	288.33
NO ₃ ⁻¹ (mg/lit)	37	44	22.5	<0.5
Ca ⁺² (mg/lit)	46	66	81 15.3	105.67 11.13
Mg ⁺² (mg/lit)	16	22	–	–
Fe ^{+2/+3} (mg/lit)	0.2	0.1	<0.01	1.77
Na ⁺¹ (mg/lit)	193	101	–	–
Borax (mg/lit)	596.1	177	–	–
Total hardness (mg/lit)	–	–	15	17.4
Zn ⁺² (mg/lit)	–	–	0.01	0.07
Elec. conductivity (μS/cm)	965	826	480	1403

4 Spray Quenching & Influence of Water Quality

4.1 Introduction

This chapter deals with the results regarding spray quenching and the influence of addition of different chemical in cooling water on spray quenching of various metals. A comparative analysis of impingement density distribution, temperature distribution and resulting heat transfer coefficients of pneumatic and hydraulic spray is presented for different flow rates and materials. The dependence of heat transfer on impingement density is discussed for pneumatic spray. The effect of addition of salts, surfactant, mixture of salts and surfactant, gases and oil in cooling water on temperature profiles and heat flux at specific positions on metal surface for spray quenching is discussed in detail.

4.2 Comparison of pneumatic atomizing & hydraulic full cone nozzle

The mass of water crossing a unit area perpendicular to the axis of spray in unit time is known as *impingement density*. The impingement density distribution is specific to the certain distance between the metal surface and the nozzle outlet. Both are inversely proportional. As this distance z increases, the impingement density decreases. The recommended distance for Pneumatic nozzle was $z = 150 \text{ mm}$, that is why, all experiments with this nozzle have been performed keeping this distance between metal surface and nozzle. In order to compare the impingement densities of the two nozzles i.e. pneumatic and hydraulic nozzle, the diameter of the circle of the cone at the metal surface should be equal. Since the cone angle of the two nozzles are 20° and 45° respectively, the distance z should be lower for the case of Hydraulic nozzle because of its higher cone angle i.e. 45° which can be calculated in the following way:

$$\tan\theta = \frac{x}{z}$$

$$x = z_1 \tan\theta_1 = z_2 \tan\theta_2$$

$$z_2 = \frac{z_1 \tan\theta_1}{\tan\theta_2}$$

$$z_1 = 150 \text{ mm} \quad \theta_1 = 10^\circ \quad \theta_2 = 22.5^\circ$$

$$z_2 = 64 \text{ mm (for hydraulic nozzle)}$$

The operating parameters of Hydraulic full cone nozzle and Pneumatic atomizing nozzle are tabulated in table 4.1. Impingement density for hydraulic full cone nozzle and pneumatic atomizing nozzle is measured using a patternator along the axis perpendicular to the axis of spray cone at a distance of 64 and 150 mm respectively. The impingement density distributions are shown in figures 4.1 and 4.2. Figure 4.1 depicts that impingement density is distributed symmetrical around the axis of cone and distributed normally. The value of impingement density distribution (IDD) is proportional to the amount of water flow at the inlet keeping the air pressure constant. On the other hand, IDD is non-symmetric for hydraulic full cone nozzle as illustrated in figure 4.2. In this figure, IDD is measured for three different water flow rates i.e. 20, 25 and 30 l/h. IDD found to be symmetric around the axis of spray only if the flow rate is 20 l/h. That is why, the experiments for analyzing the effect of water quality on heat transfer during spray quenching have been performed for this flow rate for hydraulic full cone nozzle.

Table 4.1: Operating parameters of two types of nozzles

Type of nozzle	Cone angle	Nozzle-Surface distance (mm)	Water flow rate (l/h)	Air pressure (bar)
Hydraulic nozzle	45°	64	20	—
Pneumatic atomizer	20°	150	25	3

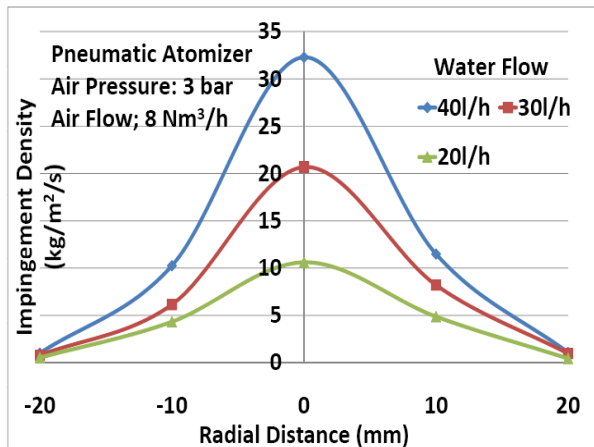


Figure 4.1: Impingement density distribution for pneumatic atomizing nozzle for varying water flow

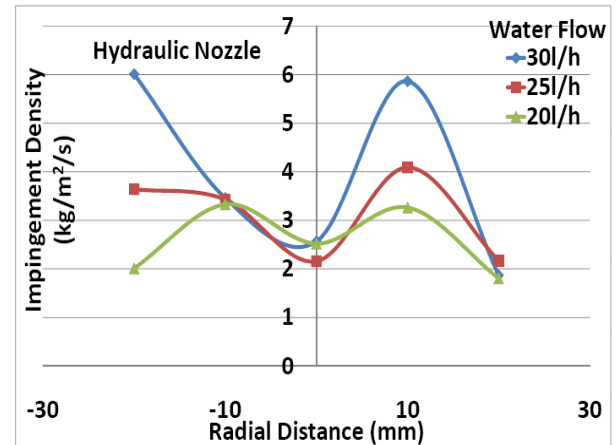


Figure 4.2: Impingement density distribution for hydraulic full cone nozzle for varying water flow

Temperature profiles for pneumatic and hydraulic nozzles are drawn in figure 4.3 while heat transfer coefficient with respect to surface temperature within film boiling region is drawn in figure 4.4. The heat transfer coefficient is approximately 10 times higher for pneumatic nozzle ($7000 \text{ W/m}^2/\text{K}$) than for hydraulic nozzle ($700 \text{ W/m}^2/\text{K}$). Similarly, when it takes 14 seconds to quench the center of the nickel disc from 600°C to 50°C with

hydraulic nozzle, pneumatic nozzle quench it in only half second. Though, the water flow has strong influence on heat transfer, the effect of air flow enhances the heat transfer to an order of magnitude. Air helps in producing the relatively fine particle and moving them with higher velocity. These two effects are the main causes of such enhancement of heat transfer for pneumatic atomizing nozzle. In order to analyze the effect of kind of metal on heat transfer during spray quenching by hydraulic full cone nozzle, discs made up of nickel and aluminum alloy AA6082 are quenched. Since the melting point of nickel is 1400 °C which is much higher than that of AA6082 (580 °C), the initial temperature are kept different as shown in figures 4.5 and 4.6. These two figures exhibit one similarity for the two material and that is Leidenfrost temperature which lies at approximately at 240 °C for the center of the disc. It can be inferred from these results that value of Leidenfrost temperature depends on the method of quenching and material properties but in case of nickel and aluminum the heat penetration coefficient ($\sqrt{\lambda\rho c_p}$) are same and that is why the leidenfrost value appears to be similar for these two kinds of metals. Although, the average heat transfer coefficient within the film boiling region lies within the same range i.e. 500 to 600 W/m²/K, it shows a slight dependence on the surface temperature for AA6082. The heat transfer coefficient measured for hydraulic spray can also be verified with that reported in the literature. Referring to figure 4.7, a water spray of impingement density of 3 kg/m²/s (figure 4.2) or 180 kg/m²/min should correspond to the heat transfer coefficient of 600 W/m²/K. Hence, the relation between HTC and impingement density is found to be in accordance with that proposed by Jeschar et al.[1]. Initial surface temperature of the

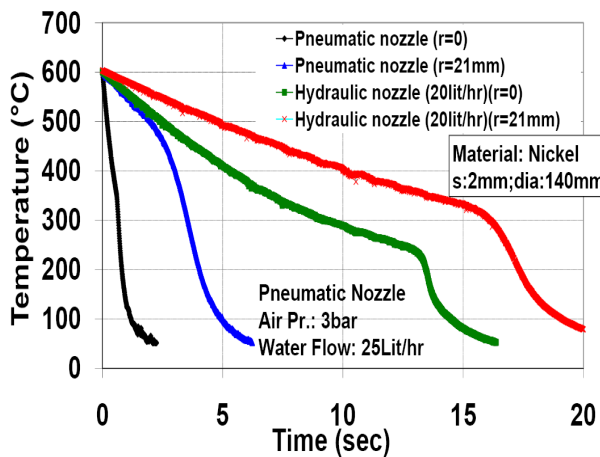


Figure 4.3: Temperature profiles of hydraulic & pneumatic nozzle

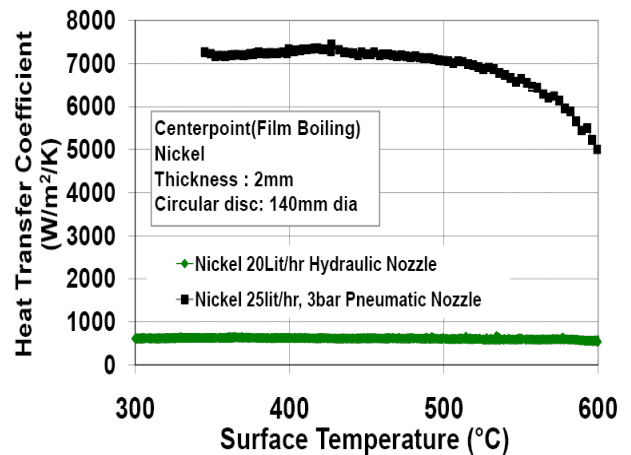


Figure 4.4: Heat transfer coefficient vs temperature for two nozzles

metal surface to be quenched is also an issue which should be addressed. For analyzing this effect, a circular nickel disc of 2 mm thickness and 140 mm diameter is quenched from 700 °C, 600 °C, 500 °C and 400 °C approximate initial surface temperatures by hydraulic full cone nozzle with a water flow of 20 l/h. The variation of temperature with time and the relation between heat transfer coefficient and surface temperature are drawn figures 4.8 and 4.9. It is evident from the two figures that leidenfrost temperature changes from 240 to 270 °C for the four cases of different initial temperatures. Temperature profiles are almost parallel to each other. However, heat transfer coefficient within film boiling region seems to be influenced by initial temperature. For initial surface temperatures of 700 °C,

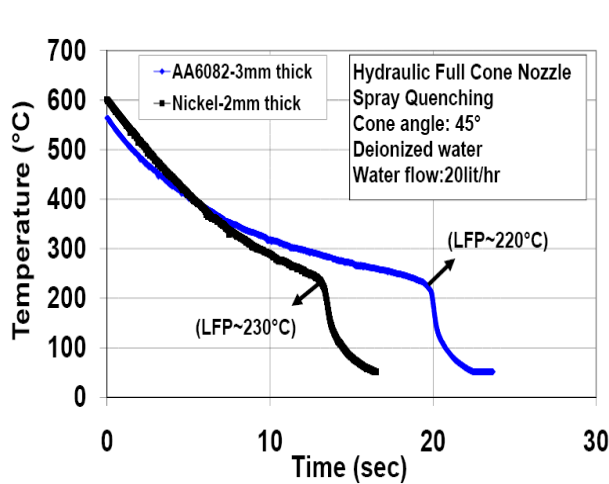


Figure 4.5: Temperature profiles for two different materials at center point of disc

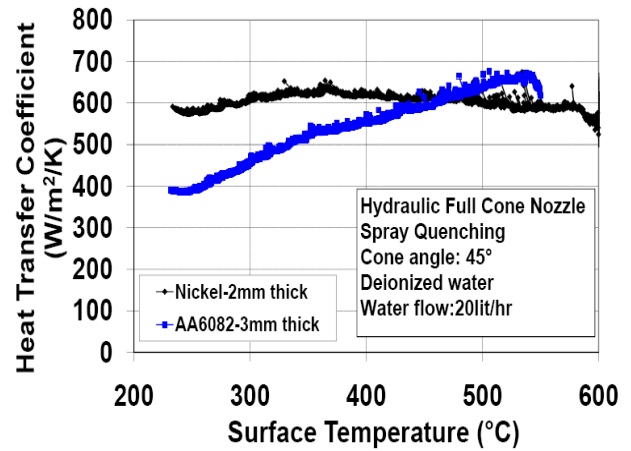


Figure 4.6: Heat transfer coefficient vs temperature for two different materials at center point of disc

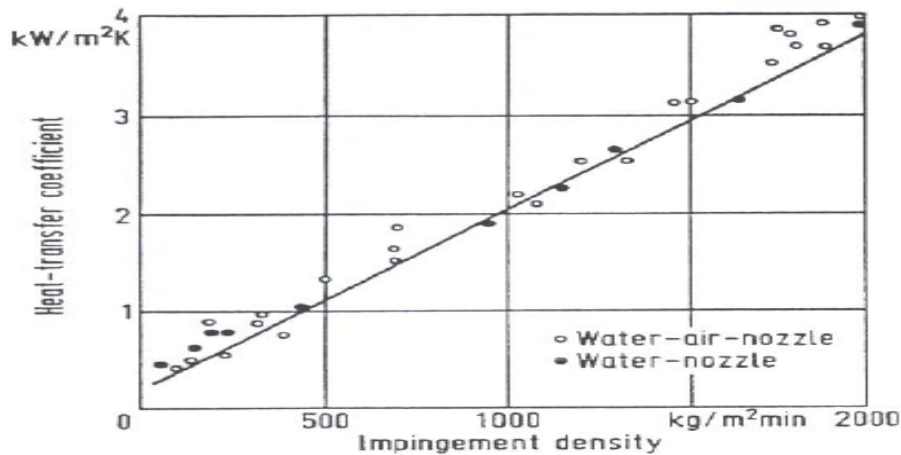


Figure 4.7: Heat transfer coefficient in the range of film boiling for spray quenching with water as a function of impingement density [Jeschar et al.]

600 °C, 500 °C and 400 °C, corresponding HTC are 720, 900, 1000 and 1100 W/m²/K respectively. So, the HTC inversely relates to the surface initial temperature within film boiling region.

It is also an issue of interest in spray quenching technique that how the temperature is distributed along the diameter of spray cone at the metal surface at different intervals of time in case of different material. The trends of temperature distribution are illustrated in figures 4.10, 4.11, 4.12 and 4.13. As the impingement density is the primary influencing parameter on heat transfer, the temperature values are also distributed relative to the impingement density distribution i.e. temperature is reduced faster at the center of the spray and the cooling rate becomes slower as the radius increases. It is noteworthy that temperature distribution curve for pneumatic atomizing nozzle is a mirror image of impingement density distribution for the same type of nozzle in figure 4.1. The temperature distribution for pneumatic nozzle is more symmetrical around the center as compared to hydraulic nozzle. When comparing hydraulic nozzle with pneumatic nozzle, the temperature differ-

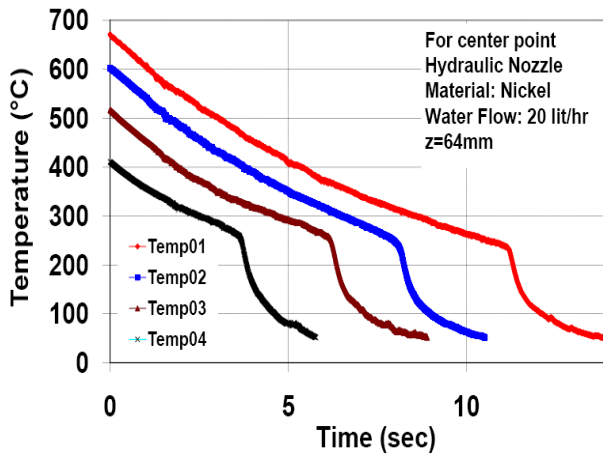


Figure 4.8: Temperature profiles with respect to initial surface temperature

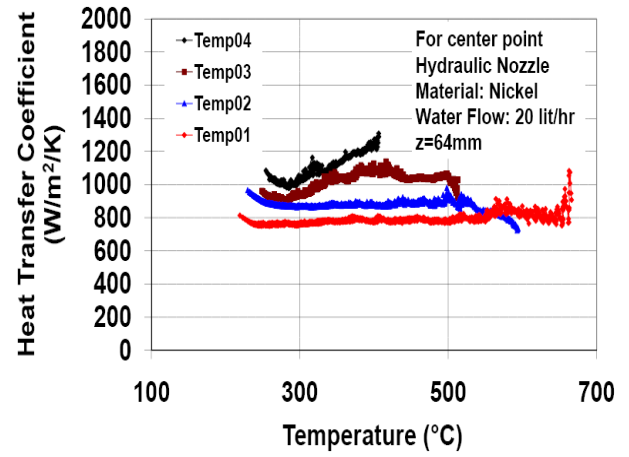


Figure 4.9: HTC VS temperature with respect to initial surface temperature

ence between center and circumference is much lower for the case of hydraulic nozzle than pneumatic nozzle. Similarly, when temperature distribution of nickel and aluminum alloys are compared, the temperature difference between center and circumference is higher in case of nickel and the reason could be the lower thermal conductivity of nickel than aluminum alloy AA6082 or AA2024 ($91 \text{ W/m/K} < 150 \text{ W/m/K}$ or 177 W/m/K).

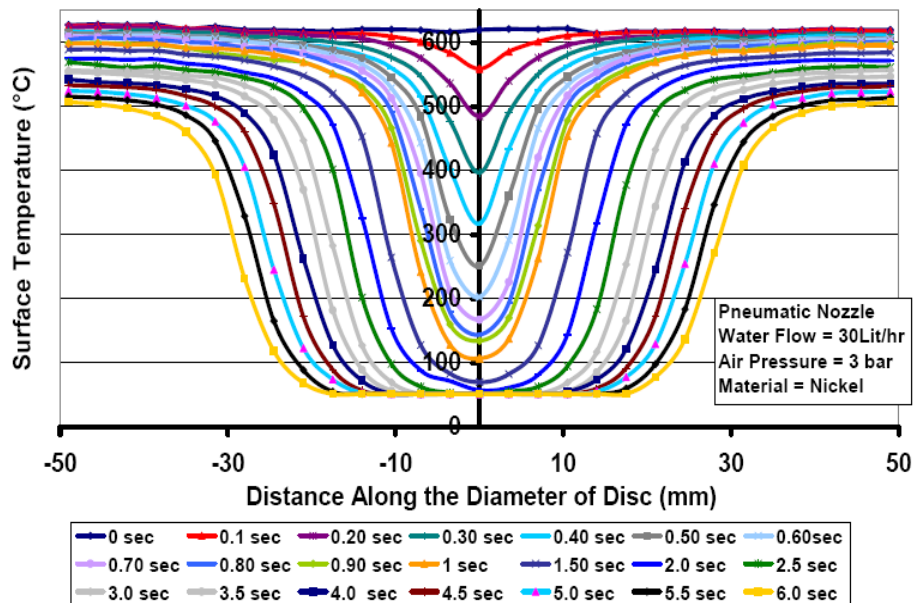


Figure 4.10: Temperature distribution along the diameter of the nickel disc for pneumatic nozzle

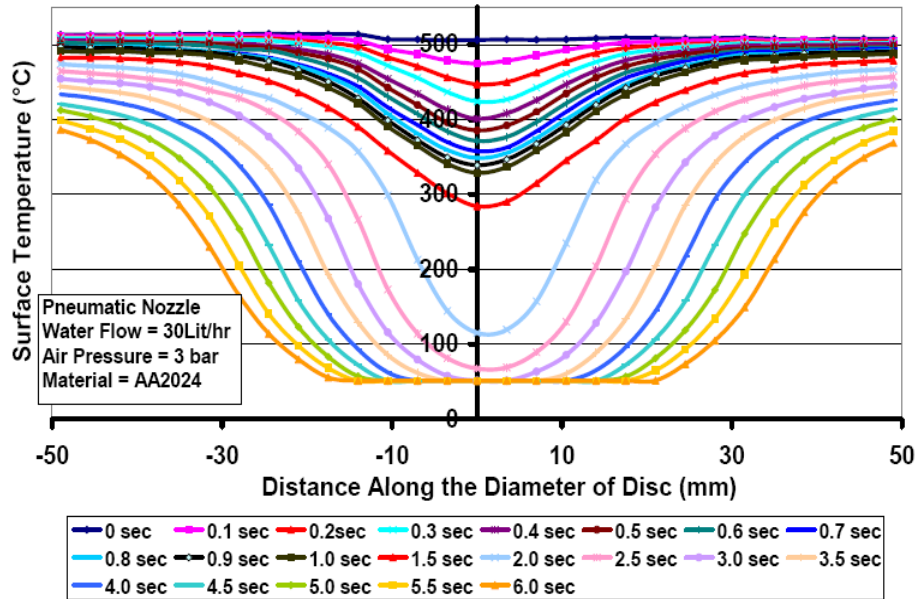


Figure 4.11: Temperature distribution along the diameter of the AA2024 disc for pneumatic nozzle

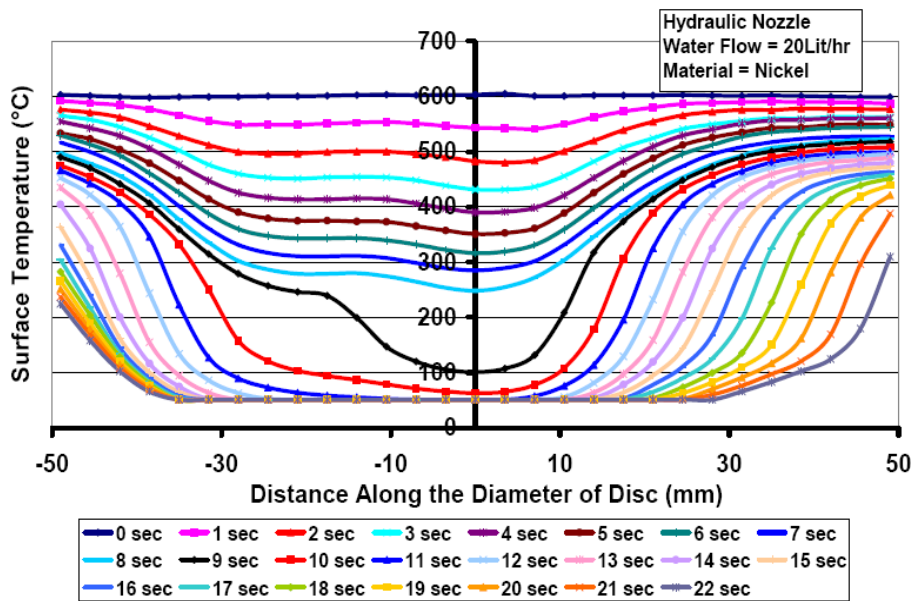


Figure 4.12: Temperature distribution along the diameter of the nickel disc for hydraulic nozzle

4.3 Influence of impingement density on heat transfer in atomized spray quenching

As we already know that atomized spray is generated by a pneumatic atomizing nozzle. Air at a certain pressure and liquid at a certain flow rate are supplied to the nozzle which generates spray of discrete fine droplets moving at very high speed. The impingement density varies with air pressure, water flow rate and also with the radius of spray cone. Impingement density is the most influential parameter on which heat removal during cooling

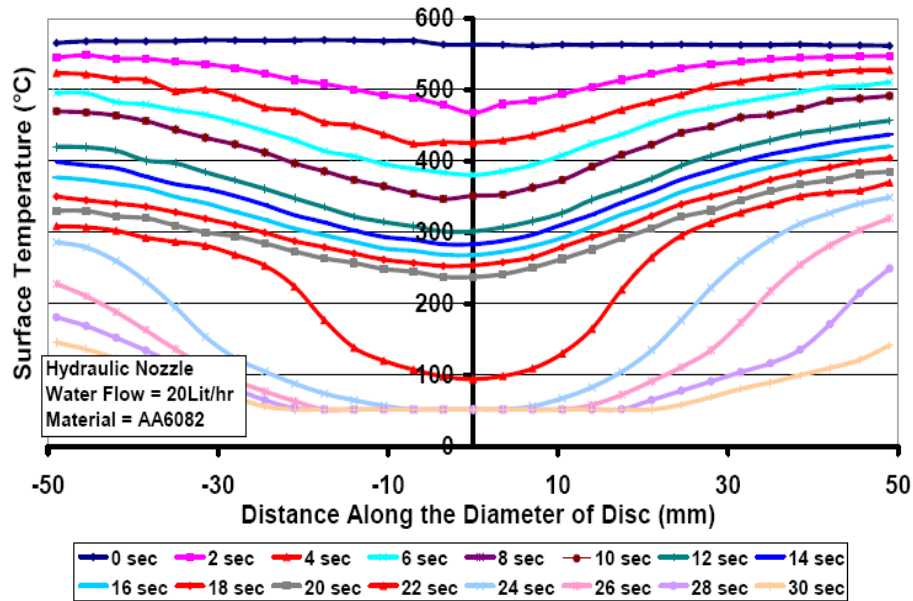


Figure 4.13: Temperature distribution along the diameter of the AA6082 disc for hydraulic nozzle

depends. A series of experiments was performed using nickel, AA2024 and inconel discs for analyzing the influence of impingement density with three different parameters of air pressure and water flow as illustrated in table 4.2. Impingement density at pressure of 3 bar was measured by patternator and it is shown previously in figure 4.1. It was tried to measure the impingement density at the air pressure of 4 bar, but the results were not accurate with the available patternator because high air pressure results in splashing of water outside the patternator's collecting bottles. This is the reason why it is mentioned as unknown in figures and table 4.2. However, the impingement density distribution along the radius with air pressure of 2 bar with 3 water flow is also presented in figure 4.14. It is obvious from the figures 4.1 & 4.14 that impingement density directly depends on water flow keeping the air pressure constant and the distribution is normal. Temperature profiles at the

Table 4.2: Operating parameters for analyzing impingement density influence

Material	Air pressure (bar)	Water flow (l/h)	Impingement density at center (kg/m ² /s)	Furnace temperature (°C)
Nickel & Inconel	3	30	21	620
	3	40	32	620
	4	40	>32	620
AA2024	3	30	21	520
	3	40	32	520
	4	40	>32	520

center of the spray and at the radial distance of 15 mm from the center are drawn for three different flow parameters of air pressure and water flow for nickel and AA2024 in figures 4.15 and 4.16. The cooling rate is not only a function of radius but also a function of the impingement density at that position. The more the impingement density at a specific point

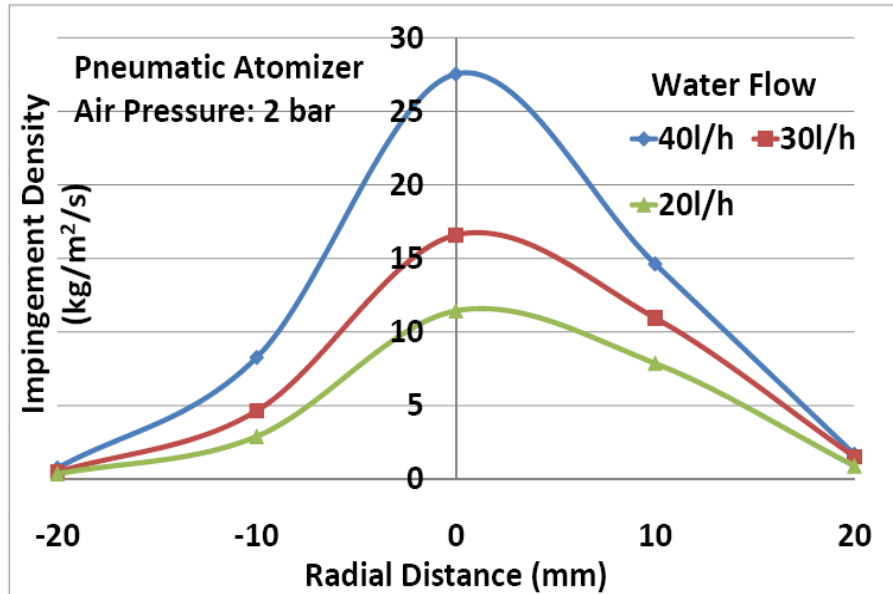


Figure 4.14: Impingement density distribution along radius at air pressure of 2 bar

is the faster is the cooling at that point. It is noteworthy that leidenfrost point also depends on the radial position. For example in figure 4.15, it moves from 300 to ~ 400 °C corresponding to the position of center and 15 mm radial distance for nickel at 4 bar air pressure and 40 l/h water flow. Similar effect can be noticed for AA2024 in figure 4.16. This effect depicts that the Leidenfrost point value is also a function of impingement density for a given spraying method and kind of metal for the case of atomized spray quenching. It is a well known fact that the method of deposition of coolant on metal surface influences the value of LFP. Heat transfer coefficient (HTC)-Surface temperature curves are plotted for nickel within film boiling region for three impingement densities at center and at the radius of 15 mm in figures 4.17 & 4.18 respectively using one dimensional analysis. For impingement density of 21 kg/m²/s, the average HTC in film boiling is 4200 W/m²/K, while for that of 32 kg/m²/s, it is 4700 W/m²/K and similarly a further increase of water flow of 40 l/h with same 4 bar pressure increased the HTC to 5700 W/m²/K. A similar effect can be noticed at the radial distance of 15 mm, where an increase of ID from 6 to 10 kg/m²/s results in increase of HTC from 1000 to 1400 W/m²/K. Similarly HTC-Surface temperature curves are also drawn for aluminium alloy AA2024 in figures 4.19 & 4.20. Although, in this case, HTC is slightly dependent on surface temperature of AA2024, impingement density shows the same characteristic effect on HTC. The HTC is independent of surface temperature at within film boiling when measured at the distance of 15 mm from center. When impingement density increases from 6.1 to 10 Kg/m²/s, HTC increases from 1000 to ~ 1200 W/m²/K. On the other hand, the LFP increases from 300 to 410 °C from center to 15 mm radial distance for AA2024.

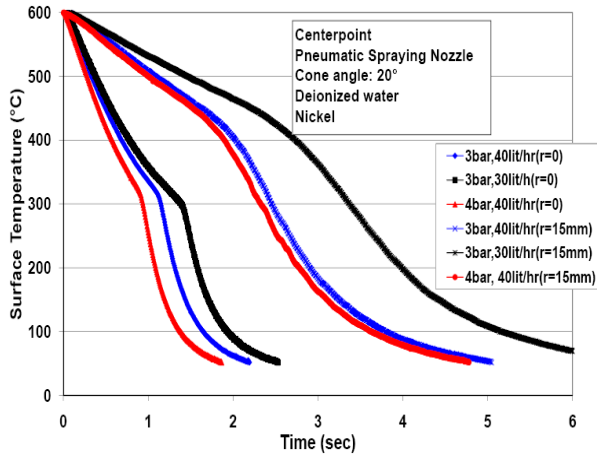


Figure 4.15: Temperature profiles for varying impingement densities at two radial positions on circular disc of nickel

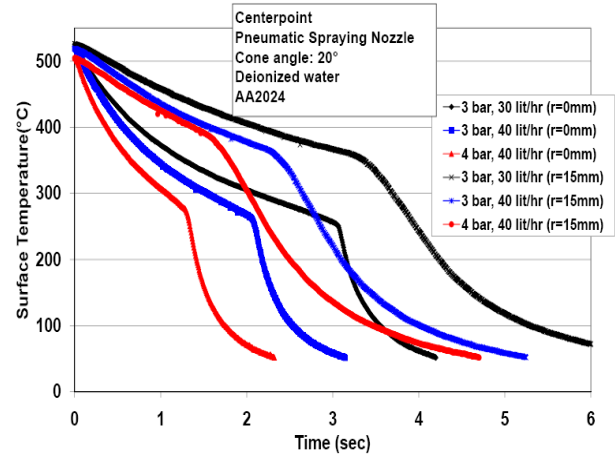


Figure 4.16: Temperature profiles for varying impingement densities at two radial positions on circular disc of AA2024

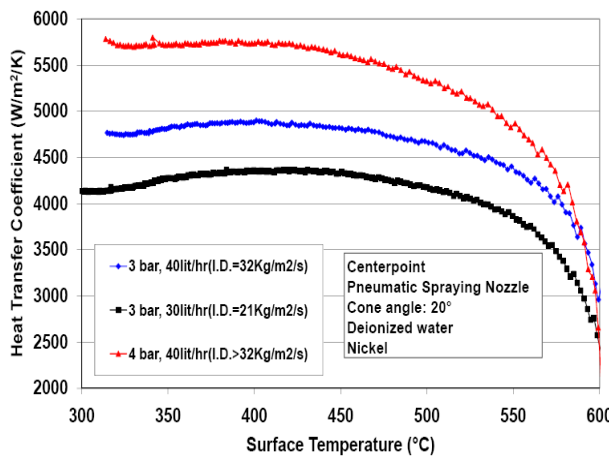


Figure 4.17: HTC-Temperature curve for varying impingement densities at center of circular disc of nickel

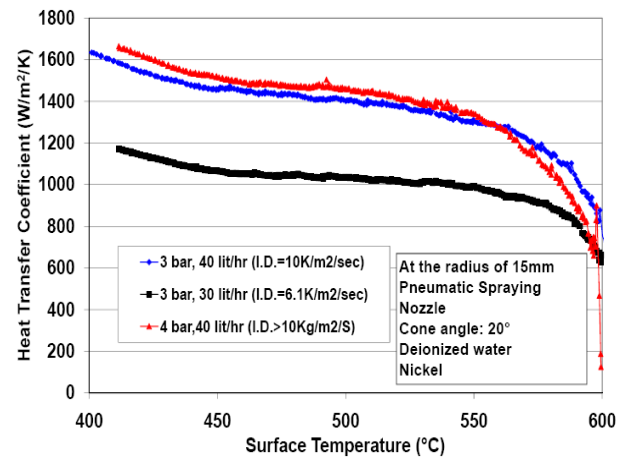


Figure 4.18: HTC-Temperature curve for varying impingement densities at radius = 15 mm on circular disc of nickel

4.4 Influence of addition of chemicals in cooling water for spray quenching

In this presented work, two methods of spray quenching have been used for analyzing the influence of water quality on heat transfer. These are atomized spray quenching and spray quenching which are carried out by pneumatic atomizing nozzle and hydraulic full cone nozzle respectively. Keeping the flow parameters constant such as water flow rate and air pressure, the water quality is altered by adding different additives in de-ionized water in different concentrations such as salts Na_2SO_4 , MgSO_4 , NaCl , NaHCO_3 , Na_2CO_3 , Borax $\text{Na}_2\text{B}_4\text{O}_7 \cdot 10\text{H}_2\text{O}$, CaCO_3 , surfactant ethoxylated ester, mixtures of salts and surfactant, gases such as air, pure oxygen and pure carbondioxide. The influence these additives on cooling phenomena which includes Leidenfrost temperature (LFP), critical heat flux (CHF), cooling time, Heat transfer coefficient (HTC) within film boiling regime, move-

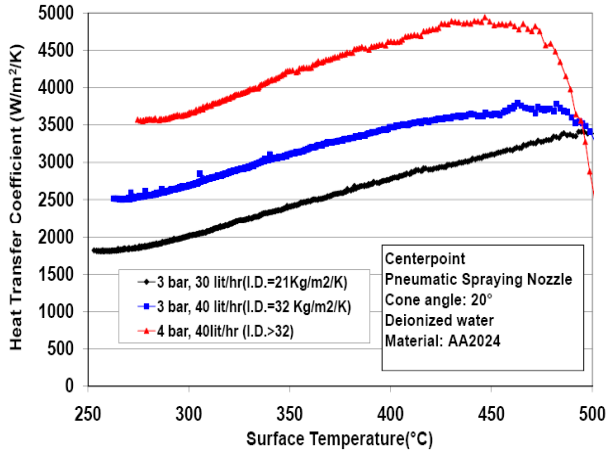


Figure 4.19: *HTC-Temperature curve for varying impingement densities at center of circular disc of AA2024*

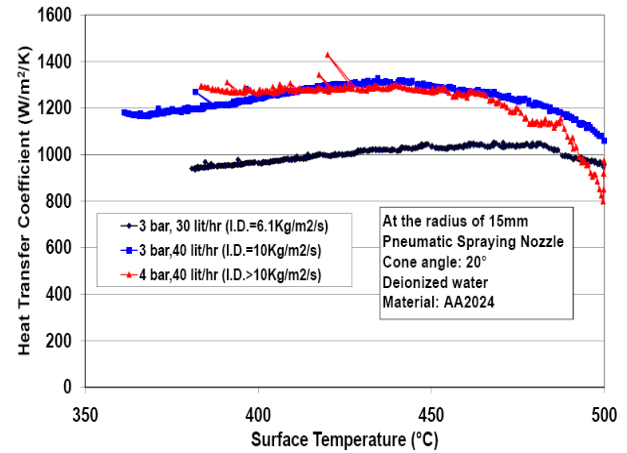
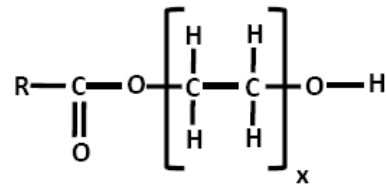


Figure 4.20: *HTC-Temperature curve for varying impingement densities at radius = 15 mm on circular disc of AA2024*

ment of wetting front has been studied. The measured values of these important features of boiling curve are summarized in table 4.3 for each specie added in cooling water. Position of maximum heat flux is regarded as the position of wetting front [27]. Ling et al. [74] non-iterative technique is used to solve the inverse heat conduction problem using MATLAB. The chemical formula of the surfactant used is:



A circular disc, made up of nickel or aluminum alloy AA6082, having geometry and material properties as given in Table 3.1, is heated to an initial temperature 600 °C approximately. Then, it is quenched by spray. Although, impingement density of the spray is the most influential parameter on heat transfer during quenching by atomized spray, it is maintained as constant by regulating constant flow of water and air. The only parameter which is altered is the concentration of additive in deionized water. Experiments also have been performed with de-ionized water for reference. Two different types of nozzles have been used with constant flow parameters as given in table 4.1. Twenty points have been selected from the center of the disc along the radius and assigned as the number of nodes for calculating the heat flux on the quenched side as shown in figure 4.21. The distance between two adjacent points is two pixels and one pixel distance 10 / 11 mm. So, a circular area of radius 45.5 mm is used for analysis. Nickel and aluminum alloy AA6082 were selected as material. Nickel can sustain at high temperature and has least tendency to be oxidized at high temperature as compared to copper. A summary of experiments carried out for analyzing influence of water quality is presented in table 4.4

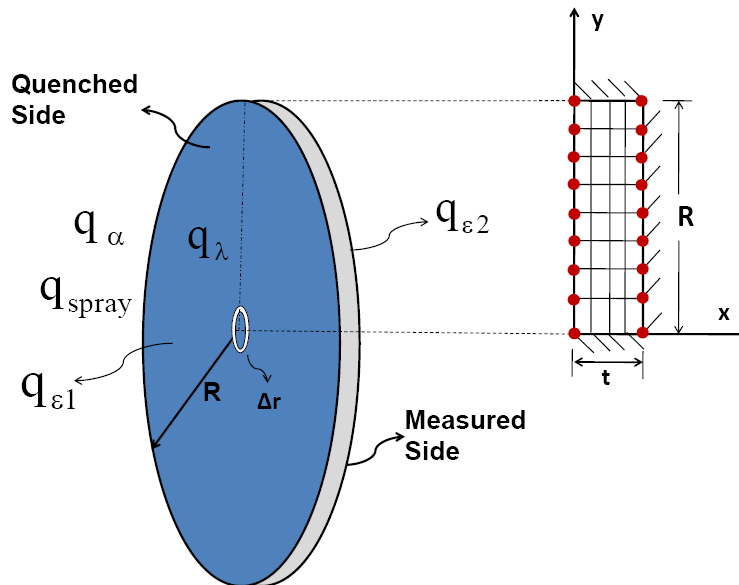


Figure 4.21: Schematic of finite element model

4.4.1 Repeatability of hydraulic spray

Before carrying out experiments for analyzing the influence of quality of water on spray quenching, it is mandatory to assess the repeatability or reproducibility of the results. The first trial for a series of experiments is to quench the metal with de-ionized water which is the reference and later the results of different water qualities are compared with this reference. The temperature profiles at three different positions on the surface of the discs are plotted for de-ionized water as coolant for three different dates of the year and shown in figures 4.22, 4.23 and 4.24 for the center of spray, at radius 17 mm and at radius 34 mm respectively. The Leidenfrost point seems to shift by 10 °C and the time to reach LFP shifts by 2 to 3 seconds. These results show that hydraulic spray is a better choice for assessing the influence of water quality on heat transfer during quenching process as compared to pneumatic spray and array of jets because hydraulic sprays show better repeatability, less variation of impingement density in radial direction, lower heat flux and absence of other fluid like air.

4.4.2 Effect of salts & their solutions

The temperature profile of the center point of the disc is plotted in figure 4.25 for deionized water and three concentrations of MgSO_4 solution. It can be analyzed from the figure that in case of pure water, Leidenfrost temperature lies at approx. 420 °C which is verified from past literature [1], but it cannot be located precisely in case of solution. LFP has increased with salt concentration which results in shortening the total time of quenching. The quenching time is decreased to 50 % from 1.2 to 0.6 seconds. A relatively stronger influence can be noticed when hydraulic spray is employed for quenching as shown in figure 4.26 for the center of the disc. The reason is that the hydraulic nozzle excludes the effect of air which is also a cooling fluid in case of pneumatic spray. A concentration of 3 g/l of MgSO_4 reduces the time of cooling from 22 to 9 second at the center of spray. The more

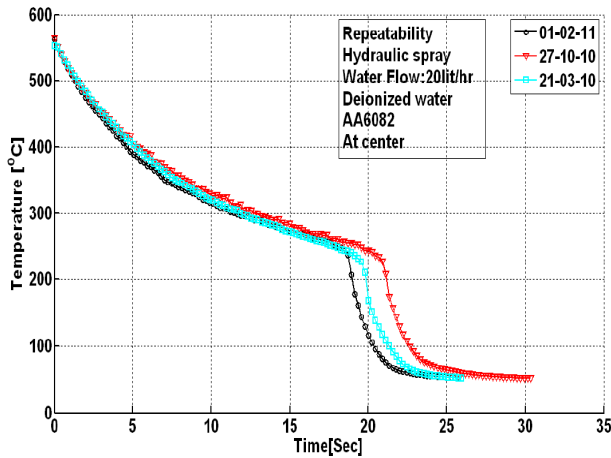


Figure 4.22: Temperature profiles for three different dates showing repeatability of hydraulic spray at center of spray

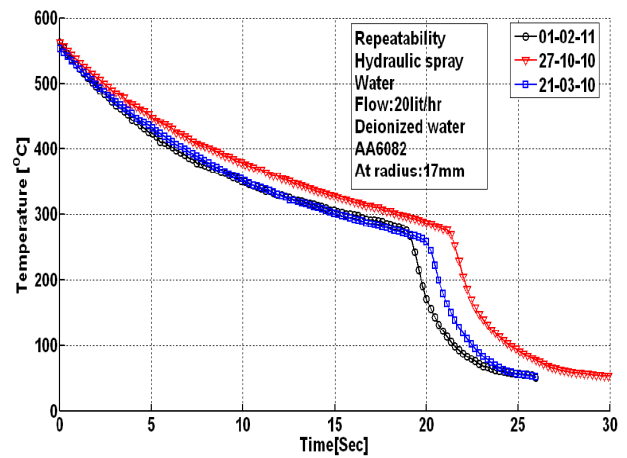


Figure 4.23: Temperature profiles for three different dates showing repeatability of hydraulic spray at radius = 17 mm

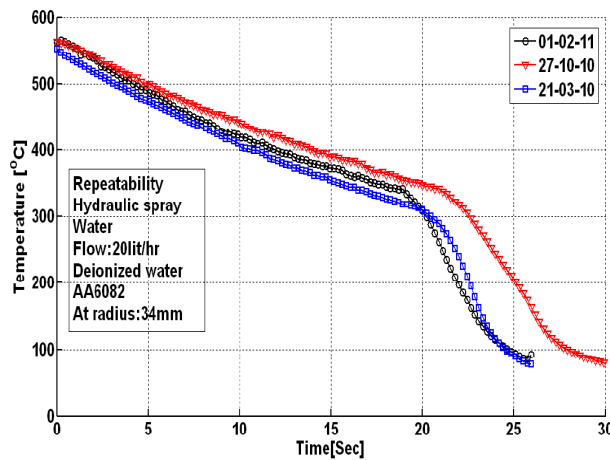


Figure 4.24: Temperature profiles for three different dates showing repeatability of hydraulic spray at radius = 34 mm

concentrated is the MgSO_4 solution, the faster is the cooling rate. Temperature profiles drawn at radius of 17 mm also show the similar effect as depicted in figure 4.27. Leidenfrost temperature is also increased for this case from 228 °C to 364 °C approximately at the center point of the disc. Boiling curve between heat flux and surface temperature is drawn in figure 4.28 for MgSO_4 solution. Presence of MgSO_4 in cooling water not only increase the heat flux in film boiling regime but also in transition and nucleate boiling. It is evident from the figure that critical heat flux increased from 1.2 to 2.17 MW/m^2 and the surface temperature corresponding to CHF (Burnout temperature) also increased from 180 °C to 220 °C when MgSO_4 solution is used as coolant for hydraulic spray. Figure 4.29 depicts that average heat transfer coefficient within film boiling region increases with increasing concentration of MgSO_4 solution in a range of 600 to 900 $\text{W/m}^2/\text{K}$. A circular area of diameter 50 pixels i.e. 45.5 mm is selected at the center of the disc and average temperature of this area is plotted versus time for all salts solution of concentration 0.5 molar. Figure 4.30 shows that MgSO_4 and Na_2SO_4 decrease the cooling time significantly. However, NaCl and NaHCO_3 did not affect to a considerable extent. Molecules of MgSO_4 and

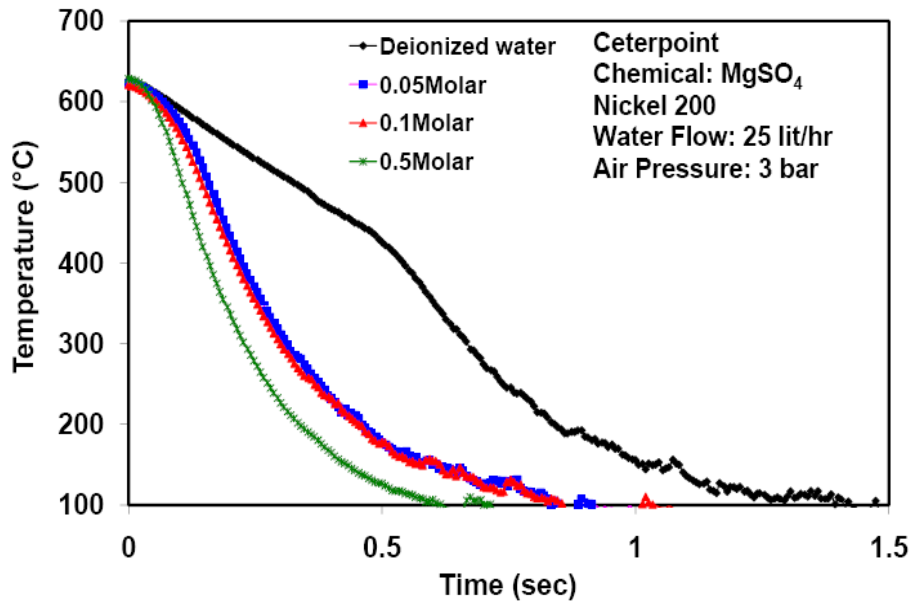


Figure 4.25: Temperature profiles for $MgSO_4$ solutions-pneumatic spray

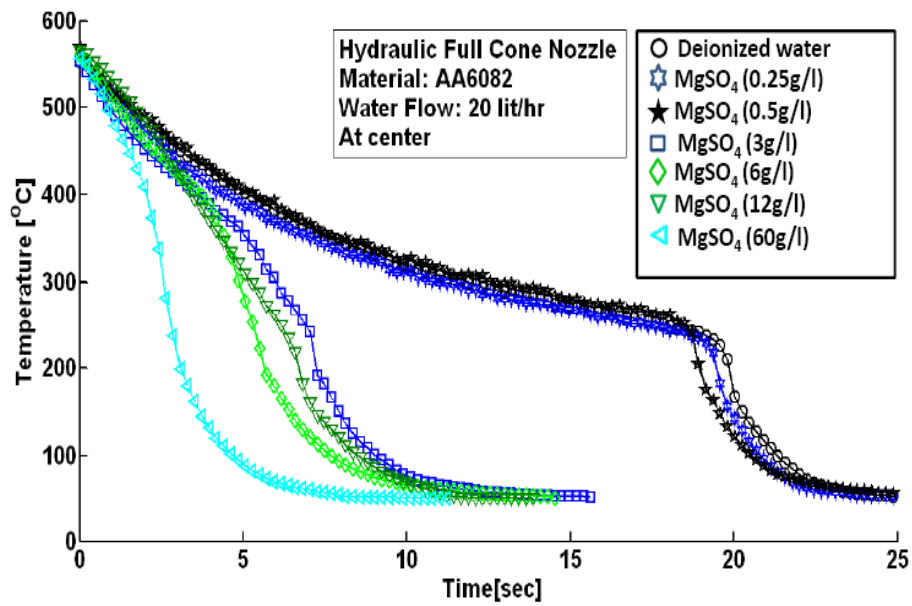


Figure 4.26: Temperature Profiles for $MgSO_4$ solutions at center of the disc-hydraulic spray

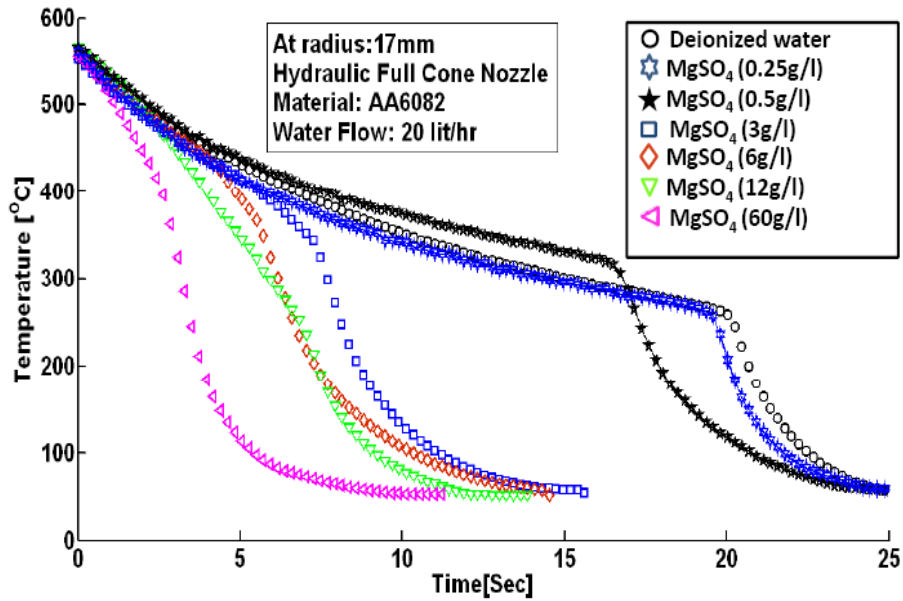


Figure 4.27: Temperature profiles for $MgSO_4$ solutions at the radius of 17 mm-hydraulic spray

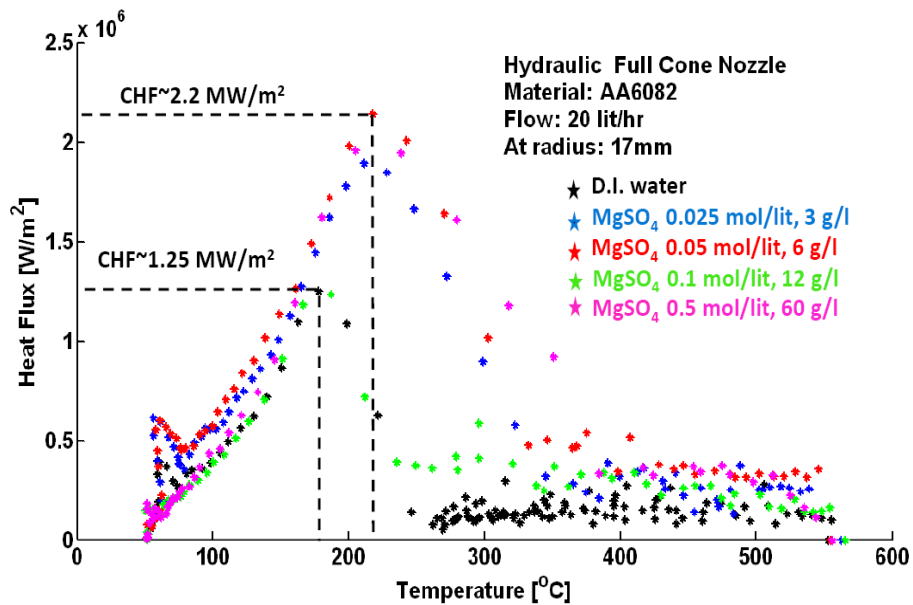


Figure 4.28: Relation between heat flux and surface temperature for $MgSO_4$ solutions-hydraulic spray

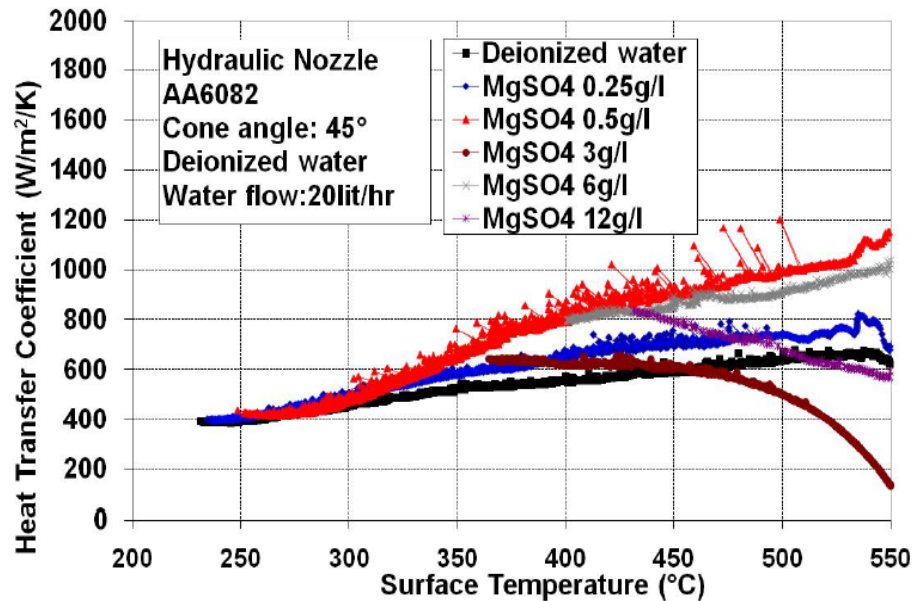


Figure 4.29: Relation between heat transfer coefficient and surface temperature for $MgSO_4$ solutions-hydraulic spray

Na_2SO_4 may precipitate faster at high temperature and deposit on the metal surface making it rougher and this surface roughness could lead to breakage of vapor film at higher temperatures. Borax ($Na_2B_4O_7 \cdot 10H_2O$) is dissolved in cooling water for secondary quenching of copper alloys. It seems to have the strongest influence on cooling as depicted in figure 4.32. As the concentration of borax is increased, the cooling rate also increases. Temperature profiles at the center of the disc show that a solution having 10 g/l of borax reduces the cooling time to half. LFP also seems to be increased with increasing concentration within a range of 228 to 384 °C. Temperature profiles at the radius of 17 mm from the center of the disc show the similar trend in figure 4.32. Curve between heat flux and surface temperature for borax solution is drawn in figure 4.33. Borax solution enhances heat flux in nucleate and transition boiling and CHF also increases from 1.2 to 1.6 MW/m^2 . Figure 4.34 gives the evidence of enhancement of HTC in film boiling region from 600 to 800 $W/m^2/K$.

Although, $CaCO_3$ solution exhibits the same trend, the influence is not much strong as shown in figures 4.35 and 4.35 for center and at radius of 17 mm respectively. $CaCO_3$ is difficult to dissolve in water. Although pulverized $CaCO_3$ is dissolved in deionized water for performing experiments, a maximum of 1 g/l concentration could be achieved with homogeneous solution. A little enhancement of heat flux in transition and nucleate boiling and also CHF can be noticed in figure 4.37. CHF is increased from 1.2 to 1.5 MW/m^2 . An enhancement from 600 to 630 $W/m^2/K$ is recorded in film boiling region for the concentration of 1 g/l.

4.4.2.1 Maximum heat flux and wetting front movement

In case of pneumatic atomizing spray, the impingement density of the spray is normally distributed in such a way that it has maximum value at the center and decreases with the radius as shown in figure 4.1. Heat flux is also distributed in similar fashion as shown in figure 4.39. Heat flux distribution is plotted with respect to radial direction at different

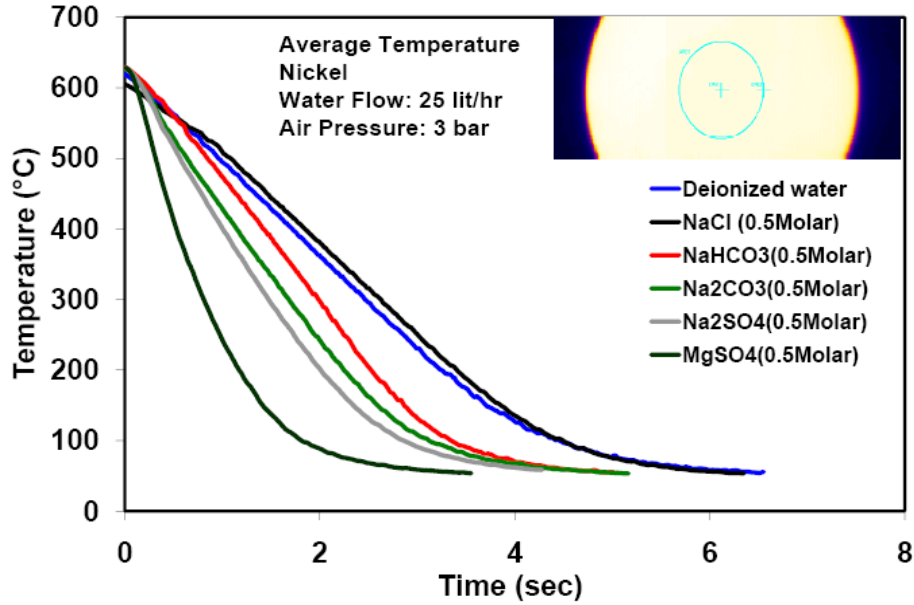


Figure 4.30: Temperature profiles of average temperature for salts solution of 0.5 molar concentration-pneumatic spray

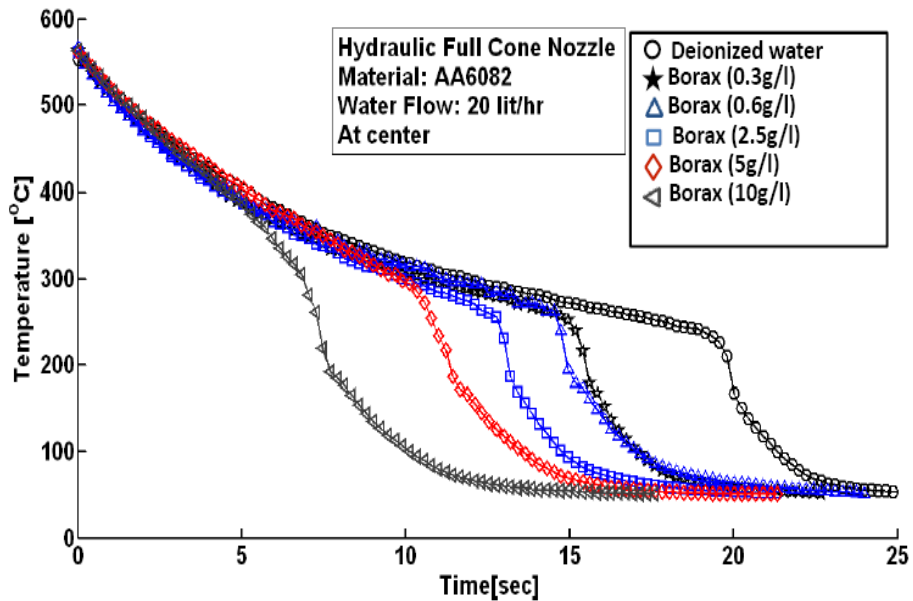


Figure 4.31: Temperature profiles for Borax solutions at center of disc-hydraulic spray

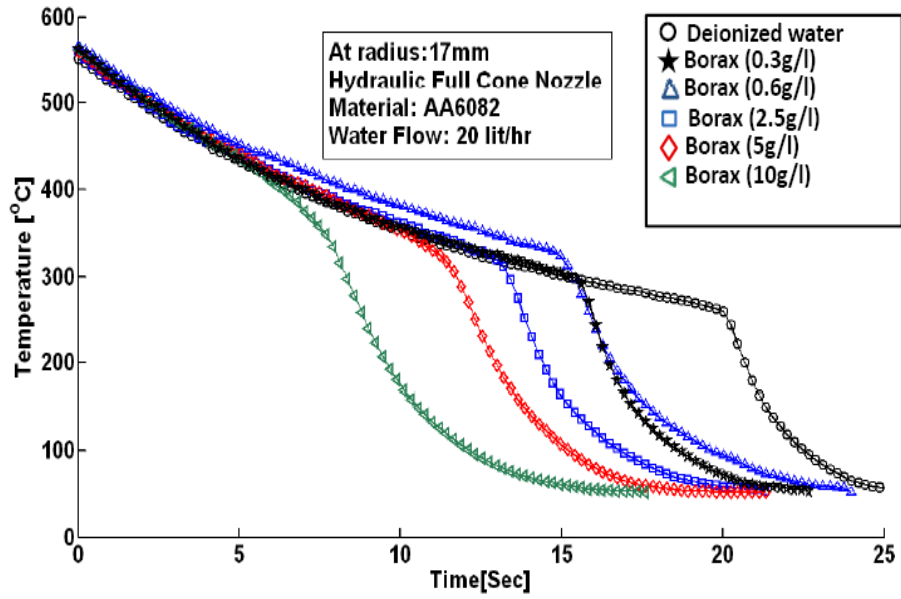


Figure 4.32: Temperature profiles for Borax solutions at the radius of 17mm-hydraulic spray

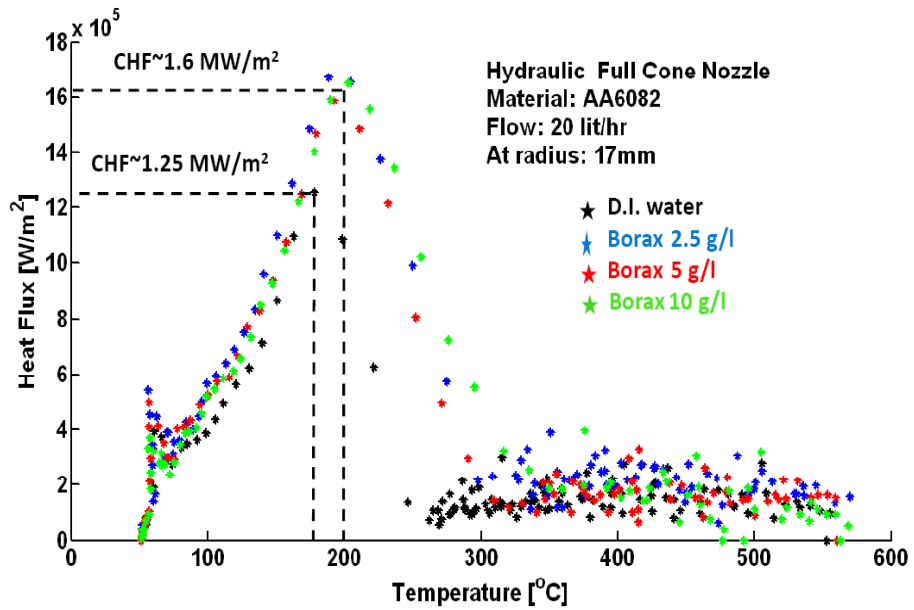


Figure 4.33: Relation between heat flux and surface temperature for borax solutions-hydraulic spray

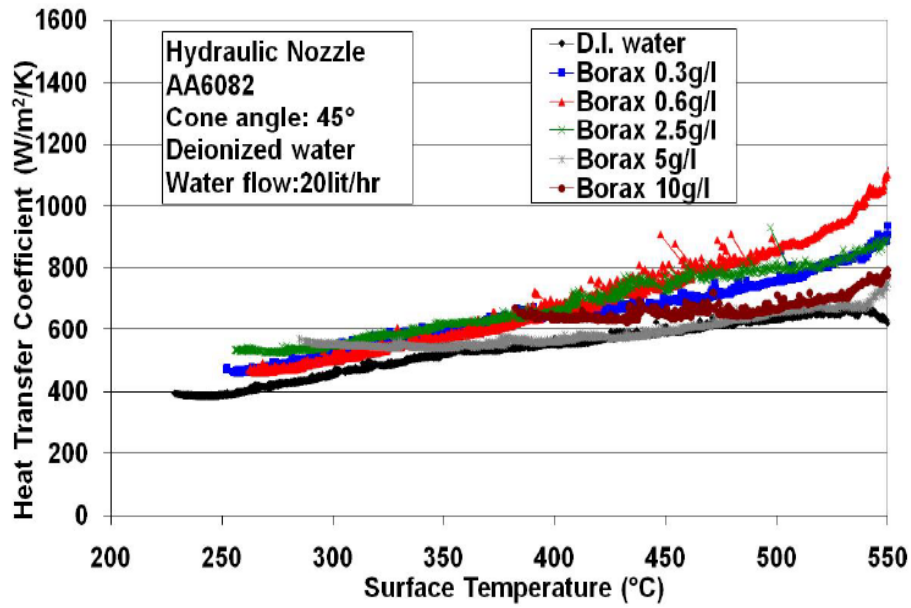


Figure 4.34: Relation between heat transfer coefficient and surface temperature for borax solutions-hydraulic spray

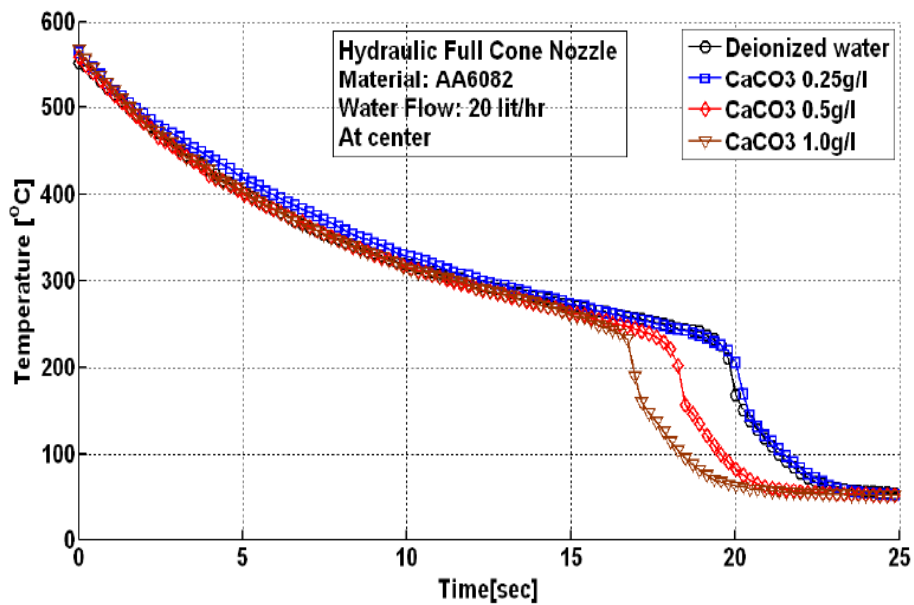


Figure 4.35: Temperature profiles for CaCO_3 solutions at at center of disc-hydraulic spray

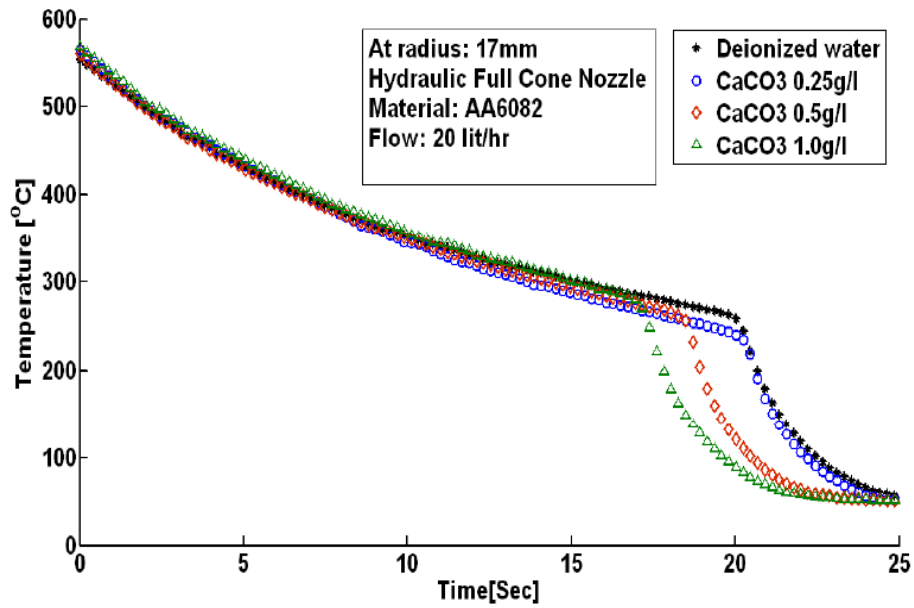


Figure 4.36: Temperature profiles for CaCO_3 solutions-hydraulic spray

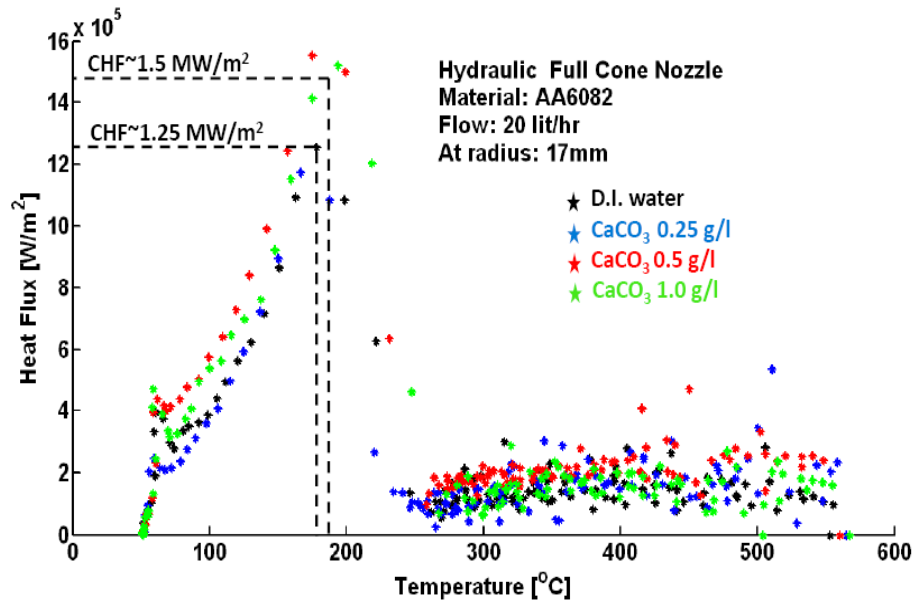


Figure 4.37: Relation between heat flux and surface temperature for CaCO_3 solutions-hydraulic spray

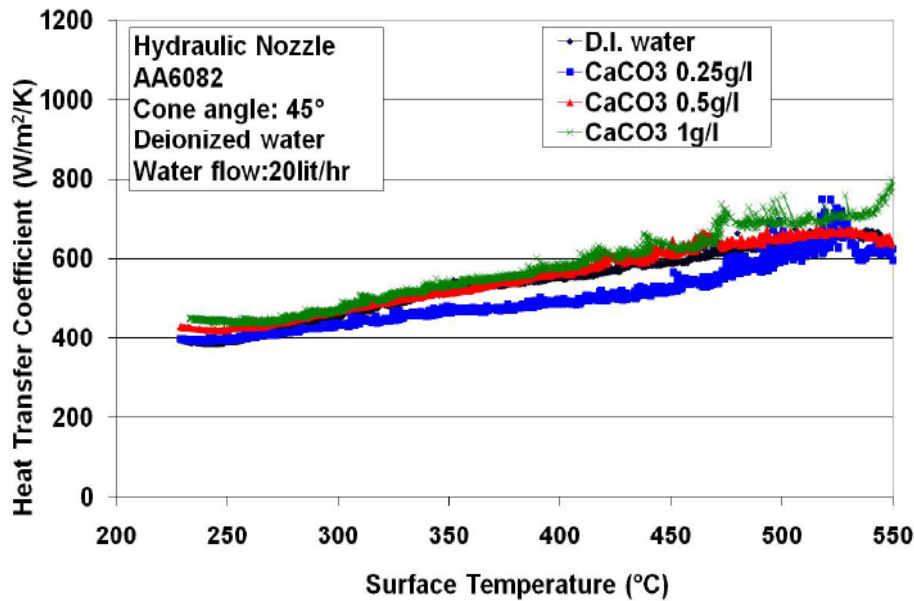


Figure 4.38: Relation between heat transfer coefficient and surface temperature for CaCO_3 solutions-hydraulic spray

point of times for Na_2SO_4 solution of concentration 7.1 g/l. Maximum heat flux lies at 5 mm from the center of the disc after 1.1 sec which is calculated to be 6 MW/m^2 . The position of maximum heat flux is assumed to be the position of wetting front. Hence, as the maximum heat flux propagates from center to the circumference wetting front also moves. The velocity of wetting front is also a question of investigation here. Wetting front is the demarcation region between wet area and dry area. Maximum heat flux position is plotted with respect to time in figure 4.40 for D.I. water and 0.5 molar solution of different salts. Slope of the curve is assumed as the wetting front velocity. MgSO_4 causes the fastest wetting front velocity while NaHCO_3 causes the slowest. This phenomenon is also apparent from the figure 4.41. Heat flux is plotted with respect to radial position at the point of time 3.3 s for all qualities of water. For MgSO_4 , maximum heat flux position is leading the other qualities.

4.4.3 Effect of surfactant

Surfactant "ethoxylated ester" is added to water in four different concentrations i.e. 50, 100, 200 and 500 ppm. It is added to the casting water in aluminium industry. The effect is opposite to that of salts. When salts increase the Leidenfrost point and reduce the film boiling region; surfactant decrease the Leidenfrost point and thereby prolong the film boiling region as shown in figure 4.42. Temperature of the central point of the circular disc is plotted against time for pneumatic atomizing nozzle. By adding the surfactant 50 ppm by weight, Leidenfrost temperature is reduced from 420 to 300 °C, while film boiling region is almost doubled from 0.5 s to 1s. However, further increase of concentration did not make significant influence. In order to optimize the secondary cooling during continuous casting of steel, the heat transfer rate from the metal surface should produce a stable surface temperature that decreases monotonically. Film boiling is deliberately promoted during the

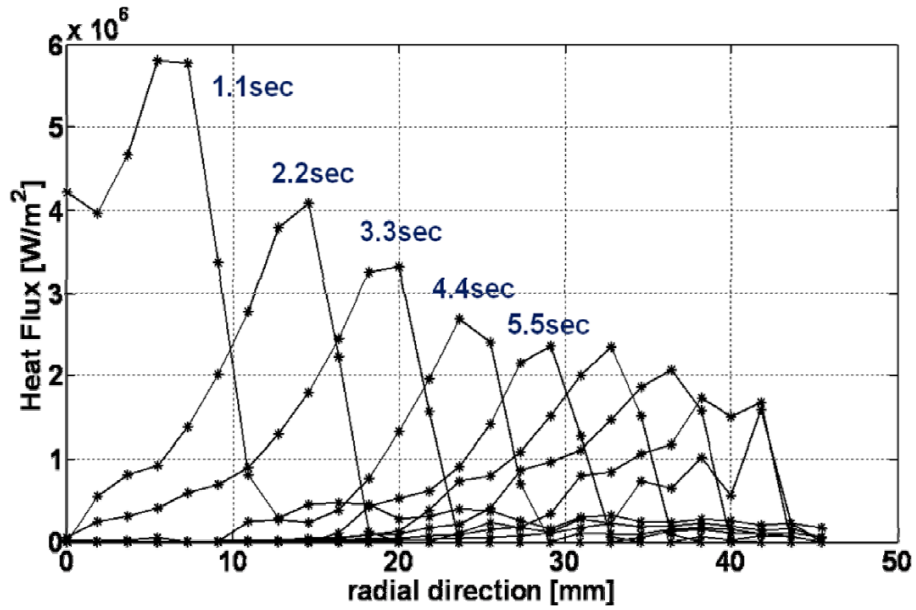


Figure 4.39: Heat flux distribution along radius of the disc-pneumatic spray

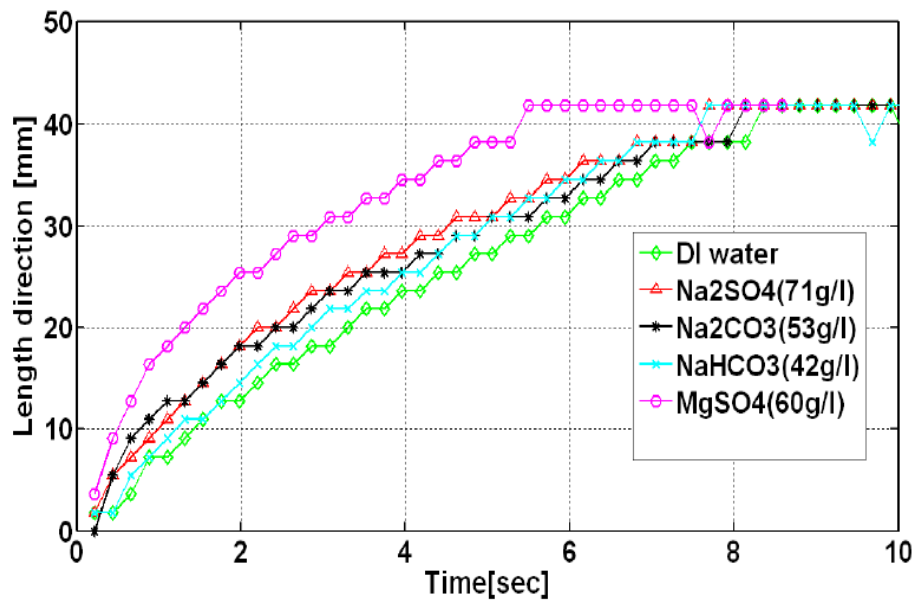


Figure 4.40: Propagation of maximum heat flux position for salts' solutions-pneumatic spray

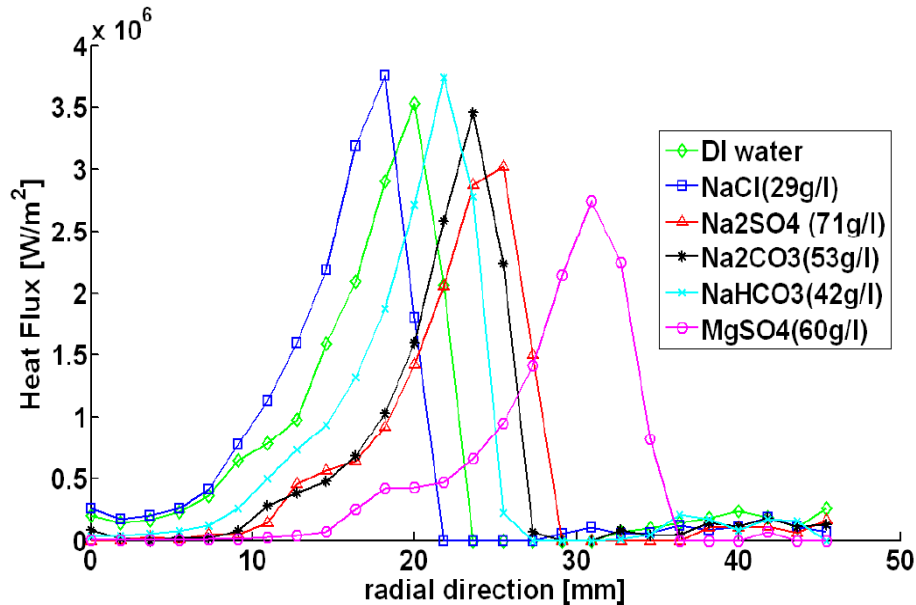


Figure 4.41: Heat flux distribution at $t = 3.3$ sec for salts' solutions-pneumatic spray

secondary cooling process in order to avoid the unstable surface temperatures and heat extraction rates that accompany nucleate/transition boiling, if the surface temperature drops too low [14]. HTC within film boiling region is plotted against surface temperature and HTC found to be independent of surface temperature and the value of HTC seems to be inversely proportional of the concentration of surfactant in cooling water and the length of film boiling region also increases with concentration of surfactant as shown in figure 4.43.

Similar results were obtained when experiments were performed using hydraulic spray with same surfactant's concentrations as shown in figures 4.44 and 4.45. A considerable shift in CHF and corresponding surface temperature of nickel is noted in figure 4.46. A concentration of 500 ppm of surfactant (ethoxylated ester) lowered the CHF value from 2 MW/m^2 to 1.6 MW/m^2 and increased the corresponding surface temperature (burnout temperature) to $100 \text{ }^\circ\text{C}$ (from 250 to $150 \text{ }^\circ\text{C}$). Similarly HTC in film boiling region for the case of hydraulic nozzle decreases from 850 to $730 \text{ W/m}^2/\text{K}$. Figure 4.47 displays the wetting front velocity for de-ionized water and four concentrations of surfactant. Wetting front velocity varies from 5 mm/s to 3 mm/s as the concentration of surfactant increases. Hence, wetting front velocity decreases with increasing surfactant concentration. This phenomenon is verified from figure 4.48. Heat flux distribution is plotted against the radius at 3.3 s after spraying starts. D.I. water leads the surfactant in maximum heat flux position.

4.4.4 Effect of mixture of salts and surfactant

From the previous results regarding the influence of water quality on heat transfer rate, one can infer that when salts e.g. MgSO_4 , borax, CaCO_3 are dissolved in cooling water they tend to enhance the heat transfer whereas; surfactant have the tendency to lower the heat transfer. A set of experiments have been performed with coolant having both species i.e. salts and surfactant in cooling water in order to assess that which specie's influence is dominant. Borax and MgSO_4 are dissolved with ethoxylated ester in such a way that

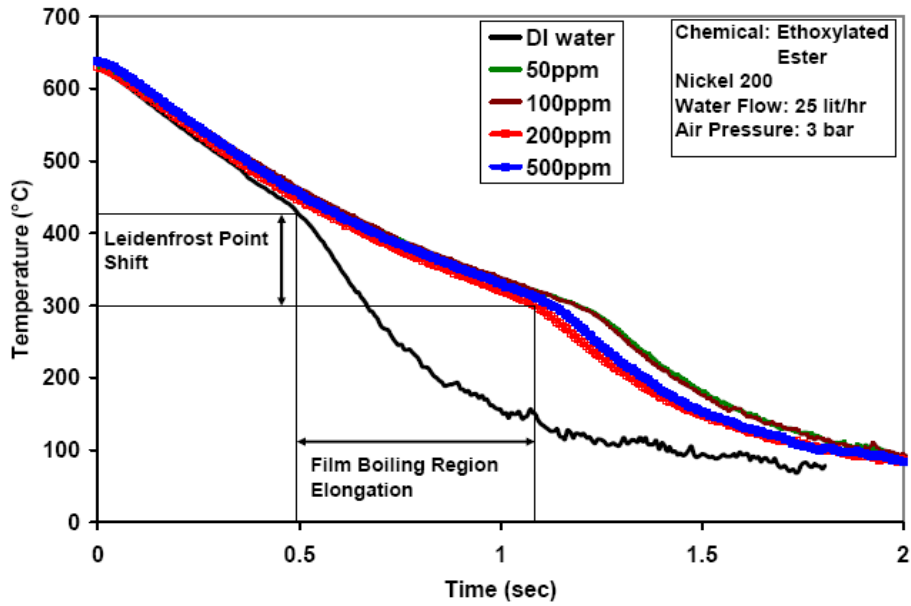


Figure 4.42: Temperature profiles for various concentrations of surfactant solution-pneumatic spray

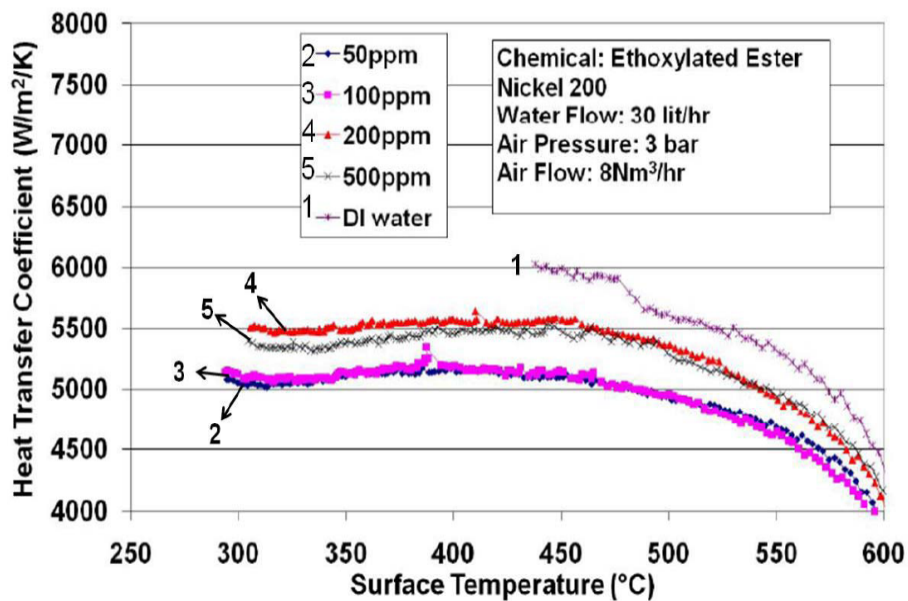


Figure 4.43: Heat Transfer Coefficient vs temperature within film boiling region for various concentrations of surfactant solution-pneumatic nozzle

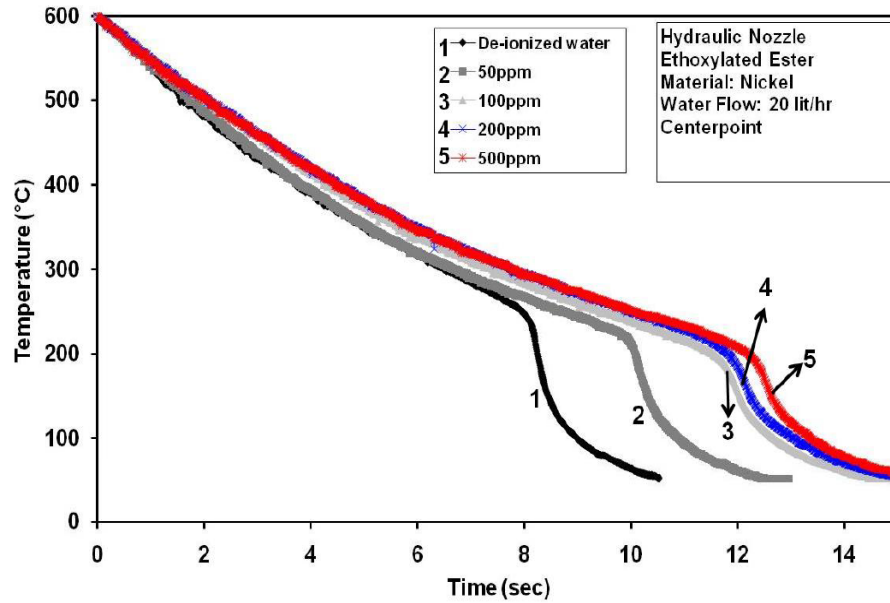


Figure 4.44: Temperature profiles for various concentrations of surfactant solution-hydraulic spray

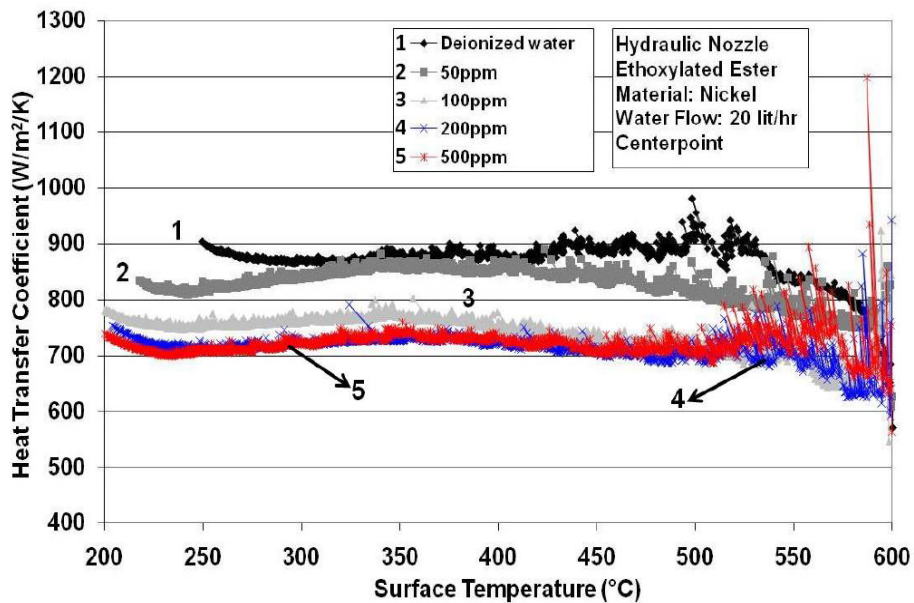


Figure 4.45: Heat transfer coefficient vs temperature within film boiling region for various concentrations of surfactant solution-hydraulic spray

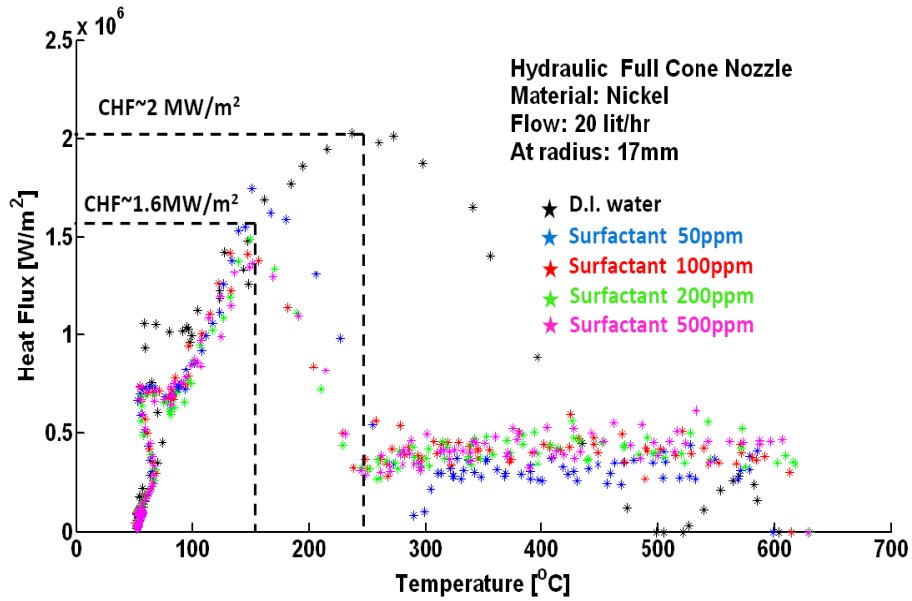


Figure 4.46: Relation between heat flux and surface temperature for various concentrations of surfactant solution-hydraulic Spray

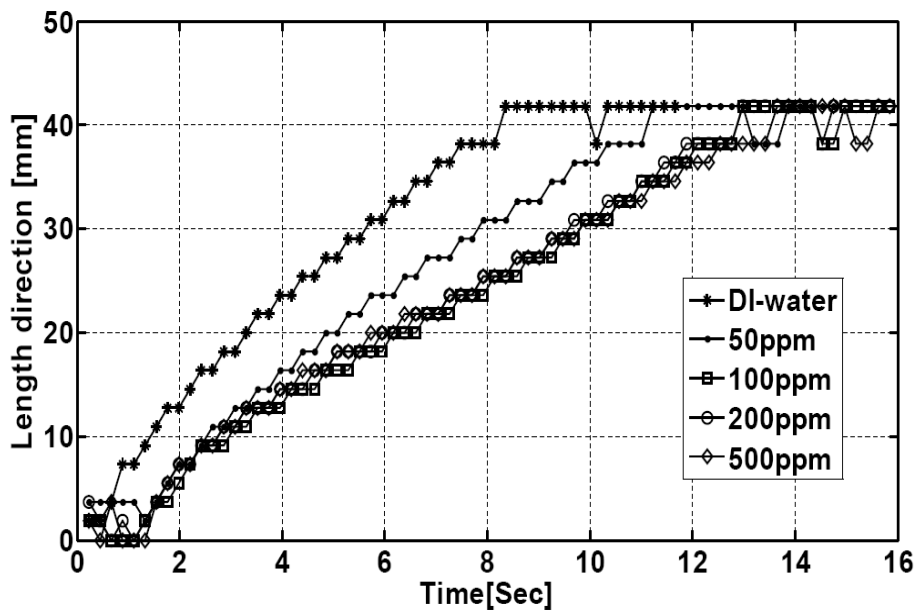


Figure 4.47: Maximum heat flux position propagation for various concentrations of surfactant solution-pneumatic spray

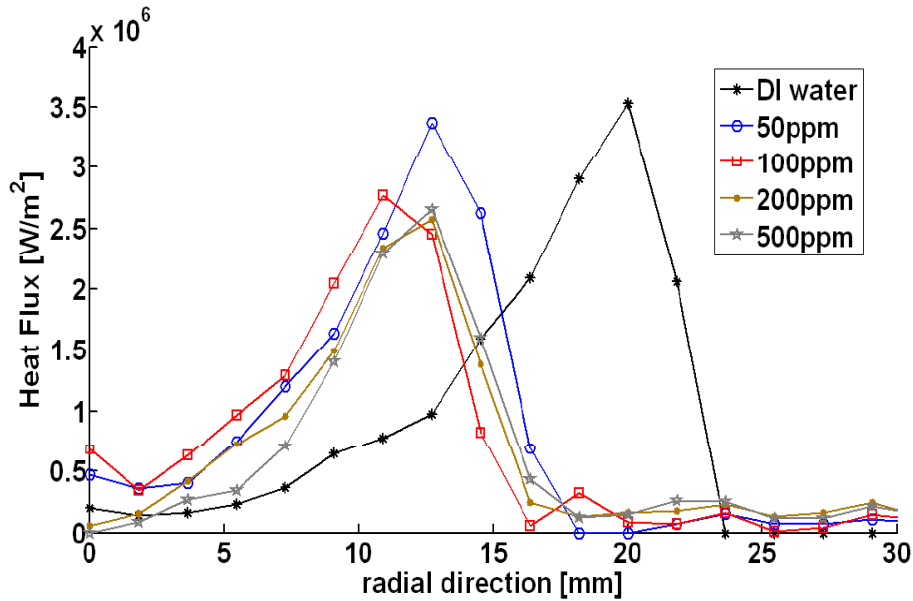


Figure 4.48: Heat flux distribution at $t = 3.3$ s for various concentrations of surfactant solution-pneumatic spray

concentrations of borax and MgSO_4 are kept constant and concentration of surfactant is varied from 50 ppm to 500 ppm. Temperature-time relationship for mixture of borax and surfactant and MgSO_4 and surfactant are shown in figures 4.49 and 4.52 and the heat flux dependence on surface temperature are shown in figures 4.50 and 4.53. HTC in film boiling curve with respect to surface temperature is plotted in figure 4.51 for mixture of borax and surfactant. For these two cases, salts showed dominant effect. Heat flux in film boiling and transition boiling regimes are considerably enhanced, even though the concentrations of borax and MgSO_4 are quite lower. It is observed from cooling curves that the cooling is faster for a mixture of 50 ppm surfactant and 3 g/l MgSO_4 than 3 g/l MgSO_4 alone. This shows that a mixture of only two species can affect cooling curve completely different as compared to individual specie.

4.4.5 Effect of dissolved gases

In order to analyze the influence of dissolved gases in deionized water, saturated oxygenated water, saturated carbonated water, aerated water and drinking carbonated water have been used as coolant for the case of hydraulic spray quenching of AA6082. Pure oxygen is injected into deionized water for 10 minutes at a pressure of 2 bar for making it saturated oxygenated water, similarly pure carbondioxide is injected for saturated carbonated water and aerated water. It can be observed from figure 4.54 that air and carbondioxide have opposite effects on cooling time at center of disc. Air increases the cooling rate and CO_2 prolongs the cooling time considerably as shown in figure 4.54 and this influence of CO_2 is also verified by that of drinking carbonated water which contains 140 mg/l of CO_2 . Heat transfer coefficient with respect to surface temperature in film boiling region is drawn in figure 4.55. Saturated CO_2 reduced the HTC from 600 to 490 $\text{W/m}^2/\text{K}$ while aerated water increased it to 700 $\text{W/m}^2/\text{K}$ as compared to deionized water.

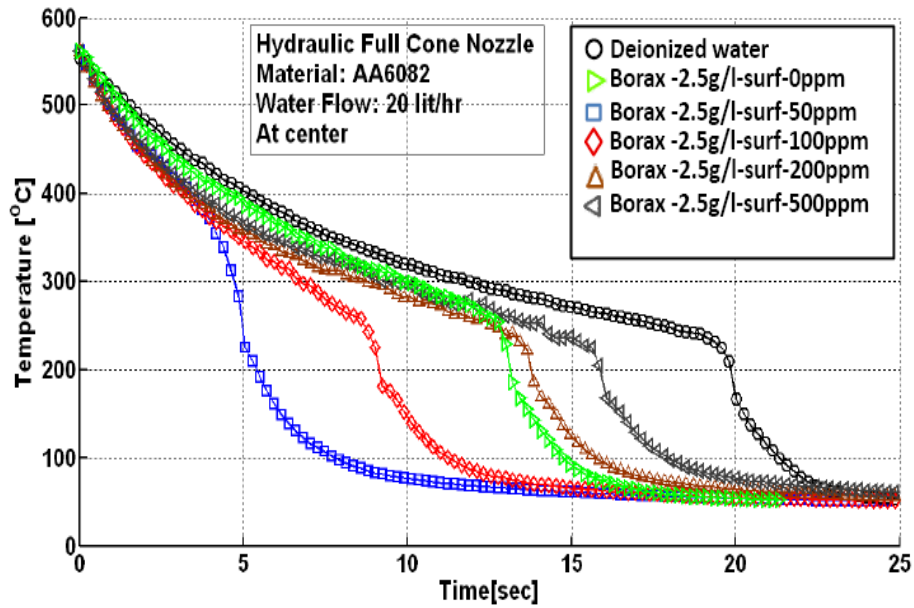


Figure 4.49: Temperature-time curve for solutions of borax and surfactant-hydraulic spray

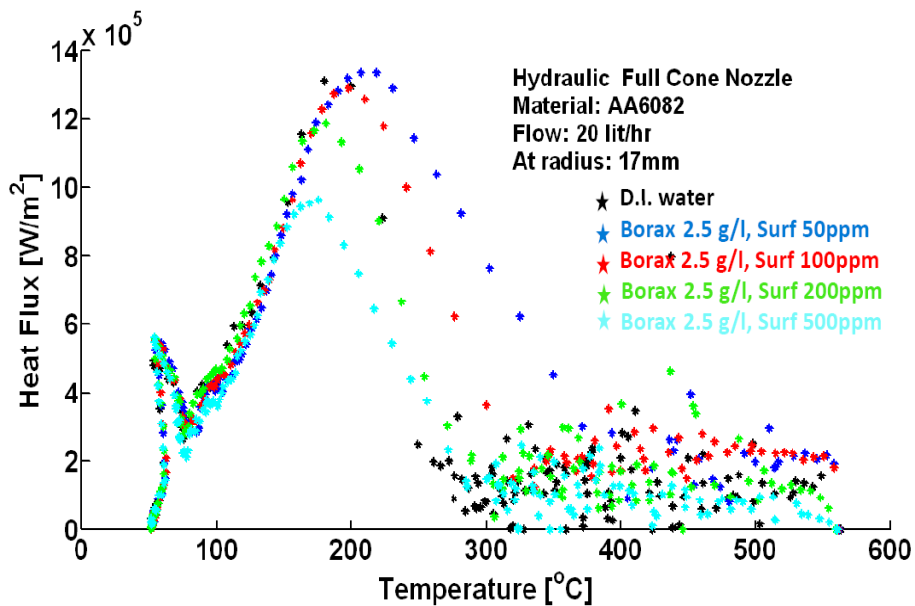


Figure 4.50: Relation between heat flux and surface temperature for solution of borax & surfactant-hydraulic spray

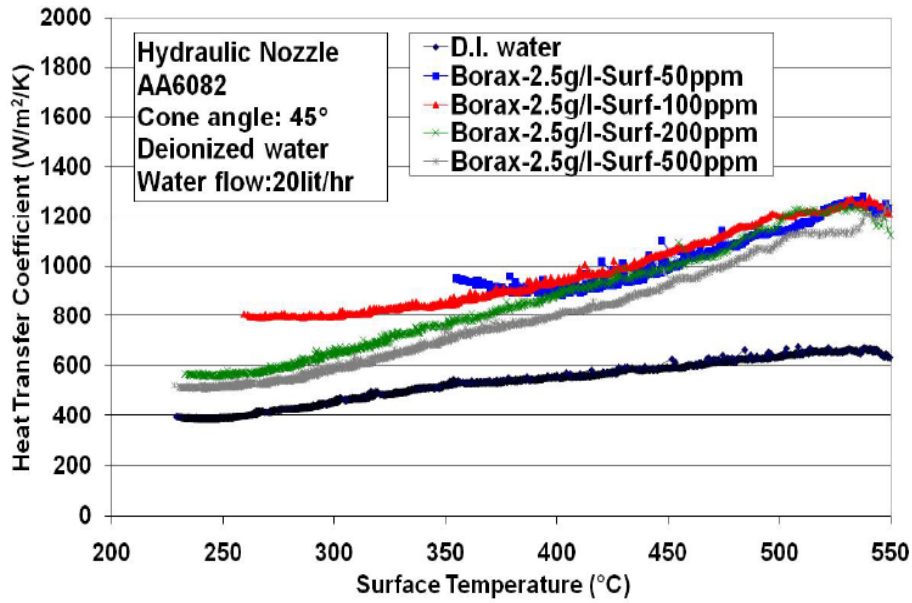


Figure 4.51: Relation between heat transfer coefficient and surface temperature for solution of borax & surfactant-hydraulic spray

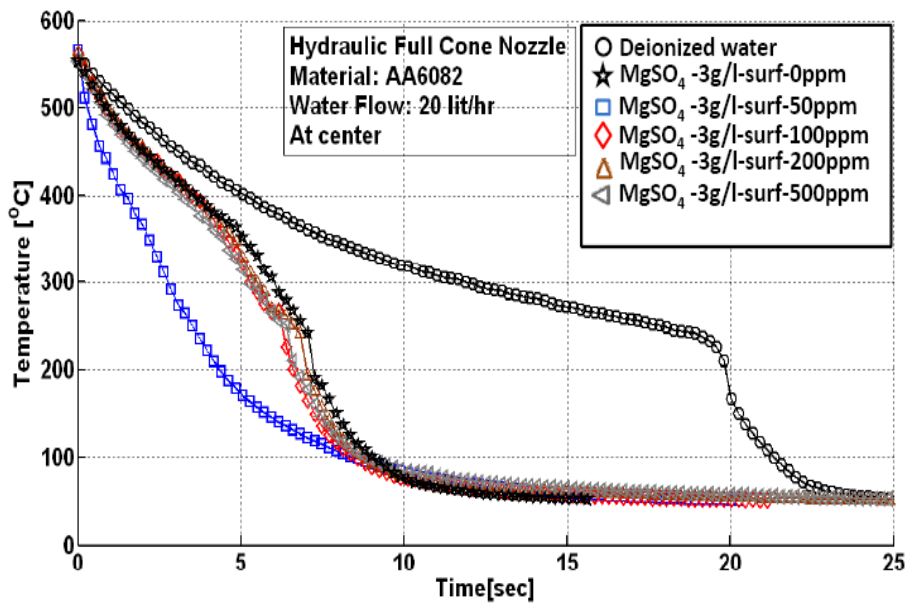


Figure 4.52: Temperature-time curve for solutions of $MgSO_4$ and surfactant-hydraulic spray

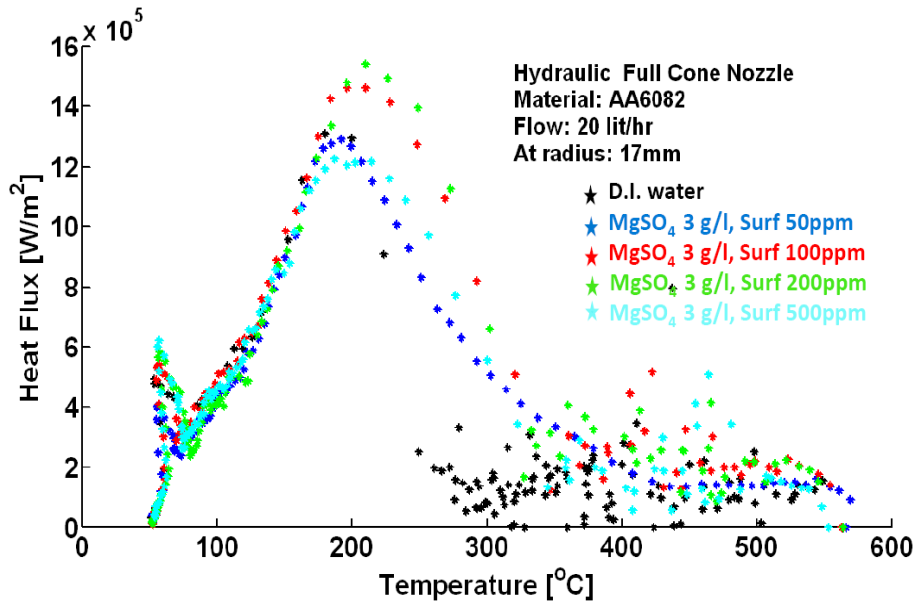


Figure 4.53: Relation between heat flux and surface temperature for solution of MgSO_4 & surfactant-hydraulic spray

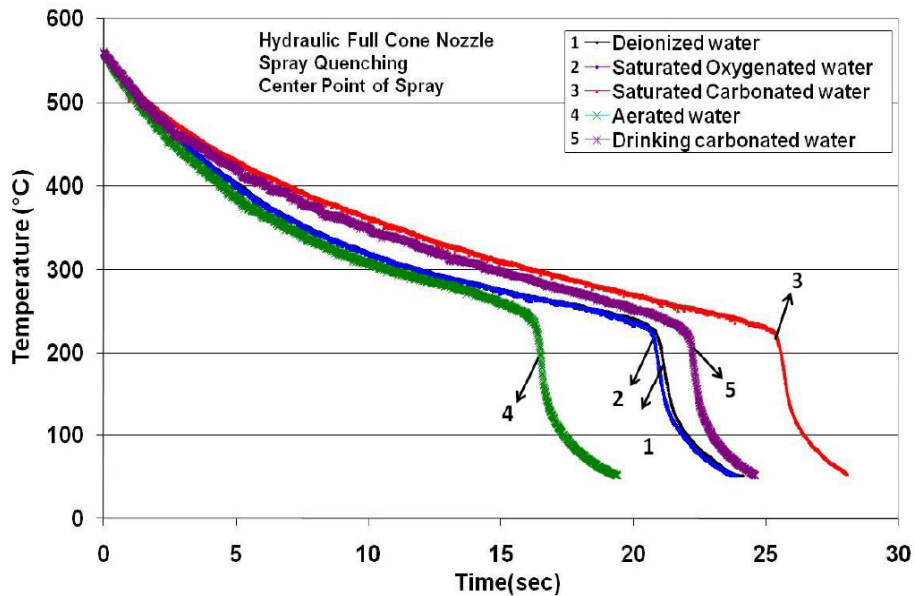


Figure 4.54: Temperature-time relation for different dissolved gases with respect to deionized water-hydraulic spray

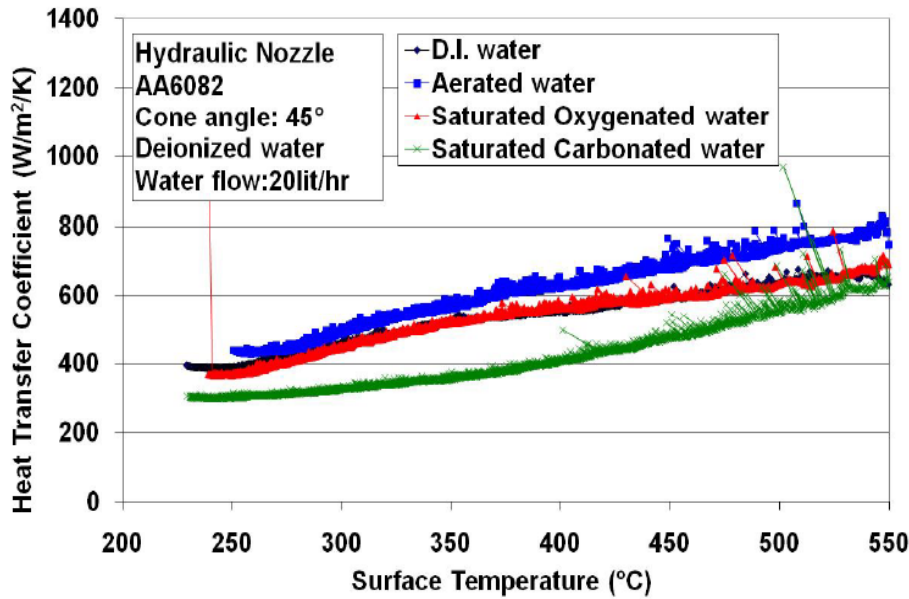


Figure 4.55: Relation between heat transfer coefficient and surface temperature for various gases dissolved in cooling water-hydraulic spray

A combination of surfactant (ethoxylated ester) and oil is dissolved in deionized water in such a proportion that surfactant concentration remains constant as 50 ppm and Oil concentration is increased as 10, 50 and 200 ppm. Increasing the Oil concentration prolongs the cooling time with an exception of Oil concentration of 200 ppm. This oil is also added to the cooling water used in secondary cooling of Aluminum ingots in industry.

pH of the coolant solution is increased by adding NaHCO_3 in deionized water to a value of 9. The cooling curves of this basic solution are plotted in figures 4.58 4.59. The change of pH exhibited almost no influence on cooling time.

Values of critical heat flux (CHF) or maximum heat flux, heat transfer coefficient in film boiling, Leidenfrost temperature, and cooling time to reach 200 °C are tabulated in table 4.3 for all kinds of ingredients added to cooling water in quenching by hydraulic spray of AA6082.

Experiments for analyzing the effect of dissolving seven different salts i.e. NaCl , Na_2SO_4 , Na_2CO_3 , NaHCO_3 and MgSO_4 , borax and CaCO_3 in water and a surfactant "ethoxylated ester" on atomized spray (water with air) and spray (water without air) cooling of hot metal surface were conducted. A circular disc is quenched by spray from 600 °C on front side and the temperature is measured by an IR camera from the back side. The heat flux on the front side is calculated using measured temperature data by solving inverse heat conduction problem. The results were compared with those using de-ionized water. It is observed that addition of salts increases the rate of heat transfer and eventually decreases the cooling time. Deposition of salts at higher temperature degrades the surface roughness and promotes the Leidenfrost temperature which promotes the nucleate boiling heat transfer. Borax and MgSO_4 increased the cooling efficiency significantly, however NaCl showed the least influence. Maximum heat flux position is used for measuring the wetting front velocity. MgSO_4 solution resulted in highest wetting front velocity. On the other hand, surfactant decreases the Leidenfrost temperature and eventually prolongs the film boiling

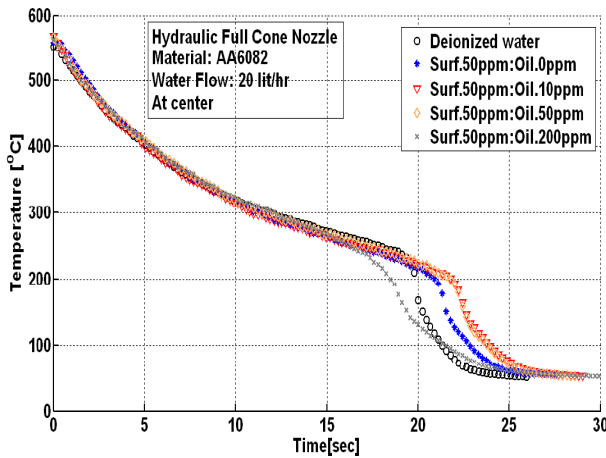


Figure 4.56: Influence of oil on temperature profile at the center of the spray

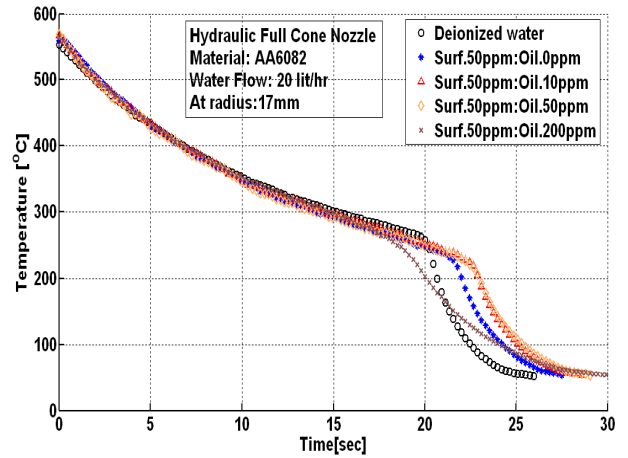


Figure 4.57: Influence of oil on temperature profile at radius of 17 mm

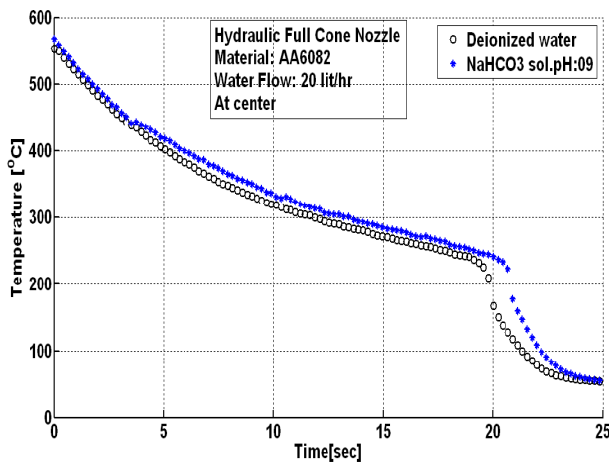


Figure 4.58: Influence of basic pH on temperature profile at the center of the spray

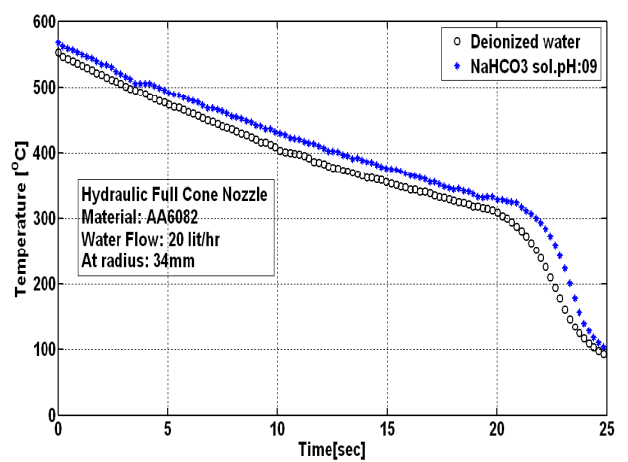


Figure 4.59: Influence of basic pH on temperature profile at radius of 34 mm

region. Addition of surfactant also decelerates the wetting front velocity. When $MgSO_4$ and borax are dissolved together with surfactant, heat flux is enhanced in film and transition boiling regimes. Cooling water saturated with CO_2 reduced the cooling rate considerably while that saturated with air caused faster cooling.

Table 4.3: Summary of important parameters of boiling curve for different kinds of ingredients in cooling water

Ingredient	Concentration	LFP (°C)	Max HF (MW/m ²)	Time to reach 200 °C (s)	HTC in film boiling region (W/m ² /K)	Metal
D.I. water	–	228	1.2	19.8	600	AA6082
MgSO ₄	0.25 g/l	228	1.4	18.9	700	
	0.5 g/l	251	1.5	18.5	900	
	3 g/l	364	1.8	7.2	600	
	6 g/l	400	1.9	6.8	900	
	12 g/l	~400	2.17	5.7	900	
	60 g/l	~430	2.17	3.0	–	
Borax Na ₂ B ₄ O ₇	0.3 g/l	251	1.5	15.4	700	
	0.6 g/l	262	1.5	14.9	800	
	2.5 g/l	255	1.65	13.1	800	
	5 g/l	284	1.65	11.3	600	
	10 g/l	384	1.6	7.5	660	
CaCO ₃	0.25 g/l	228	1.17	20	546	
	0.5 g/l	229	1.52	18.2	623	
	1.0 g/l	232	1.55	16.9	630	
D.I. water	–	250	2.0	8.2	890	Pure Nickel
Surfactant ethoxylated ester	50 ppm	220	1.6	10	850	
	100 ppm	191	1.4	11.5	760	
	200 ppm	203	1.4	11.8	730	
	500 ppm	194	1.34	12	730	
D.I. water	–	228	1.2	19.8	600	AA6082
MgSO ₄ (3g/l)+ethox. ester	50 ppm	–	1.3	4.4	1070	
	100 ppm	370	1.45	6.6	1025	
	200 ppm	370	1.54	7.0	970	
	500 ppm	370	1.2	6.6	622	
Borax (2.5 g/l)+ethox. ester	50 ppm	355	1.3	5.5	1036	
	100 ppm	259	1.27	9.2	1000	
	200 ppm	233	1.18	13.9	1020	
	500 ppm	225	0.95	15.8	950	
Carbonated water(drinking)	HCO ₃ ⁻¹ (190 mg/l)	230	1.4	22.8	550	
Saturated CO ₂ water	Pure CO ₂ injected for 10 min	225	–	25.6	490	
Saturated O ₂ water	Pure O ₂ injected for 10 min	228	–	20	600	
Aerated water	Pressurized air (2 bar)	250	1.6	16	700	

Table 4.4: Summary of experiments for water quality

Kind of Nozzle	Solvent	Chemical	Concentration					Material		
Pneumatic atomizing nozzle (air Pr: 3 bar air flow: 8 Nm ³ /h, Water flow: 30 l/h)	Salts	NaCl	0.05 M	0.1 M	0.5 M			Pure nickel (Circular disc $\phi = 140$ mm, thickness = 2 mm), initial temp:600 °C		
			2.9 g/l	5.8 g/l	29 g/l					
		NaHCO ₃	0.05 M	0.1 M	0.5 M					
			4.2 g/l	8.4 g/l	42 g/l					
		Na ₂ SO ₄	0.05 M	0.1 M	0.5 M					
			7.1 g/l	14.2 g/l	71 g/l					
		MgSO ₄	0.05 M	0.1 M	0.5 M					
			6 g/l	12 g/l	60 g/l					
		Na ₂ CO ₃	0.05 M	0.1 M	0.5 M					
			4.2 g/l	8.4 g/l	42 g/l					
		Organic solvents	Ethoxylated ester	50 ppm	100 ppm	200 ppm	500 ppm			
			Carbonated water							
	Antifrost		50/50							
	Industrial casting water	Al-Industry	Fresh	1 week later						
		Al-Industry	Prob1	Prob2						
Cu-Industry		A90	K1							
Hydraulic full cone nozzle (water flow : 20 l/h)	Organic solvents	50ppm Surf. plus Oil	No oil	10 ppm	50 ppm	200 ppm		AA6082 (Circular disc $\phi = 140$ mm, thickness = 3 mm), initial temp : 560 °C		
		Ethoxylated ester	50 ppm	100 ppm	200 ppm	500 ppm				
	Salts	Borax	0.3 g/l	0.6 g/l	1g/l	2.5 g/l	5 g/l		10 g/l	
		CaCO ₃	0.25 g/l	0.5 g/l	1 g/l					
		MgSO ₄	–	–	0.025 M	0.05 M	0.1 M		0.5 M	
	0.25 g/l		0.5 g/l	3 g/l	6 g/l	8.4 g/l	60 g/l			
	Mixture	MgSO ₄ plus ethoxylated ester	3 g/l	3 g/l	3 g/l	3 g/l				
			50 ppm	100 ppm	200 ppm	500 ppm				
		Borax plus ethoxylated ester	2.5 g/l	2.5 g/l	2.5 g/l	2.5 g/l				
	Gases	Pure O ₂	2 bar	10 min						
		Pure CO ₂	2 bar	10 min						
		Air	2 bar	10 min						
	pH = 9	By adding NaHCO ₃								
	Mold with 7 orifices	Organic solvent	Ethoxylated ester	50 ppm	100 ppm	200 ppm	500 ppm			Pure nickel

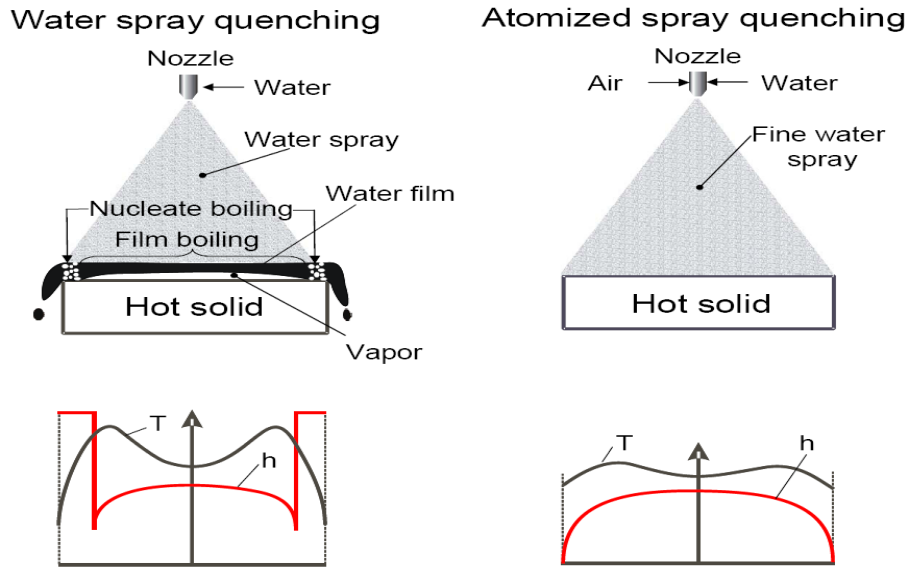


Figure 4.60: Principle of atomized spray cooling

4.5 Local control of atomized spray quenching

An advantage with spray quenching compared to bath quenching (when the whole part is submerged into a liquid bath) is that different areas of the component can be individually cooled which can be regarded as locally defined quenching. This allows control of the surface heat flux at thicker and thinner sections and therefore gives the opportunity to get a uniform cooling of the whole component which reduces residual stresses in the material. Depending on the shape of the component, different types of spray nozzles are used at different areas to get the correct heat flux "q", that a certain type of spray nozzle can generate. Figure 4.60 schematically illustrates the quenching of a hot slab from a temperature higher than Leidenfrost temperature. In water spray quenching a vapor layer forms. The heat is mainly transferred by conduction through the vapor. At the edges, the vapor layer collapses immediately. Thus nucleate boiling occurs at these locations and the heat transfer coefficient HTC drastically increases. As a result the temperature rapidly decreases. With atomized spray quenching, the profile of the heat transfer coefficient matches with the required condition of minimizing stresses and distortion. It is proven with the infrared thermography that even at the edges no nucleate boiling occurs. In this study, the heat transfer characteristics are investigated in more detail. It was measured to which extent the heat transfer is enhanced in comparison with the traditional spray quenching because of the contact between droplets and surface. It is a question to which range the impingement density can be increased before a closed liquid film forms as in traditional spray quenching. In metal quenching an array of nozzles is necessary. Therefore, in this work the local heat transfer with overlapping sprays is presented. Overlapping sprays increase the homogeneity in heat transfer rates and thus cause reduced stresses and distortion while quenching. The aim of the measurements of the atomized spray quenching was to find out the influence of the main parameters for the enhancement of heat transfer such as impingement density of the spray, use of multiple sprays, air pressure, water flow rate etc. Impingement density is the most influential parameter which can be defined as mass of water passing

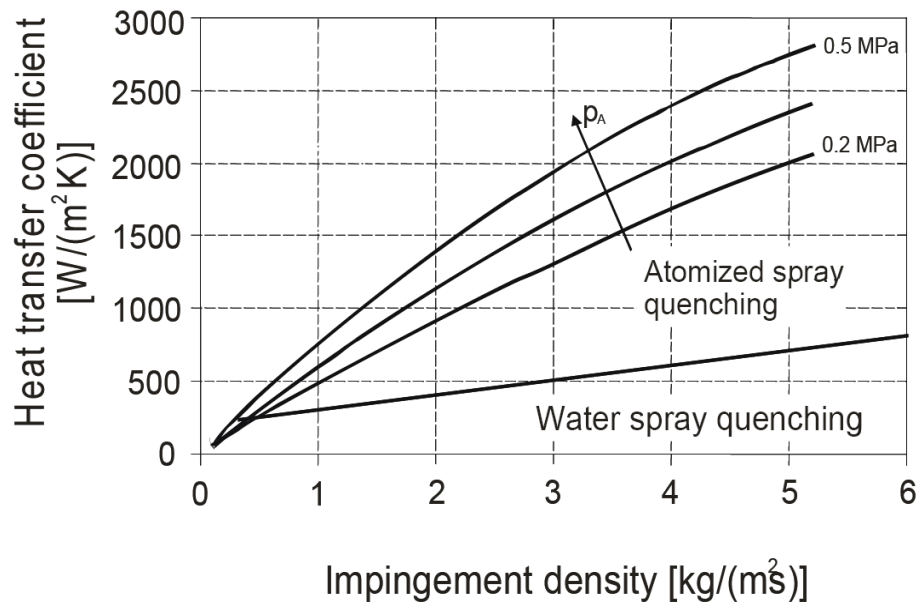


Figure 4.61: Relation between heat transfer coefficient versus impingement density and air pressure [Jacek Krol [10]]

through unit area in unit time. Figure 4.61 shows comparison of atomized spray quenching with traditional spray quenching. It is evident that for a heat transfer coefficient $1000 \text{ W/m}^2/\text{K}$, the required impingement density for water spray is about $8 \text{ kg/m}^2/\text{s}$, but $1.8 \text{ kg/m}^2/\text{s}$ for atomized spray quenching. For a constant impingement density the droplet velocity increases with the air pressure. Therefore, the droplet contact time between surface and droplet increases. As a consequence, the amount of heat transferred from surface to droplet also increases.

The heat transfer coefficient of atomized spray quenching is presented in figure 4.62 depending on the surface temperature for a low $1.4 \text{ kg/m}^2/\text{s}$ and a high $33 \text{ kg/m}^2/\text{s}$ impingement density. For both impingement densities, the heat transfer coefficient is independent of the surface temperature for the values above the Leidenfrost temperature i.e. in film boiling regime. It can be seen that the Leidenfrost temperature increases only slightly with impingement density from about $290 \text{ }^\circ\text{C}$ for $1.3 \text{ kg/m}^2/\text{s}$ to about $315 \text{ }^\circ\text{C}$ for $33 \text{ kg/m}^2/\text{s}$. Even for the impingement density of $33 \text{ kg/m}^2/\text{s}$, which produced a heat transfer coefficient of about $10000 \text{ W/m}^2/\text{K}$, a water film does not form above Leidenfrost temperature. The surface always remains dry above Leidenfrost temperature. The advantage of the atomized spray quenching is demonstrated in figure 4.63 for the quenching of an edge. The spray center is directed to locations at different distances ranging from $x = 0 \text{ mm}$ to 25 mm from the spray center. This figure illustrates the sequences of the temperature on the top surface in the spray center and on the bottom surface directly below the edge. The temperature profiles for the spray center remains almost the same and the temperature gradients on the bottom surface directly below the edge are nearly independent from the cooling of top surface. Only if the spray is directed nearly to the edge, the bottom surface cools down a little bit faster. This happens due to the superposed airflow. Vapor film does not collapse at the edges and therefore nucleate boiling is avoided at the edges. This leads to uniform heat flux throughout the surface of the metal sheet. Figure 4.64 presents the quenching of

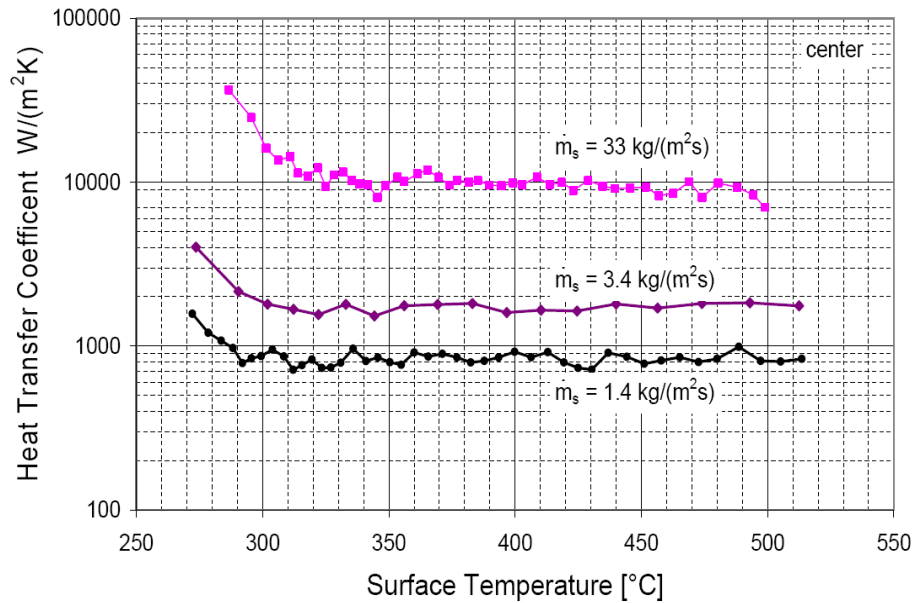


Figure 4.62: Relation between heat transfer coefficient of atomized spray quenching and surface temperature within film boiling region during atomized spray quenching [Jacek Krol [10]]

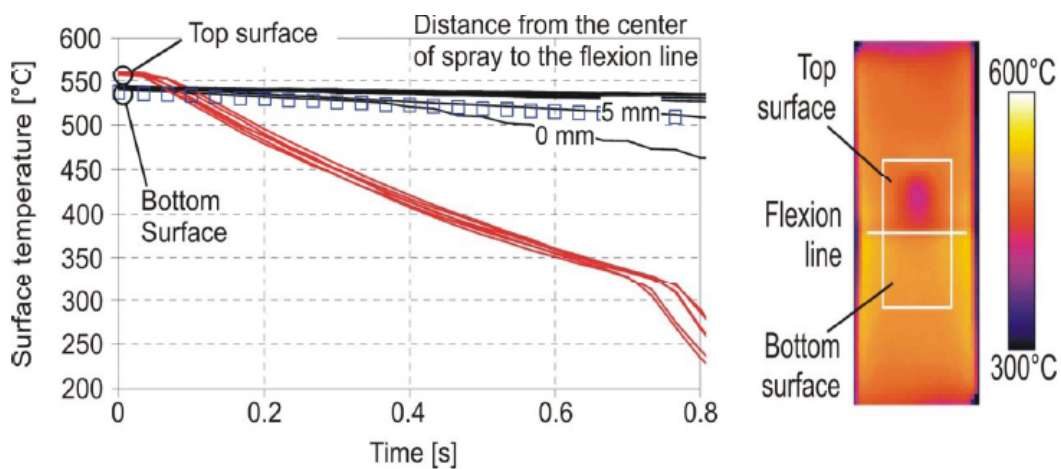


Figure 4.63: Quenching of an edge: temperature profile (left), picture from infrared camera [F. Puschmann]

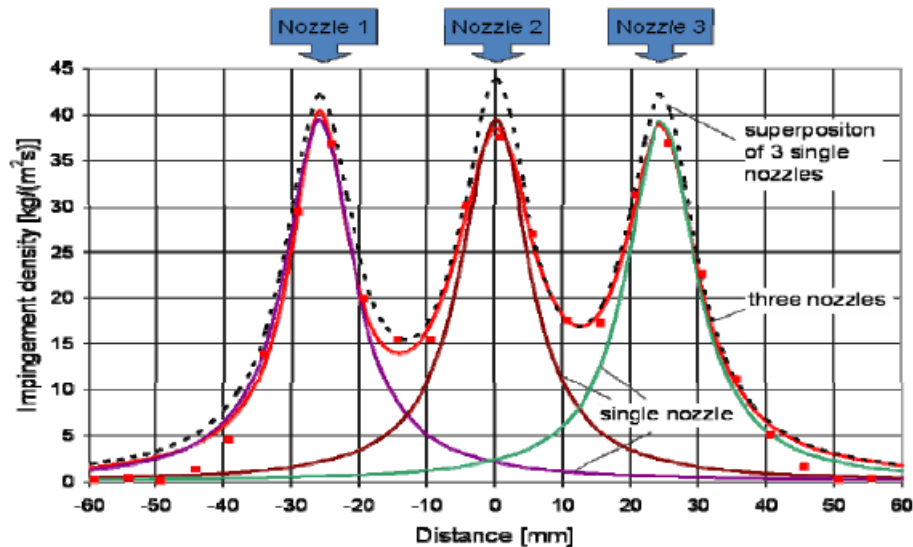


Figure 4.64: Effect of overlapping sprays on impingement density [Jacek Krol [10]]

an aluminium sheet by three nozzles with flat spray pattern. They were arranged in line array with a distance of 35 mm between them. The resultant impingement density is more uniform than the individual nozzle. With individual nozzle, the impingement density near the circumference of the spray cone is very low as compared to the center which results in the variation of cooling rates. To eliminate this significant variation, array of nozzles are used installed with the effective spacing. The minimum impingement density of the overlapping spray appears to be 15 kg/m²/s i.e. 40 % of the maximum impingement density. Figure 4.65 shows curves for the spray center and also for the position between nozzles 1 and 2 and for the position between nozzles 2 and 3. The temperature profile for the spray center and for two points remains almost the same until Leidenfrost temperature is reached. The corresponding local profiles of the temperature are shown in figure 4.66 for specific times. For times before 2.8 second the profiles are very homogenous which demonstrates a uniform profile of the heat transfer coefficient. For these times, all profiles are still above Leidenfrost temperature, which is about 280 °C. Only below LFP, the profile is uneven because of the imperfect distribution of the impingement density of the nozzles.

Atomized spray cooling reaches with values up to 10,000 W/m²/K much higher heat transfer coefficients than spray cooling. The heat transfer coefficient is mainly determined by the impingement density. To obtain a given heat transfer coefficient, the atomized spray quenching requires less amount of water than the traditional spray quenching. An array of nozzles produces more uniform quenching profiles than a single nozzle. With this quenching technique, the water layer does not form on the hot surface with temperature above the Leidenfrost temperature, and the nucleate boiling does not occur at the edges like in case of water spray quenching or immersion quenching where the immediate collapse of the vapor film at the edges results in extremely high stresses and distortions.

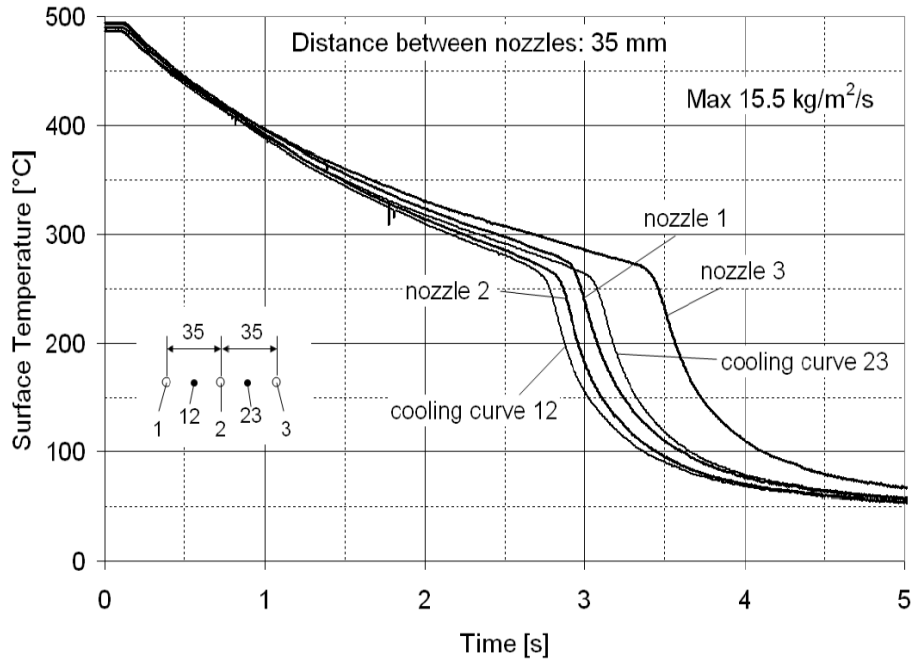


Figure 4.65: Time dependent temperature profile of aluminium sheet with three nozzles [Jacek Krol [10]]

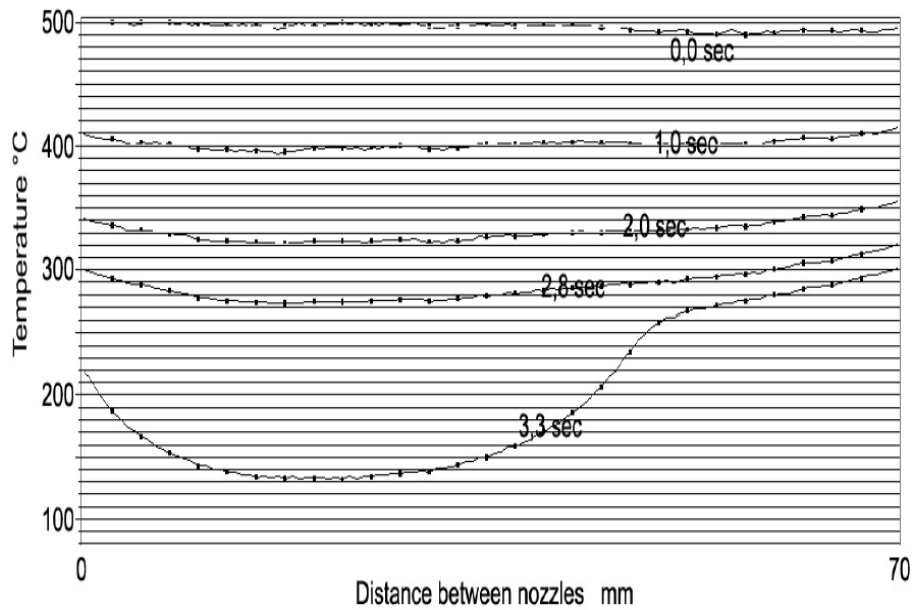


Figure 4.66: Spatial temperature profile aluminium sheet with three nozzles [Jacek Krol [10]]

5 Influence of Water Velocity on Quenching by Array of Water Jets

5.1 Introduction

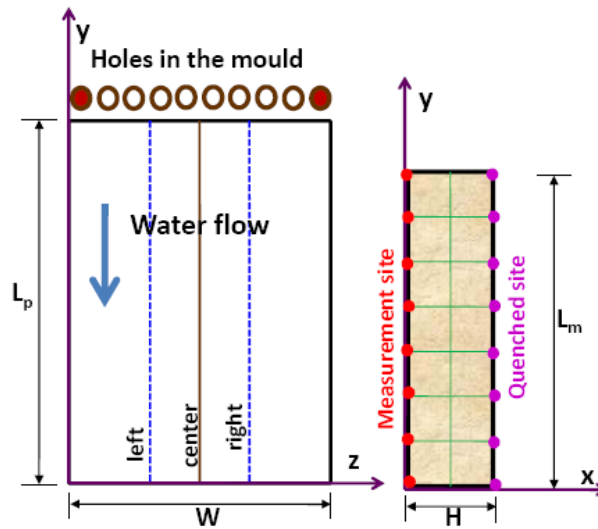
This chapter comprises of the results and discussion concerning to the influence of water velocity on quenching by array of jets or multiple jets. As mentioned earlier, the array of jets are generated by using two devices named as molds. One generates seven parallel jets of diameter 2.5 mm at an angle of 60° from horizontal plane and other one generates eight parallel jets of diameter 4.78 mm at an angle of 60° . These molds are actually a small section of the actual mold used in secondary cooling of DC casting of aluminum ingots. Vertical rectangular plates of materials nickel, AA2024 and Inconel are quenched by these jets. The temperature profiles at different vertical distance, distribution of heat flux with respect to time and space and wetting front velocity are calculated for the two kinds of molds. Wetting front velocity is also measured by high speed camera and its measured and calculated values are presented with respect to different jets' velocities.

5.2 Mold with higher water flow

A rectangular sheet, made up of pure nickel having thermo-physical properties as mentioned in table 3.1 and dimensions as mentioned in table 5.2 is subjected to quenching by array of eight water jets. The cooling component employed for this purpose is a mould having eight orifices of diameter 4.78 mm as shown in figure 3.11. This component is actually a small portion of the real mould used in direct chill casting of aluminum ingots at Alunorf GmbH. Influence of water velocity or flow, which is one of the most important parameters in quenching rate, on heat flux is analyzed by performing experiments with scheme presented in table 5.1. The water jet velocity is adjusted by changing the water flow rate of the hydraulic pump. Two different values of the outlet velocity are regulated i.e. 1.0 m/s, 1.5 m/s corresponding with water flow rate of 516.8 l/h and 777.2 l/h respectively. As the nickel sheet is heated by the furnace, the furnace temperature is set to 630°C . However, it decreases during movement of the hot sheet from furnace to cooling unit in ambient conditions. This is the reason, why we observe different values of initial surface temperatures within a range of $20 - 30^\circ\text{C}$ as shown in table 5.1. The nozzle head is fixed at the top of the hot rectangular plate and maintained in static conditions. So, the analysis excludes the casting speed. The effective length L_m considered for the analysis is 156 mm because the nozzle head is not located at the top edge of the nozzles in order to avoid the splashing of water to the other side of the sheet. 44 mm of the length of the sheet from the top is allowed for the water jets to strike the sheet parallel to its length as shown in figure 5.1.

Table 5.1: Detail of experiments for water jet quenching of nickel plate

Experiments	Average initial temperature			Average temp. on surface	Experimental conditions
	Left	Center	Right		
Exp-A	584.7	586.9	585.9	585.8	Water velocity 1.0 m/s Flow rate 516.8 l/h
Exp-B	593.8	595.5	592.1	593.8	
Exp-C	592.6	594.8	593.3	593.6	
Exp-D	593.9	593.6	594.0	593.8	Water velocity 1.5 m/s Flow rate 777.2 l/h
Exp-E	620.2	617.3	614.9	617.5	

**Figure 5.1:** Schematic of finite element model

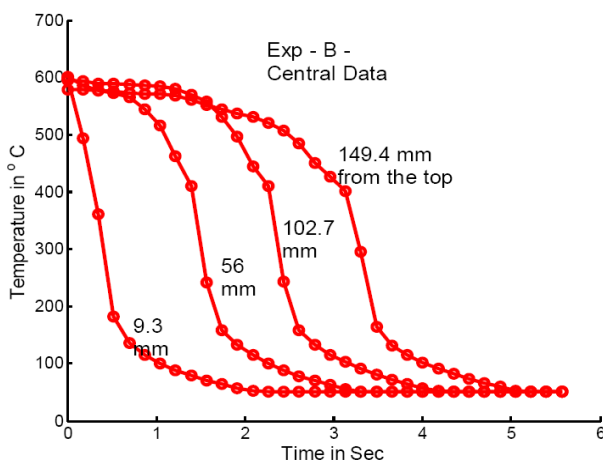
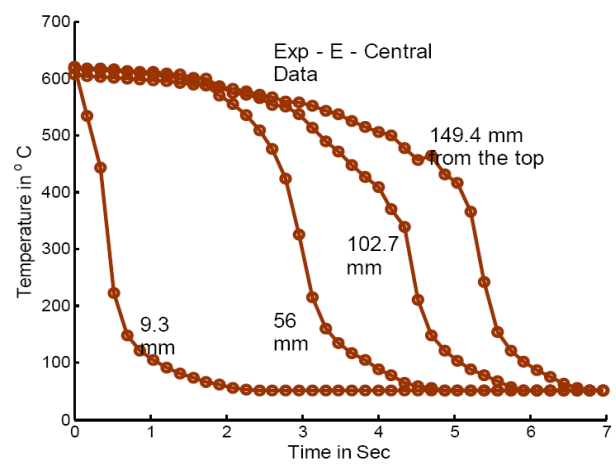
Temperature profiles measured at four different locations are plotted in figures 5.2 and 5.3. Figure 5.2 exhibits temperature profiles for water jets velocity of 1 m/s and figure 5.3 for 1.5 m/s. It can be observed from these figures that, at the distance of 9 from the top of the sheet, the temperature of the higher jet velocity decreases a little faster than the lower velocity and, on the other hand, at the distance of 56, 103 mm and 150 mm from the top, the temperature gradient is lower in lower velocity case when compared to the higher velocity. In order to evaluate heat flux, the non-iterative finite element method described in chapter 2 is applied to the 2D structure as shown in figure 5.1. It is assumed that there is no variation in the cooling characteristics of the sheet in the width direction. The 2D model of $2 \times 156 \text{ mm}$ dimension having 5×67 elements are schematically represented in figure 5.1. All thermal boundaries are assumed to be insulated except quenched surface for the sake of simplicity. A uniform time step of magnitude numerically equal to the diffusive time of the structure is used and it is defined as in [74]

$$\text{Diffusive time} = \frac{(\text{Distance between quenching and measurement side})^2}{\text{Thermal diffusivity}} \quad (5.1)$$

So, the diffusive time is 0.174 sec, total number of nodes in length direction are 68 pixels and number of nodes in thickness direction is 3 pixels (1 pixel equal to 0.769 mm for these

Table 5.2: Geometry & specific properties of nickel

Sheet length	L_p	200 mm
Width	w	110 mm
Thickness	H	2 mm
Density	ρ	8909 kg/m ³
Specific heat	c_p	444 J/kg/K
Thermal conductivity	λ	90.9 W/m/K

**Figure 5.2:** Temperature profile for nickel for jet velocity 1 m/s**Figure 5.3:** Temperature profile for nickel for jet velocity 1.5 m/s

set of experiments).

5.2.1 Calculated heat flux

The instantaneous heat flux distribution along the length of the sheet for two different velocities of water jets at four different times is presented in figures 5.4 and 5.5. From these figures it can be observed that the position of maximum heat flux changes with time. It starts from the place where the jets strike the surface of metal and then moves downward with time and finally reach at the bottom of the plate. If it is assumed that the position of maximum heat flux lies at the point of demarcation between film boiling and nucleate boiling i.e. wetting front, the velocity of movement of this point with time can be regarded as *wetting front velocity*. This hypothesis was enunciated by Monde and coworkers [27] and discussed in detail in section 2.2.2. The value of maximum heat flux and its position depends on the water jet velocity. For the two velocities, the position and the maximum heat flux values are almost same for at time 0.87 seconds, however, at times 1.7 and 2.6 seconds the values of maximum heat flux for jet velocity of 1 m/s are almost two third of the maximum heat flux for jet velocity of 1.5 m/s and similarly the positions of maximum

heat flux lie ahead for jet velocity of 1 m/s as compared to that of 1.5 m/s i.e for 1 m/s it lies at 0.06 m and 0.1 m at 1.7 and 2.6 sec respectively whereas for 1.5 m/s it lies at 0.04 m and 0.06 m for 1.7 and 2.6 sec respectively.

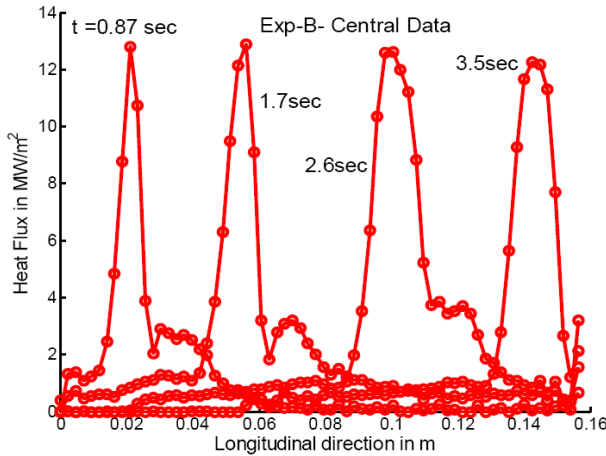


Figure 5.4: Heat flux distribution for nickel for jets' velocity 1 m/s

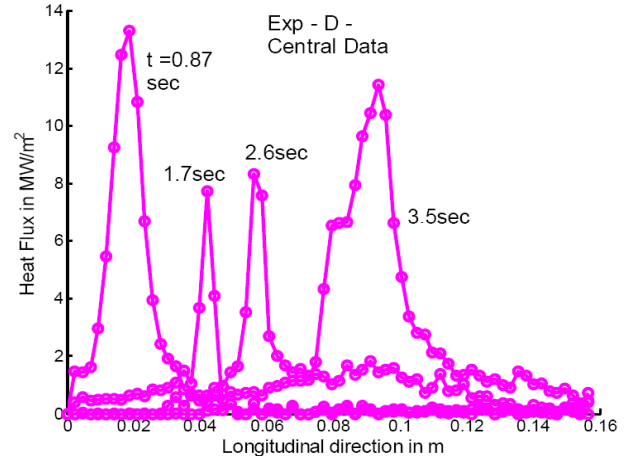


Figure 5.5: Heat flux distribution for nickel for jets' velocity 1.5 m/s

5.2.2 Maximum heat flux propagation

When the wetting front starts moving, the surface temperature drops sharply. Consequently, the surface heat flux increases drastically and reaches its maximum value [27]. The position of maximum heat flux with respect time for jet velocity of 1 m/s and 1.5 m/s is plotted in figures 5.6 and 5.7. These figures clearly depict that, in the initial stage, Higher jet velocity propagates the maximum heat flux faster than lower jet velocity, however, afterwards it always lag behind the lower jet velocity curve. The wetting front reaches the bottom of the sheet much faster in case of lower jet velocity. This fact can be further verified through the velocity of maximum heat flux MaxHF propagation. In order to determine

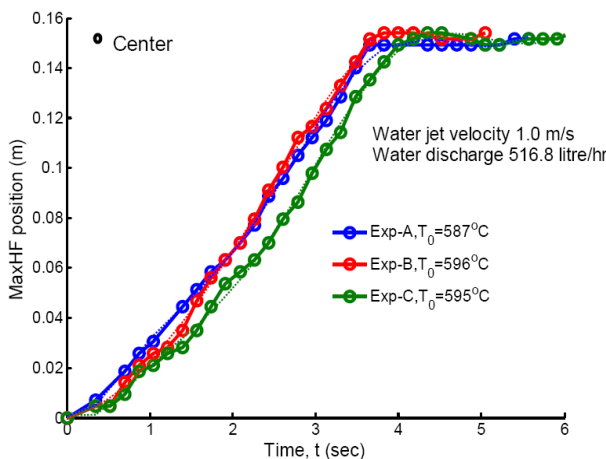


Figure 5.6: Maximum heat flux propagation for nickel for jets' velocity 1 m/s

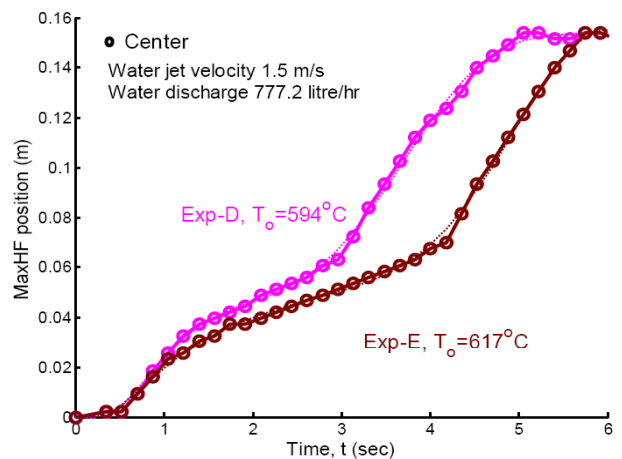


Figure 5.7: Maximum heat flux propagation for nickel for jets' velocity 1.5 m/s

the MaxHF propagation velocity, the MaxHF position data are fitted with least-squares method to a suitable polynomial and then polynomial equation is differentiated. Figures 5.8 and 5.9 represent the MaxHF propagation velocity as a function of time. Although, the curves drawn for both higher and lower jet velocity follow the same trends but their peaks and the time at which they reach at the peak varies significantly. This figure reveals the effect of water velocity on the MaxHF propagation. The wetting front reaches the bottom of the sheet at 4.3 sec in the case of 1 m/s water jet velocity while it takes 6 sec to reach the bottom of sheet in case of 1.5 m/s jet velocity. This phenomenon shows that increase in water velocity delays the MaxHF propagation velocity and eventually decrease the wetting front velocity.

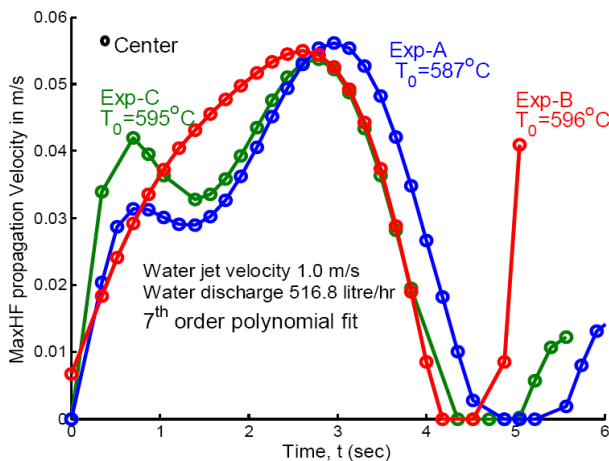


Figure 5.8: MaxHF propagation velocity for nickel for jets' velocity 1 m/s

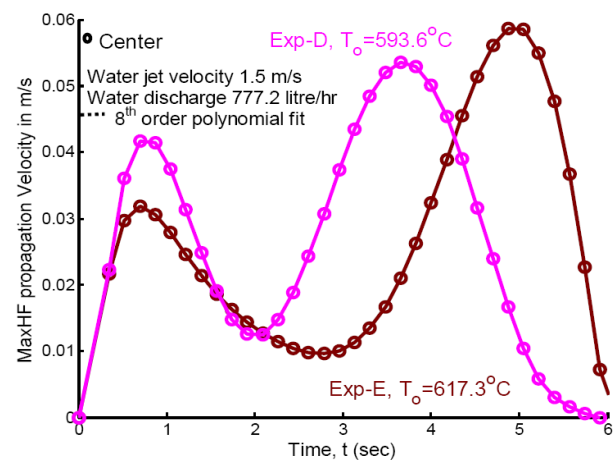


Figure 5.9: MaxHF propagation velocity for nickel for jets' velocity 1.5 m/s

5.2.3 Surface heat flux & temperature

Increase in water velocity delays the MaxHF propagation. To understand this fact quantitatively, an attempt is made to plot the surface heat flux as a function of temperature. For that, 20 mm left to the central line and 20 mm right to the central line of plate is modeled along with the central line as shown in figure 5.1. From the above three mentioned simulations, the nodes which lie near the center of the FEM mesh are considered for the heat flux vs. temperature plot. A trend line has been fitted for the two different velocity of water as shown in figure 5.10. The film boiling (above 400 °C), nucleate and transition boiling (120 - 400 °C), and free convection (below 120 °C) regions can be easily recognized from the figure 5.10. Increase in water velocity, decreases the MaxHF. For water velocity of 1.5 m/s, the heat flux curve shifts toward the lower temperature side and also shrinks when compared to the heat flux curve of water velocity 1 m/s. The heat flux in the nucleate boiling and film boiling zone is higher for lower water velocity. But in the free convection zone, heat flux in higher water velocity is greater than the lower water velocity case. Therefore, increase in water velocity and flow does not increase the heat extraction from the hot surface. But, the temperature at which MaxHF occurs is independent of cooling water velocity because for both of the water velocity, the MaxHF occurs nearly at 140 - 145°C.

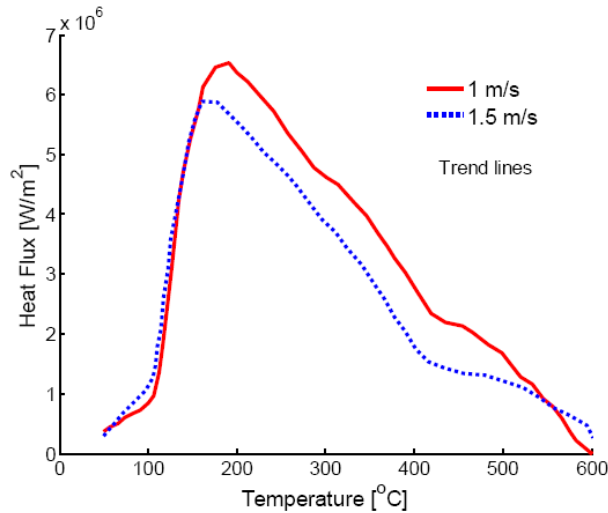


Figure 5.10: Heat flux as a function of surface temperature for two jet velocities

5.2.4 Importance of IHCP

Instead of solving the inverse heat conduction problem IHCP, one can simply evaluate the heat flux based on the temperature measurement at the back side of the plate assuming that the temperature on the quenched and measurement sites are equal. But, the temperature at the measured and quenched sides are not equal because of the finite conductivity of the material, specially , in transition and nucleate boiling regions. To verify this fact, the temperature difference between the quenched and measurement site nodes are plotted along the length of the plate as shown in figure 5.11. The temperature difference reaches a maximum value of around 125 °C in the wetting front region. Even though the thickness of the Nickel sheet is 2 mm, the temperature difference is not in the negligible range in wet region. This temperature difference has a huge impact on the heat flux estimation. Therefore, one can not avoid the IHCP. Other than the wetting front zone, the temperature difference is less than 20 °C for both the water velocity, therefore, one dimensional analysis can be carried out within . At the exact location of wetting front, the maximum temperature difference occurs.

The influence of cooling water velocity and quantity of flow on the heat flux is analyzed. It is observed that the increase in water velocity and flow does not increase the heat extraction from the hot surface. This fact is verified through the maximum heat flux (MaxHF) propagation and its velocity on time. Increase in water velocity delays the MaxHF propagation and also decreases the maximum heat flux value.

5.3 Mold with lower water flow

A mold, having seven orifices of diameter 2.5 mm each, is also installed and used for quenching three kinds of metals i.e. nickel, AA2024 and Inconel 600 with array of seven parallel water jets impinging at an angle of approximately 60° with axis perpendicular to the surface of metal. This mold is shown in figure 3.12. The volume flow rate of water is varied from 111 l/h to 228 l/h in seven stages so that quenching takes place with four

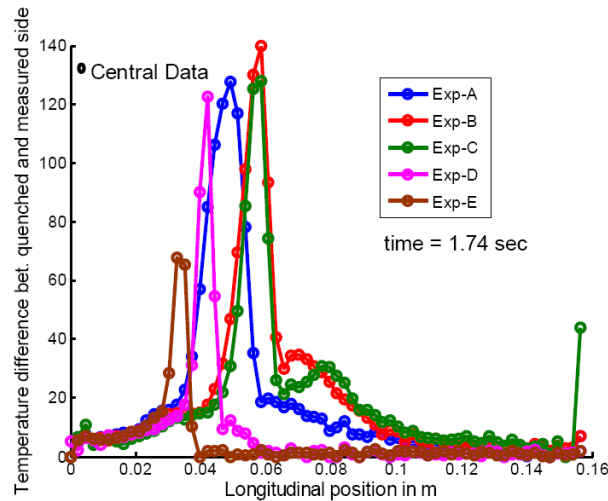


Figure 5.11: *Temperature difference between measured and quenched side*

different water jet velocities varying from 0.9 m/s to 1.84 m/s. The results of Inconel were not acceptable due to its very low conductivity, so they are not included in this discussion. The first step after installing the mold is to assess the repeatability of experiment with this cooling component. For that purpose, a nickel sheet having dimensions of $70 \times 140 \times 2$ mm is heated to 600 °C and 800 °C and quenched four times for each case with the same jet velocity of 1.24 m/s. In order to assess the repeatability of experiments, temperature profiles, heat flux profile at specific position and wetting front velocity have been drawn and compared for all four repeated experiments. Temperature profiles have been drawn in figures 5.12 and 5.13 for two specific position i.e. 51 mm and 110 mm from the top of the rectangular sheet at the central vertical line for the initial surface temperatures of 600 °C and 800 °C respectively. Figures depict that the curves are almost overlapping to each other. However, the fluctuation can be observed for the case of initial temperature of 800 °C at the distance of 110 mm from the top of the sheet. Due to the manual arrangement of experimental set up, this sort of minor fluctuation is unavoidable. Because of this fluctuation, this mold have not been used for examining the influence of water quality during quenching. The next assessment is the distribution of heat flux along the central line of the sheet at a specific distance from the top. Figures 5.14 and 5.15 show the relation between heat flux and time at a distance of 51 and 110 mm from top when the initial surface temperatures are 600 °C and 800 °C respectively.

Maximum heat flux position, shown by the peak of the curve, lies on the same time for the four repeated experiments i.e. at two seconds in figure 5.14 and at fifth second in figure 5.15. Maximum heat flux position is drawn with respect to time and plotted in figures 5.16 and 5.17 for four repeated experiments. Wetting front velocity found to be same in all four similar cases. When comparing for initial surface temperature, wetting front velocity is higher for lower initial surface temperature i.e. 29 mm/sec for 600 °C than for higher initial surface temperature i.e. 19 mm/sec for 800 °C.

Variation of temperature with respect to times for AA2024 for four velocities is drawn in figures 5.18 and 5.19. As the velocity increases from 0.9 to 1.5 m/s, the cooling rate also increases for the two positions of 53 and 96 mm from the top edge of the sheet. However,

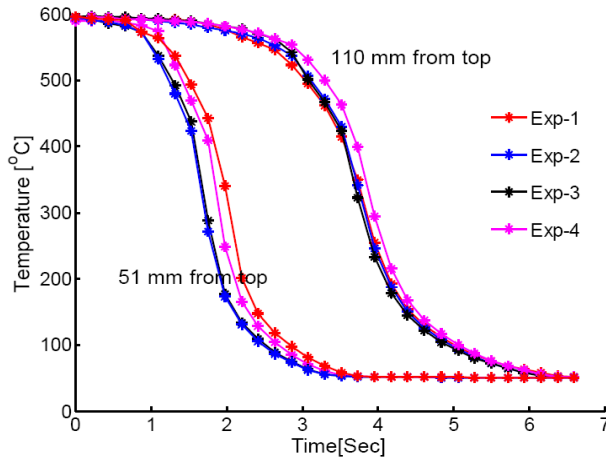


Figure 5.12: Temperature-time curves for four repeated experiments at different positions for initial temperature ≈ 600 °C

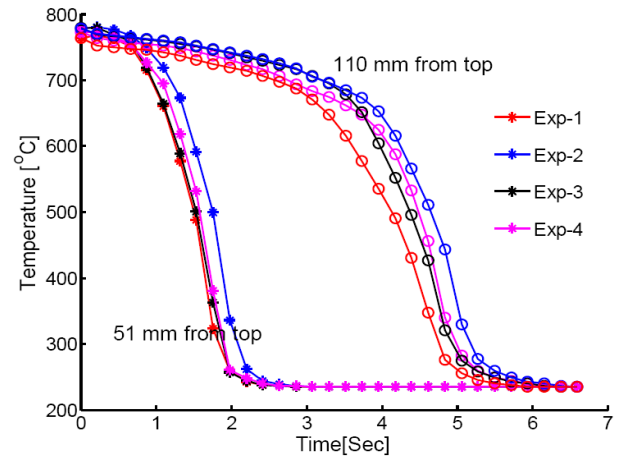


Figure 5.13: Temperature-time curves for four repeated experiments at different positions for initial temperature ≈ 800 °C

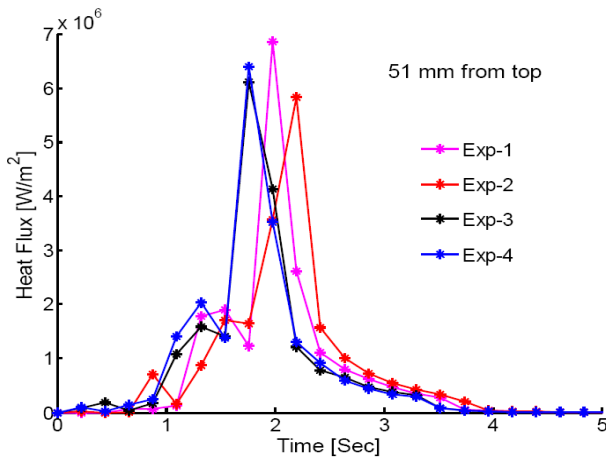


Figure 5.14: Heat flux-time curves for four repeated experiments at specific position for initial temperature ≈ 600 °C

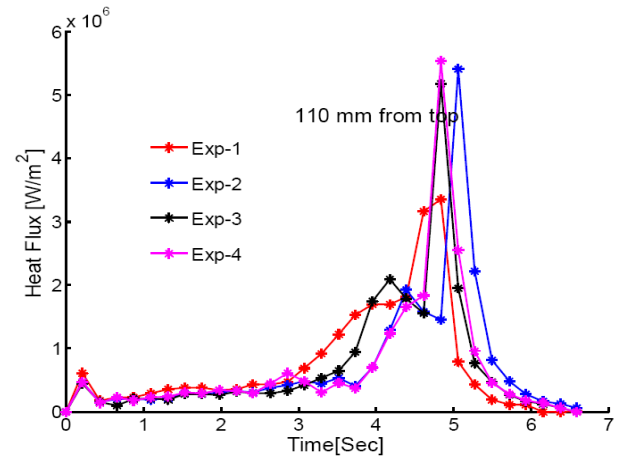


Figure 5.15: Heat flux-time curves for four repeated experiments at specific position for initial temperature ≈ 800 °C

the highest velocity of 1.8 m/s seems to be exceptional, and the cooling rate is slower in this case. It may occur due to the fact that at higher jet velocity, the jet rebounds after striking the metal surface and only a fraction of the amount of water cools the lower area of the hot sheet. The heat flux distribution over the length of AA2024 sheet is drawn in figures 5.20 and 5.21 for two points of time i.e. 3.3 seconds and 5.5 seconds. The distance of position of maximum heat flux from the top of the sheet increases with increasing the water jet velocity. However, the same exception of maximum jet velocity of 1.8 m/s is repeating in this case also. Maximum heat flux propagation velocity is plotted in figure 5.22 for four jet velocities for AA2024. The lowest jet velocity of 0.9 m/s results in the lowest wetting front velocity i.e. ≈ 9.5 mm/s while the other three higher jet velocities result in higher wetting front velocity i.e. ≈ 17 mm/s.

The relation of average heat flux with surface temperature for all positions on the central line of AA2024 sheet is presented in figure 5.23 for four jet velocities. These curves are very difficult to draw because of a higher degree of noise, especially in transition and nucleate

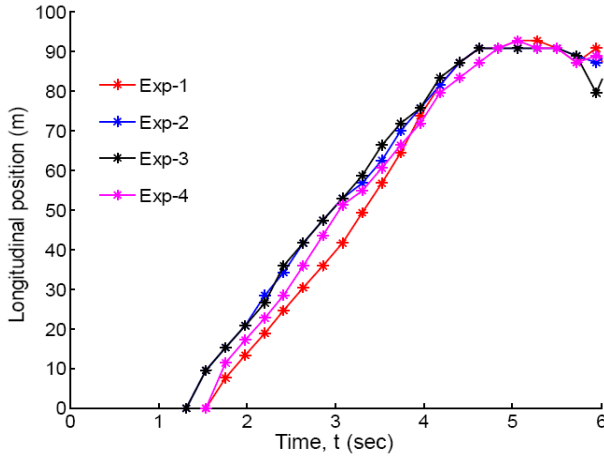


Figure 5.16: Wetting front propagation for four repeated experiments for initial surface temperature $\approx 600\text{ }^{\circ}\text{C}$

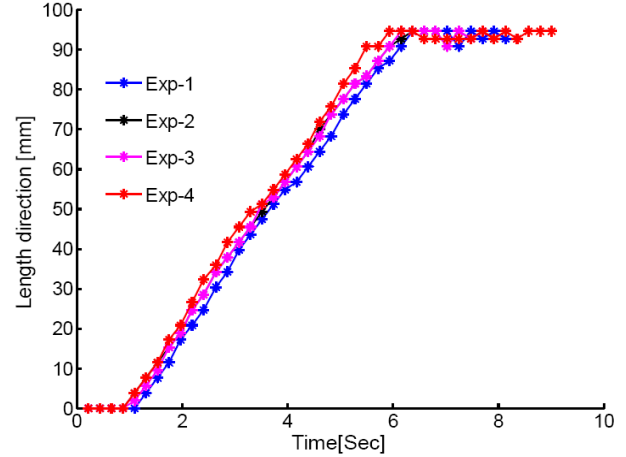


Figure 5.17: Wetting front propagation for four repeated experiments for initial surface temperature $\approx 800\text{ }^{\circ}\text{C}$

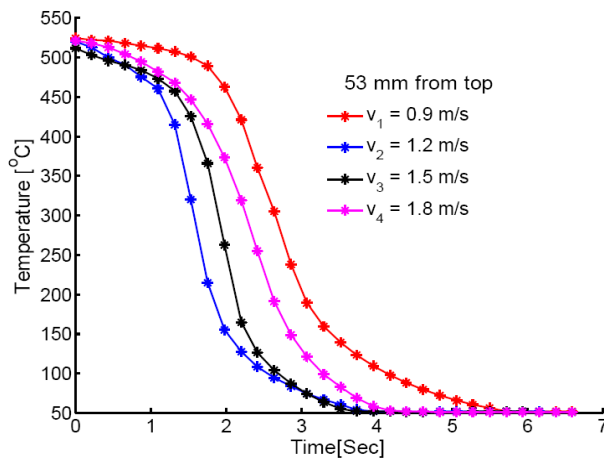


Figure 5.18: Temperature profile at a distance of 53 mm from top for AA2024 for four jets' velocities

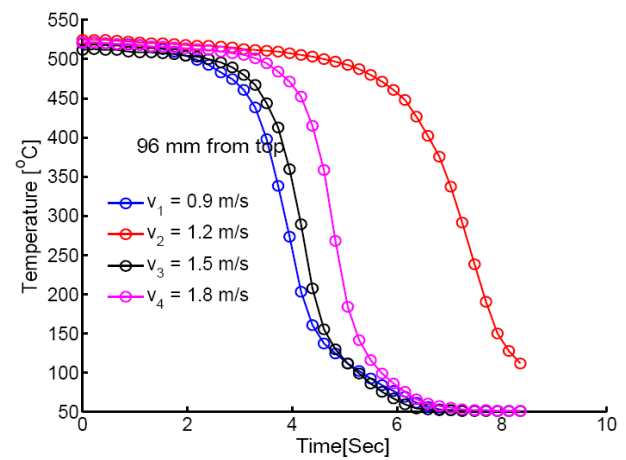


Figure 5.19: Temperature profile at a distance of 96 mm from top for AA2024 for four jets' velocities

boiling region. These are the average curves drawn by curve fitting for the actual points. The critical heat flux lies between 2 to 3 MW/m² at surface temperature of $\sim 180\text{ }^{\circ}\text{C}$ for the four cases. It is difficult to locate the exact value of Leidenfrost point in this diagram because they are approximate curves. However, it can be concluded that higher the jet velocity, higher the average heat flux at a specific surface temperature.

Experiments were repeated for four jets' velocities for nickel. The velocities are varied as 0.9, 1.2, 1.5 and 1.8 m/s. The results show almost the same trend as shown in case of AA2024. The temperature profiles for the two positions i.e. 53 and 96 mm from the top of the sheet are shown in figures 5.24 and 5.25. The cooling rate increases with increasing jets' velocity with the exception of velocity of 1.8 m/s. Heat flux distribution along the length of the sheet is plotted in figures 5.26 and 5.27. The maximum heat flux position lies at higher distance for higher velocity with exception of jet velocity of 1.8 m/s. Similar effect can be noticed in figures 5.28 and 5.29. In these figures heat flux is drawn with respect to time at a certain position on the central line of the nickel sheet. Higher velocities

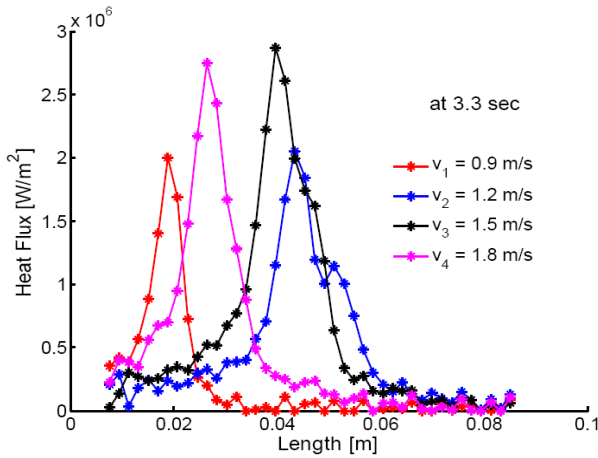


Figure 5.20: Heat flux-length curves for AA2024 for four jets' velocities at 3.3 second

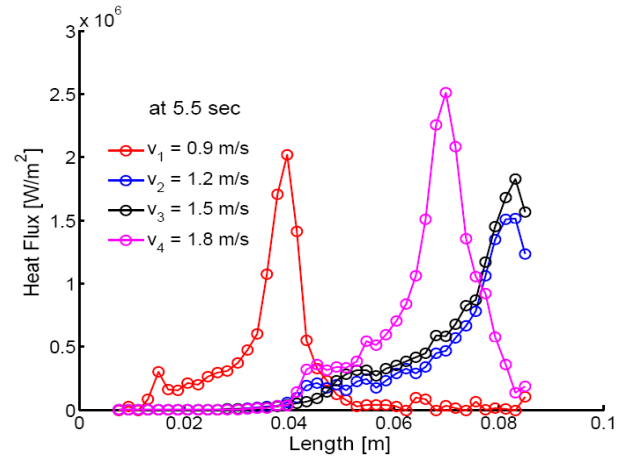


Figure 5.21: Heat flux-length curves for AA2024 for four jets' velocities at 5.5 second

lead to faster movement of position of maximum heat flux. and this is verified slopes of maximum heat flux propagation or wetting front velocities in figure 5.30. Wetting front velocity for the jet velocity of 0.9 m/s is ~ 16 mm/s whereas; for the jet velocity of 1.5 m/s, it is calculated as ~ 28 mm/s. However, the highest jet velocity shows exceptional result of again reducing the wetting front velocity which may be due to the fact that at highest velocity the water jet rebounds after the first strike and only a fraction of total amount of water flow is used to quenching the remaining portion of the nickel sheet.

The average heat flux of all the selected points at the central line are plotted against the surface temperature for nickel sheet in figure 5.31. The maximum or critical heat flux lies at 6 MW/m^2 at the temperature of 200°C . Comparing this value of critical heat flux with that of AA2024, one notice that it is two or three times higher than that of AA2024 with the same flow. It means that the heat flux not only depends on water through put, but it also depends on thermo-physical properties of the metal. The Leidenfrost point seems to be approximately 400°C for this kind of cooling method.

5.4 Measurement of wetting front velocity by high speed camera

In earlier sections of this chapter about the calculated wetting front velocities, the cases of spray quenching and quenching by array of jets were discussed. It was assumed that position of maximum heat flux is the position of wetting front and then the movement of this point was regarded as the propagation velocity or wetting front velocity. Those results can be validated by actual measurement of wetting front velocity with the help of high speed camera. The experiment plan for this analysis is made in two categories. At first, atomized spray quenching is analyzed for three materials i.e. AA2024, nickel and Inconel 600 with three different impingement densities as shown in figures 5.32 and 5.33 and secondly, quenching by seven jets of orifice diameter of 2.5 mm is analyzed for same three materials i.e. AA2024, nickel and Inconel 600 for four different jet outlet velocities as shown in figures 5.34 and 5.35. The images are captured by the camera with a frequency

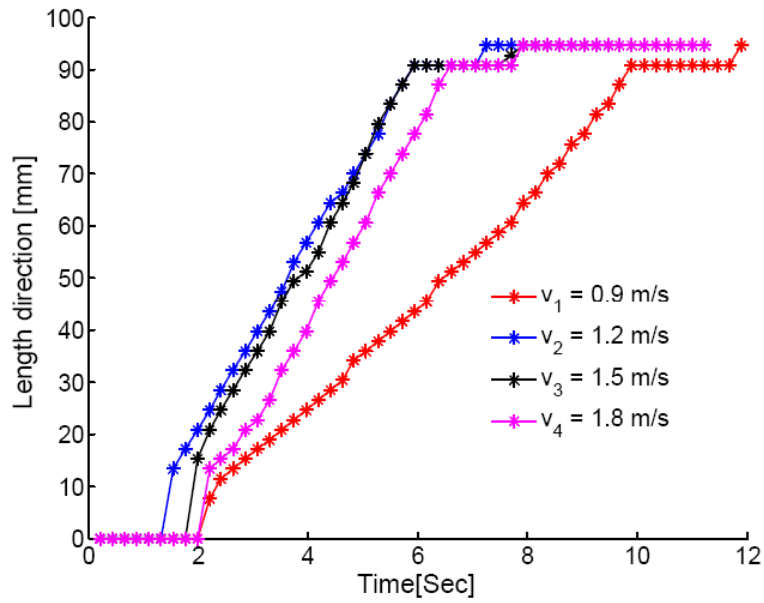


Figure 5.22: Maximum heat flux propagation for AA2024 for four jets' velocities

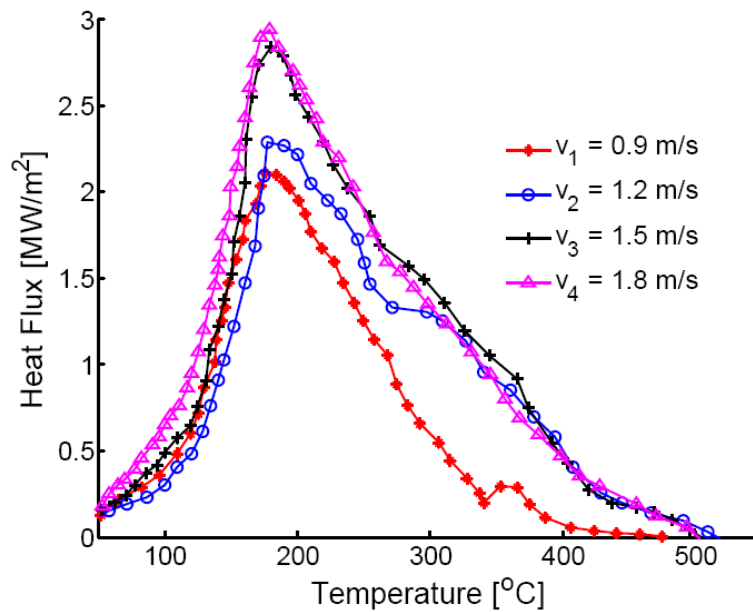


Figure 5.23: Heat flux as a function of surface temperature for AA2024 for four jets' velocities

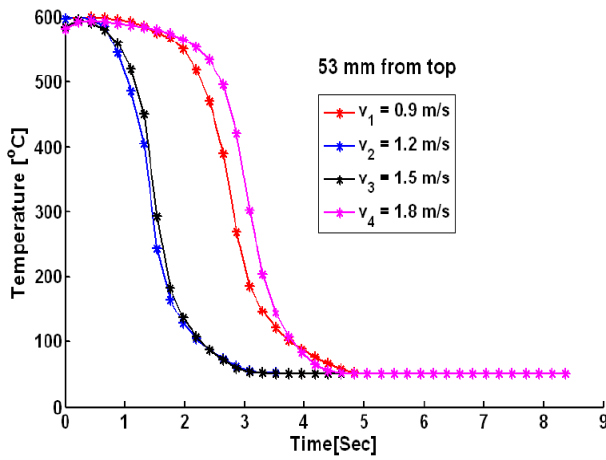


Figure 5.24: Temperature profile at a distance of 53 mm from top for nickel for four jets' velocities

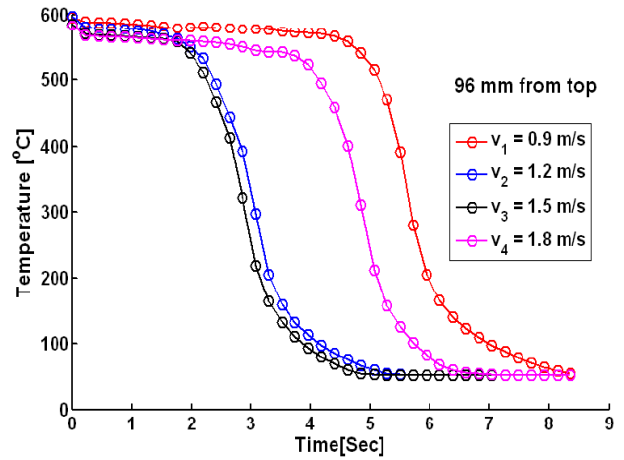


Figure 5.25: Temperature profile at a distance of 96 mm from top for nickel for four jets' velocities

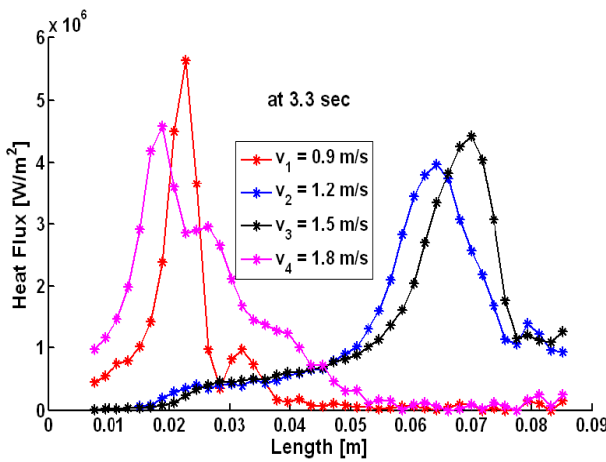


Figure 5.26: Heat flux-length curves for nickel for four jets' velocities at 3.3 second

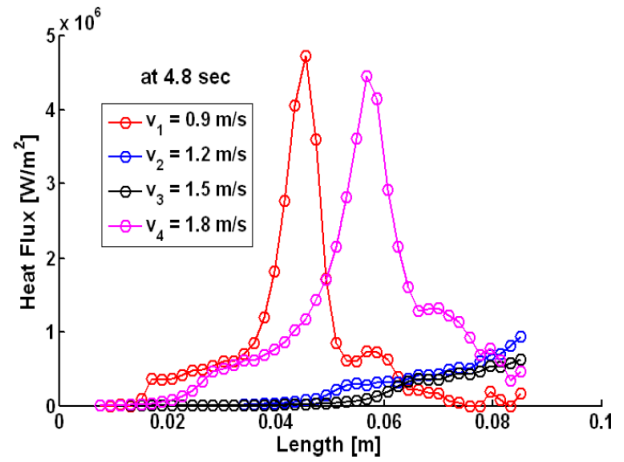


Figure 5.27: Heat flux-length curves for nickel for four jets' velocities at 5.5 second

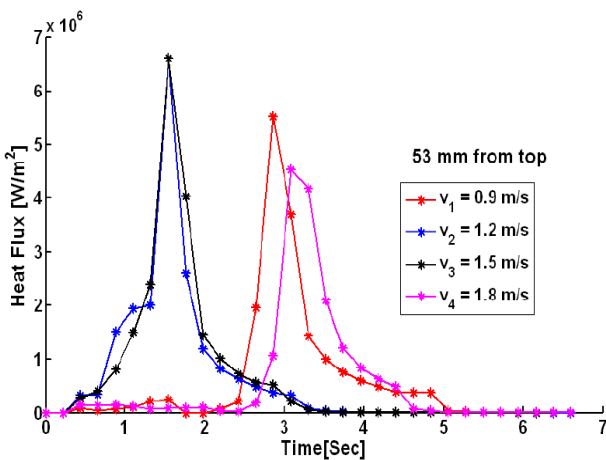


Figure 5.28: Heat flux-time curves for nickel for four jets' velocities at 3.3 second

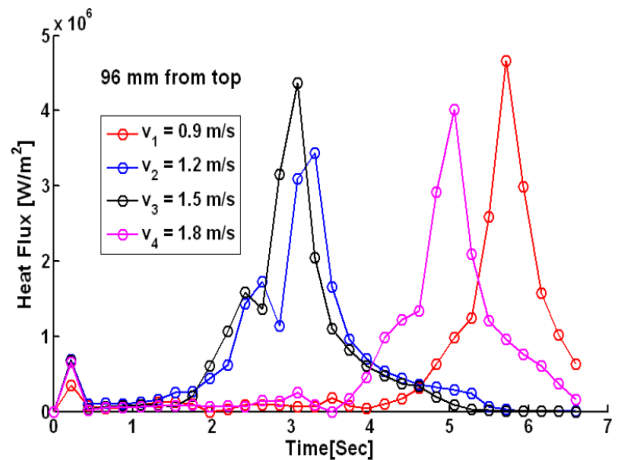


Figure 5.29: Heat flux-time curves for nickel for four jets' velocities at 5.5 second

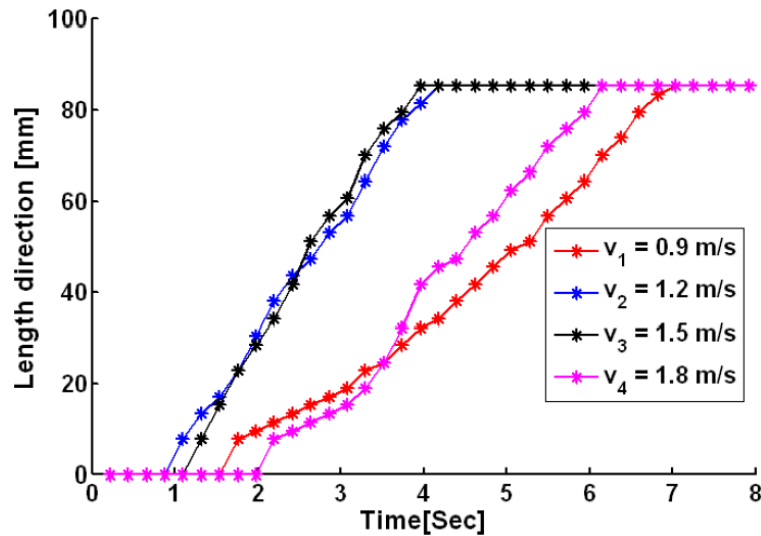


Figure 5.30: Maximum heat flux propagation for nickel for four jets' velocities

of 50 Hz for spray and with a frequency of 125 Hz for jets. After the experiments have been performed, the pictures of every 25th image for spray and every 50th image of jet quenching are saved and the wetting front position is measured using the actual scale on the picture. This means that the wetting front position after every 0.5 second and 0.4 second is measured for the two methods of quenching respectively.

Results for atomized spray quenching for three metals are depicted in figures 5.36, 5.37 and 5.38 for AA2024, nickel and Inconel respectively. The curves are drawn between wetting front position in mm and time. The relations seemed to be almost linear. Therefore, each curve can be represented by a straight line by performing linear regression and the slope of this approximate straight line is regarded as the wetting front velocity. It is obvious from the figures that wetting front velocity has a direct relation with the impingement density i.e. higher the impingement density faster will be the wetting front velocity. For example, the wetting front velocity is 3.5 mm/s for impingement density of 21 kg/m²/s whereas; it is 5 mm/s for impingement density of 32 kg/m²/s for AA2024 referring to figure 5.36. Similarly, wetting front velocities are 2.4, 3.3 and 3.9 mm/s for impingement densities of 21, 32 and >32 respectively for nickel as shown in figure 5.37. (The third and highest impingement density could not be measured by patternator because the water splashes out of the collecting tubes at the high air pressure of 4 bar which results in less weight of collected water.) Same trend can be observed for Inconel 600 in figure 5.38.

Results for quenching by array of seven water jets are shown in figures 5.39, 5.40 and 5.41 for AA2024, nickel and Inconel respectively. The wetting front velocity is almost constant throughout the quenching process. Jets with four different velocities i.e. 0.9, 1.2, 1.5 and 1.8 m/s were employed to quench rectangular sheets. Wetting front velocity in this case depends directly on jets' exit velocity. Figure 5.39 illustrates that when the outlet jets' velocities are raised from 0.9 to 1.5 m/s, the wetting front velocity also increases from 15.8 to 21.8 mm/s but increasing the jet's velocity further to 1.8 m/s results in opposite way. This confirms the fact that there must be an optimum maximum jet's velocity beyond which the wetting front velocity starts decreasing and in the present case it is 1.5 m/s as

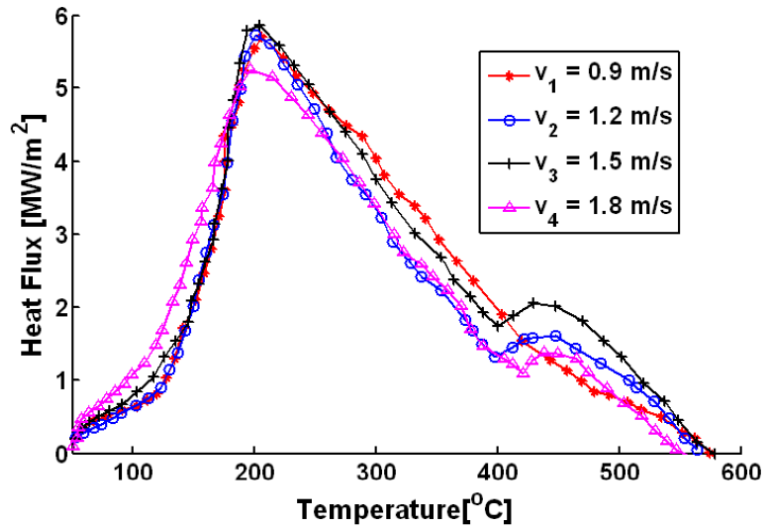


Figure 5.31: Heat flux as a function of surface temperature for nickel for four jets' velocities

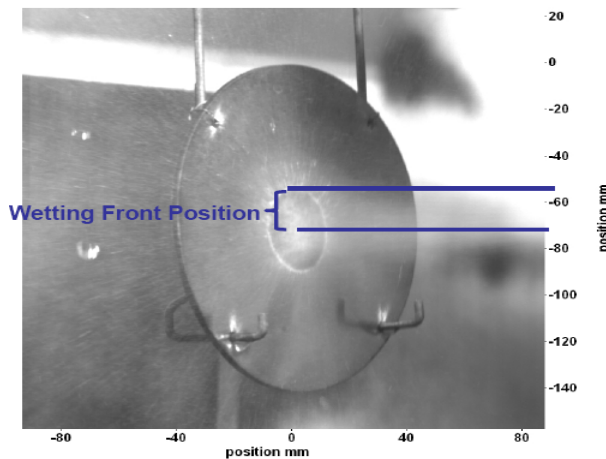


Figure 5.32: Visual estimation of wetting front velocity for spray quenching by high speed camera at initial stage

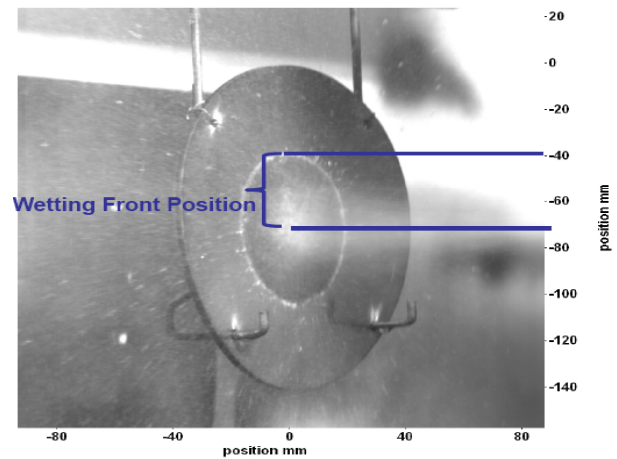


Figure 5.33: Visual estimation of wetting front velocity for spray quenching by high speed camera at later stage

illustrated in all three cases of metals. This trend is more clear from figures 5.40 and 5.41.

It is important to note that the wetting front velocity may also depend on factors other than the impingement density of jets' outlet velocity e.g. the thermo-physical properties of metal, its surface structure and/or its thickness.

The relation between wetting front velocity measurement by high speed photography or by solving inverse heat conduction problem and water jets velocity is plotted in figure 5.42 for three materials i.e. AA2024, nickel and Inconel 600. Initially, the wetting front velocity increases with jet's velocity. However, once the jet velocity reaches to 1.8 m/s, the wetting front velocity decreases. So, in this setup, 1.5 m/s jet's velocity might be the highest optimum velocity and when it is increased further, the wetting front velocity start decreasing.

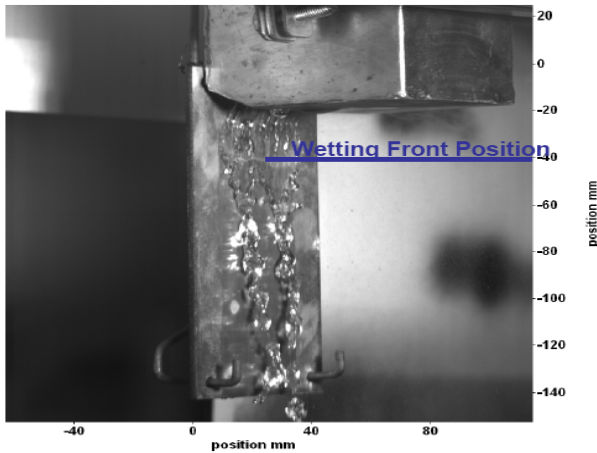


Figure 5.34: Visual estimation of wetting front velocity for jet quenching by high speed camera at initial stage

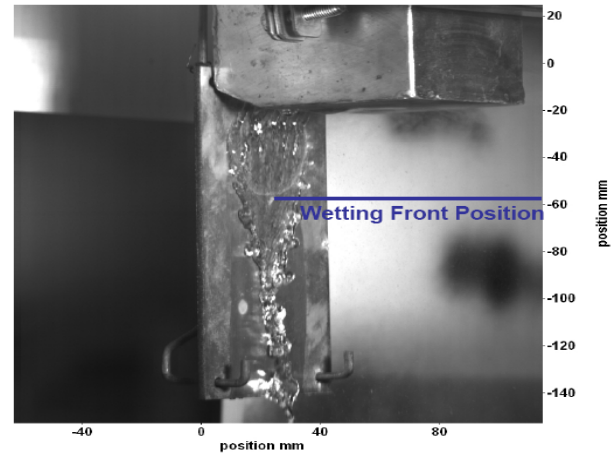


Figure 5.35: Visual estimation of wetting front velocity for jet quenching by high speed camera at later stage

5.5 Surface roughness & its influence

Surface roughness consists of surface irregularities which result from the various machining processes. These irregularities combine to form surface texture. Roughness includes the finest (shortest wavelength) irregularities of a surface. Roughness generally results from a particular production process or material condition.

Roughness height

It is the height of the irregularities with respect to a reference line. It is measured in millimeters or microns or micro inches. It is also known as the height of unevenness.

Roughness width

The roughness width is the distance parallel to the nominal surface between successive peaks or ridges which constitute the predominate pattern of the roughness. It is measured in millimeters.

Roughness width cut off

Roughness width cut off is the greatest spacing of respective surface irregularities to be included in the measurement of the average roughness height. It should always be greater than the roughness width in order to obtain the total roughness height rating.

Waviness

This refers to the irregularities which are outside the roughness width cut off values. Waviness is the widely spaced component of the surface texture. Waviness includes the more widely spaced (longer wavelength) deviations of a surface from its nominal shape. This may be the result of workpiece or tool deflection during machining, vibrations or tool runout.

In our case, we did not employ the method of roughness measurement to find out the surface roughness of metal sheet because the equipment was unavailable. That is why, we

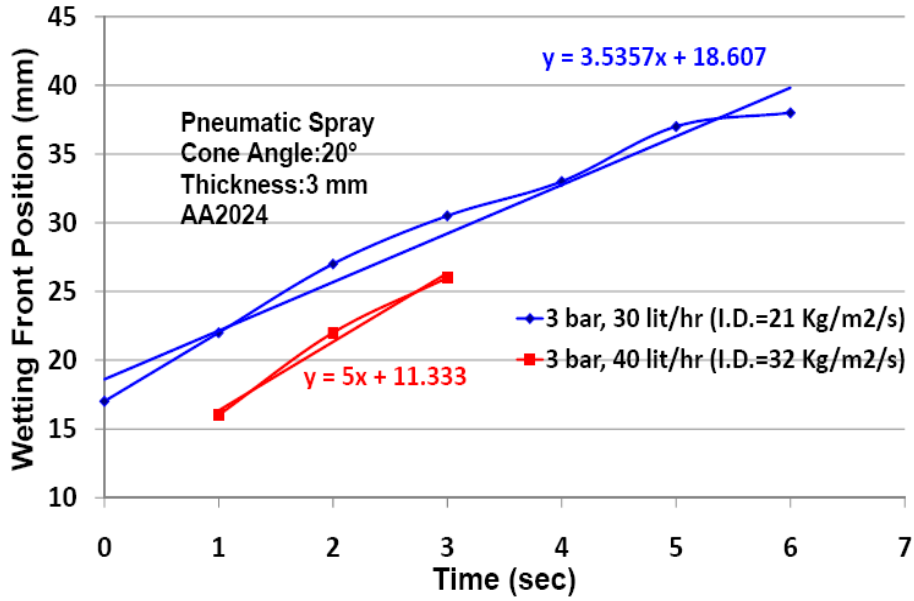


Figure 5.36: Wetting front propagation during spray quenching for AA2024 at different impingement densities

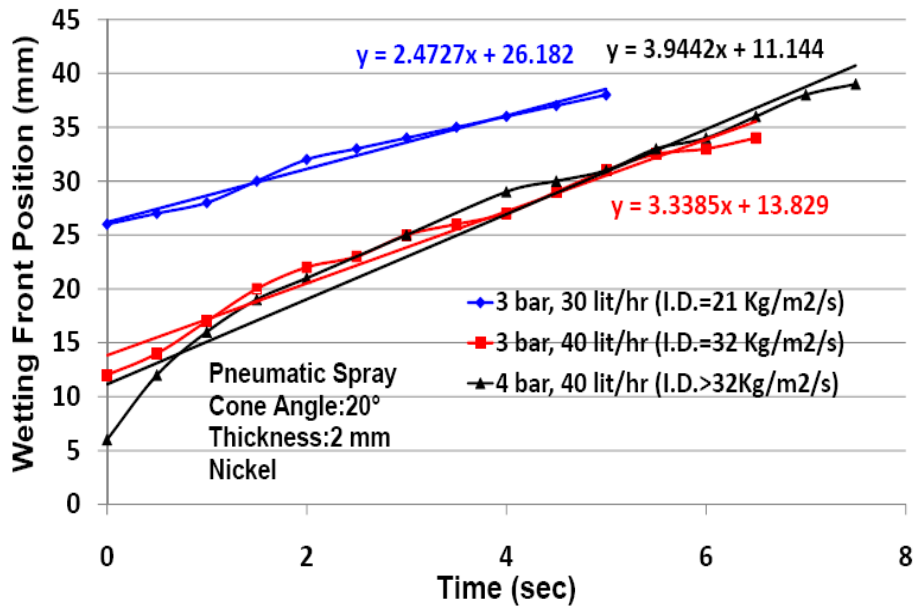


Figure 5.37: Wetting front propagation during spray quenching for nickel at different impingement densities

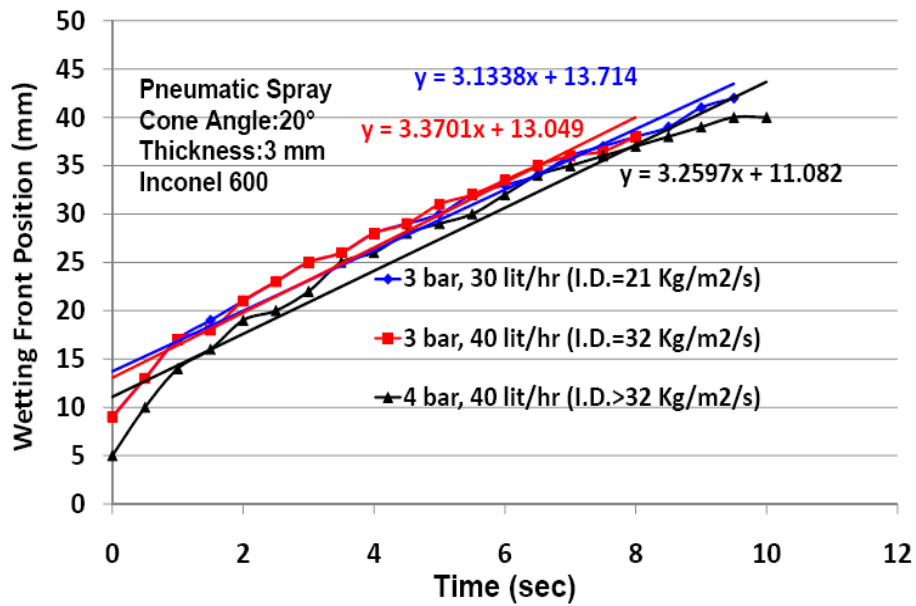


Figure 5.38: Wetting front propagation during spray quenching for Inconel 600 at different impingement densities

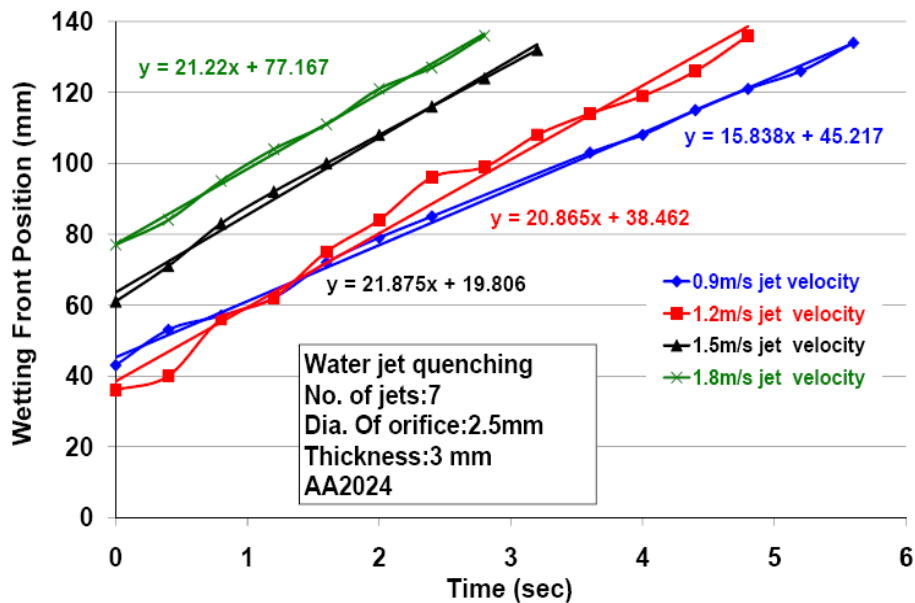


Figure 5.39: Wetting front propagation during jets' quenching for AA2024 at different jet velocities

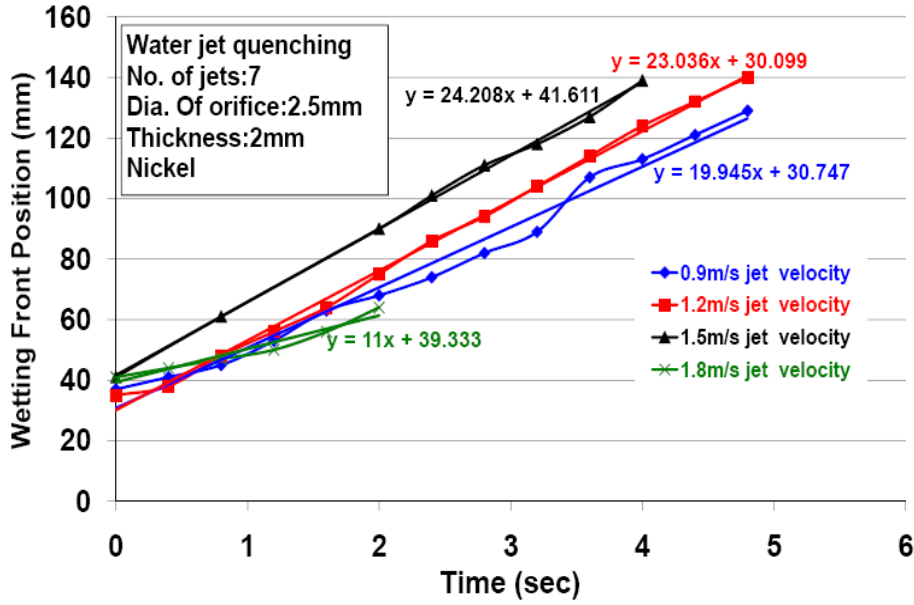


Figure 5.40: Wetting front propagation during jets' quenching for nickel at different jet velocities

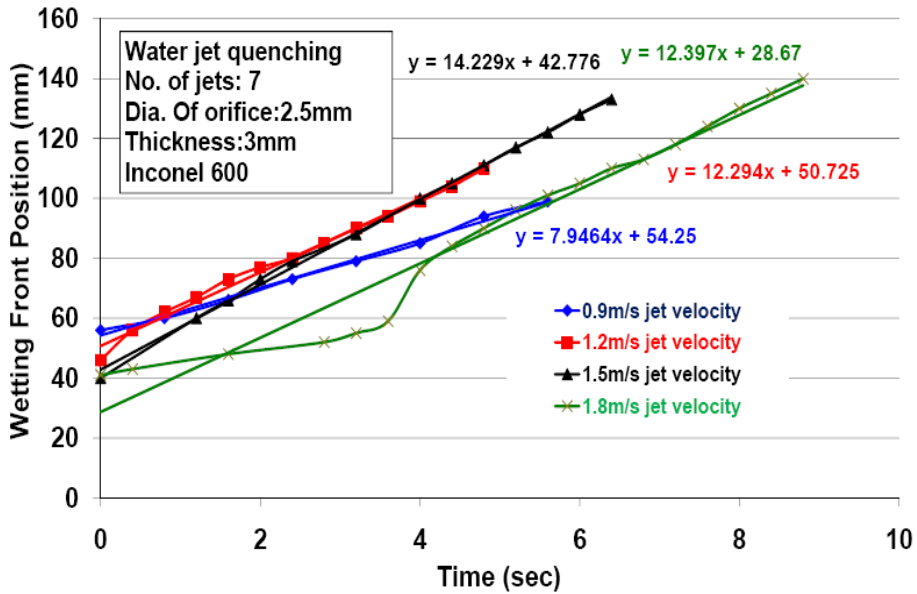


Figure 5.41: Wetting front propagation during jets' quenching for Inconel 600 at different jet velocities

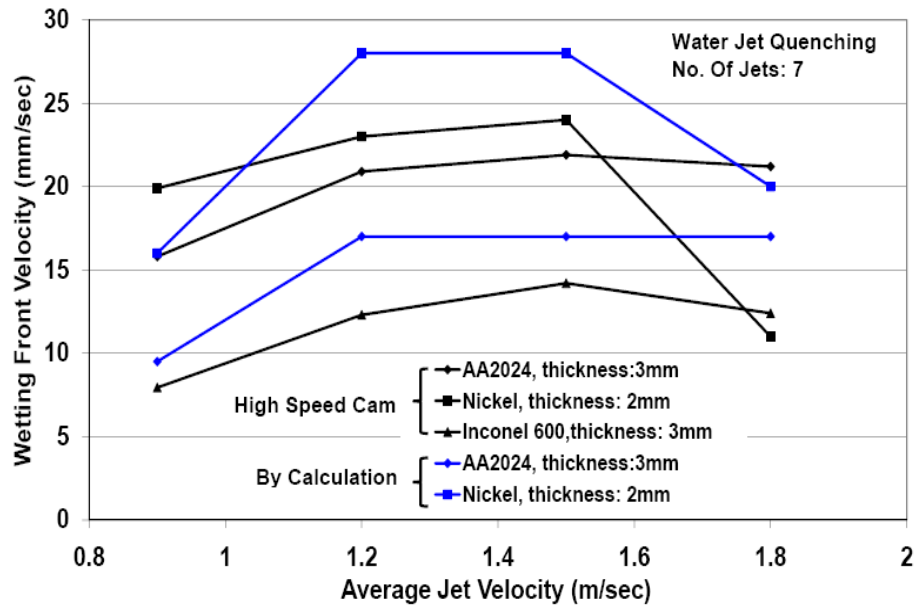


Figure 5.42: Variation of wetting front velocity with respect to jet velocity for three materials

used the numbers written on the sand papers to show the surface roughness produced by those papers. The selected sand paper numbers were 40, 60. Greater the number is lower will be the surface roughness produced by the sand paper. Table 5.3 shows the range of surface roughness caused by different manufacturing processes. Table 5.4 summarizes the results of experiments performed for analyzing the influence of surface roughness. It seems that the roughness developed by these sand papers was not that significant to affect the heat transfer and Leidenfrost temperature values. This is why, it is required that more rough surfaces are developed and then this effect should be analyzed.

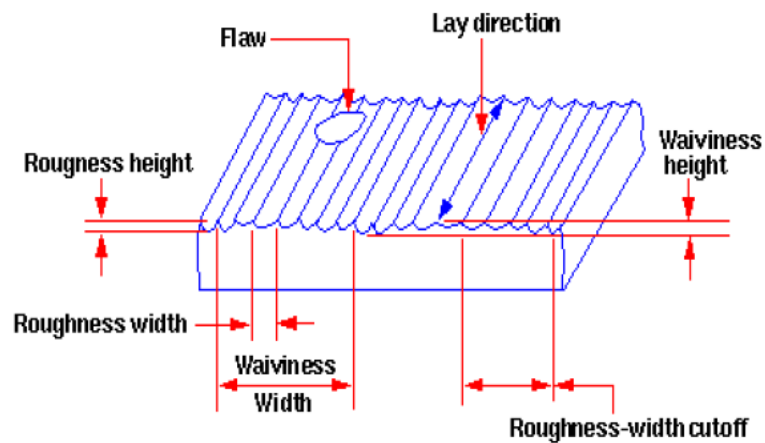


Figure 5.43: Measurement of surface roughness

Table 5.3: Obtainable range of surface roughness in microns

Manufacturing process	With difficulty	Normally	Roughing
Sand casting		6.3 – 12.5	
Permanent mold	0.8 – 1.6	1.6 – 6.3	12.5 – 25
Die casting		0.8 – 3.2	
Forging	1.6 – 3.2	3.2 – 25	
Extrusion	0.4 – 0.8	0.8 – 6.3	
Rolling	0.4 – 0.8	0.8 – 3.2	
Flame cut		25 – 50	
Hack saw cut		6.3 – 50	
Bandsaw, chipping		3.2 – 50	
Filing	0.8 – 1.6	1.6 – 12.5	
Emery polish	0.1 – 0.4	0.4 – 1.6	1.6 – 3.2
Shot blast	1.6 – 3.2	3.2 – 50	
Tumbling		0.2 – 12.5	
Abrasive belt		0.1 – 6.3	
Fiber wheel brushing	0.1 – 0.2	0.2 – 0.8	0.8 – 1
Cloth buffing	0.012 – 0.05	0.05 – 0.1	
Shell milling	1.6 – 3.2	3.2 – 25	25 – 50
Drilling	3.2 – 6.3	6.3 – 25	
Planing & shaping		1.6 – 12.5	
Face milling	0.8 – 1.6	1.6 – 12.5	12.5 – 50
Turning	0.2 – 1.6	1.6 – 6.3	6.3 – 50
Boring	0.2 – 1.6	1.6 – 6.3	6.3 – 50
Reaming	0.4 – 0.8	0.8 – 6.3	6.3 – 12.5
Cyl. grinding	0.025 – 0.4	0.4 – 3.2	3.2 – 6.3
Centerless grinding	0.05 – 0.4	0.4 – 3.2	
Internal grinding	0.025 – 0.4	0.4 – 3.2	3.2 – 6.3
Surface grinding	0.025 – 0.4	0.4 – 3.2	3.2 – 6.3
Broaching	0.2 – 0.8	0.8 – 3.2	3.2 – 6.3
Super finishing	0.025 – 0.11	0.1 – 0.4	
Honing	0.025 – 0.11	0.1 – 0.4	
Lapping	0.006 – 0.05	0.05 – 0.4	
Milling, spiral bevel	1.56 – 3.2	3.2 – 12.5	12.5 – 25
Milling with form cutter	1.6 – 3.2	3.2 – 12.5	12.5 – 25
Hobbing	0.8 – 3.2	3.2 – 12.5	12.5 – 25
Shaping	0.4 – 1.6	1.6 – 12.5	12.5 – 250
Planing	0.4 – 1.6	1.6 – 12.5	12.5 – 50
Shaving	0.4 – 0.8	0.8 – 3.2	
Grinding, criss cross	0.4 – 0.8	0.8 – 1.6	
Grinding	0.1 – 0.4	0.4 – 0.8	
Lapping	0.05 – 0.2	0.2 – 0.8	

Table 5.4: Summary of results of experiments for surface roughness

Kind of metal	Composition	Thickness (mm)	Surface roughness (No. of sand paper)	Average impingement density (kg/m ² /s)	Leidenfrost temperature (°C)
Aluminium alloy AA2024	AlCu4Mg1, (Al: 92.4-97.8 %, Cu:2.0-4.9 %, Mg:0.15-1.8 %)	3	Polished	2.4	240-245
				3.55	
				5	
			40	2.4	240-245
				3.55	
				5	
			60	2.4	240-245
				3.55	
				5	
Nickel alloy Inconel 600	Ni:72 %, Cr:14-17 %, Fe: 6-10 %, Magnesium 1 %	0.3	Polished	2.4	280-290
				3.55	
				5	
			Rough	2.4	280-290
				3.55	
				5	
Pure aluminum	Al 100 %	0.8	Polished	1.4	230-240
				2.8	
				5	
			40	1.4	230-240
				2.8	
				5	
			Highly rough	1.4	230-240
				2.8	
				5	
Copper alloy L49	CuNi9Sn2	4	Polished	2.8	280-290
				5	
Copper alloy B14	CuSn5	4	Polished	5	270
Copper alloy K12	SE-Cu	2.7	Polished	5	260
Copper alloy K75	CuCr0,3Ti0,15Si0,002	3	Polished	5	230

6 Conclusion

Two types of spray have been employed for quenching hot metals i.e. pneumatic spray (liquid with air) and hydraulic spray (only liquid). Hot circular discs, of diameter 140 mm and thickness 2 - 3 mm, made up of nickel, AA6082, AA2024 etc. were subjected to quenching by these pneumatic and hydraulic spray. The impingement density, being the most influential parameter on heat transfer rate, is distributed as a normal distribution for pneumatic atomizing nozzle and symmetric with respect to spray cone axis while, for hydraulic full cone nozzle, it showed variable distribution. The most symmetric one for hydraulic spray was at water flow of 20 l/h. The heat transfer coefficient in film boiling regime was found to be 10 times higher for pneumatic spray than hydraulic spray for the given nozzles. The initial surface temperature has shown a little influence on Leidenfrost temperature and heat transfer coefficient in film boiling region. LFP increased to range of 15 °C when the initial surface temperature was decreased from 700 to 400 °C. The temperature distribution along the diameter of the disc for the two types of spray shows that the temperature gradients are much higher for pneumatic spray than hydraulic spray and, similarly, when temperature distribution profiles are compared for AA6082 and nickel, they are more uniformly distributed in case of AA6082 because of higher thermal conductivity of aluminum.

Atomized spray cooling reaches with values up to 10,000 W/m²/K within film boiling region which is much higher heat transfer coefficients than hydraulic spray cooling. The heat transfer coefficient is primarily dependent on the impingement density. To obtain a given heat transfer coefficient, the atomized spray quenching requires less amount of water than the conventional spray quenching. An array of nozzles produces more uniform quenching profiles than a single nozzle. With this quenching technique, the water layer does not form on the hot surface with temperature above the Leidenfrost temperature, and the nucleate boiling does not occur at the edges like in case of immersion quenching where the immediate collapse of the vapor film at the edges results in extremely high stresses and distortions. The influence of additives in cooling water on heat transfer in quenching process was one of the primary goal of this work. As the target process was secondary cooling of non-ferrous metals, the experiments were started with array of jets to mimic the secondary quenching in DC casting. The main problem with this method was that the heat flux magnitudes were much higher because of high flow rate of coolant and the effect of low concentrations of additives in cooling water were not possible to realize with the given experimental set-up. Later, the jets were substituted by pneumatic spray and then hydraulic spray was finally selected for water quality analysis so that the influence of air is also excluded. Experiments for analyzing the effect of dissolving seven different salts i.e. NaCl, Na₂SO₄, Na₂CO₃, NaHCO₃ and MgSO₄, borax and CaCO₃ and a surfactant "ethoxylated ester" in cooling water on heat transfer for atomized spray (with air) and spray cooling of hot metal surface were conducted. The results were compared with those of de-ionized water. It was observed that addition of salts increases the heat transfer in film boiling, transition boiling and nucleate boiling regimes. Deposition of salts at higher temperature may degrade the

surface roughness and promote the Leidenfrost temperature (LFP) which may promote the nucleate boiling heat transfer. It has been observed in all cases of salt solutions that LFP was shifted to a higher temperature and consequently the film boiling region is shortened. Borax and MgSO_4 increased the cooling efficiency significantly while NaCl showed the least influence. An addition of only 3 g/l of MgSO_4 shortened the time of cooling to 50 % i.e. from 20 sec to 10 s. The critical heat flux was increased from 1.2 to 2.2 MW/m^2 and the surface temperature corresponding to CHF point increased by 50 °C from 170 to 220 °C. Maximum heat flux position was assumed to be the position of wetting front and its propagation was assumed as wetting front velocity. MgSO_4 solution resulted in highest wetting front velocity. Similarly, a concentration of 2.5 g/l of Borax in cooling water enhanced the CHF from 1.25 to 1.6 MW/m^2 and the corresponding surface temperature was increased by 30 °C. Other salts also exhibited the same trend with a bit less intensity. On the other hand, the surfactant ethoxylated ester (which is normally added to cooling water in secondary cooling of DC casting of aluminum ingots) solution decreased the LFP from 420 to 300 °C for pneumatic spray and eventually the film boiling region was prolonged which is contrary to the most of the research carried out in the past. Same trend was observed when the experiments were repeated for hydraulic spray. Almost all the researcher reported that surfactant enhances the heat transfer in quenching process and some related this effect to either surface tension or viscosity. It was observed that addition of surfactant also decelerates the wetting front velocity. When MgSO_4 and borax were dissolved together with surfactant, heat flux was enhanced in film and transition boiling regimes. This shows the dominant effect of salts over surfactant. A number of water samples from aluminum and copper casting industries were also utilized as coolant for carrying out quenching experiments. Because of the fact that real industrial water contains various ions e.g. Ca^{+2} , Mg^{+2} , Na^{+1} , Fe^{+2} , Cl^{-1} , SO_4^{-2} , PO_4^{-2} , CO_3^{-2} etc., it is extremely difficult to predict the influence of every component individually when they are present together in cooling fluid. This is why, the individual influence of some important salts and surfactant are only presented in this thesis. However, two instances of mixture of salt and surfactant are also presented. Nonetheless, it is still a question that how to assess the effect of ingredients present in real industrial water on heat transfer so that the resulting heat flux can be predicted. The industrial water used for secondary cooling in DC casting process varies considerably with respect to the concentration of its ingredients, therefore, results of water sample from one industry do not apply to the water sample from other industry. Cooling water saturated with CO_2 reduced the cooling rate considerably while that saturated with air caused faster cooling. Saturated CO_2 reduced the HTC in film boiling region from 600 to 490 $\text{W/m}^2/\text{K}$ while aerated water increased it to 700 $\text{W/m}^2/\text{K}$ as compared to deionized water. This fact shows that dissolved gases affect the cooling rate when cooling water is saturated with gases and negates the hypothesis of Cui et al. [6], [54] which says that gases have very little effect on spray cooling because gases escape from the fluid as soon as it touches the hot surface.

The array of water jets ejecting from mold at an angle of 60° with horizontal plane were also employed for quenching rectangular metal sheets. Two types of molds were utilized; one generates eight jets of diameter 4.78 mm and other generates seven jets of diameter 2.5 mm. The influence of cooling water velocity on the heat flux was analyzed. It was observed in both cases that the increase in water velocity does not, in all cases, enhance the heat extraction from the hot surface. This fact is verified through the maximum heat flux

(MaxHF) magnitude and its propagation velocity. The relation between water jet velocity and maximum heat flux and wetting front velocity was direct until an optimum value of jet velocity and beyond that the relation becomes inverse. The wetting front velocity was also measured by high speed photography for verifying that inference.

In this work, stationary source of water jets has been used. However, in secondary cooling of DC casting, the solidifying strand of metal and position of mold move relative to each other. That is why, it is recommended that the experimental set up should be modified in such a way that hot metal sheet remains stationary and the mold should move upward. The sheet cannot be moved because it is very difficult to move the IR camera with exactly the same velocity as that of the metal sheet (measured surface). Secondly, it is recommended to analyze the influence of surface roughness on heat transfer during quenching of metals by producing more rough surfaces similar to cast surface with known surface roughness values.

List of Tables

3.1	Specification of different materials of metal samples	32
3.2	Algorithm for the calculation of heat of conduction	38
3.3	Example composition of cooling water in cast-house of copper and aluminum	44
4.1	Operating parameters of two types of nozzles	46
4.2	Operating parameters for analyzing impingement density influence	51
4.3	Summary of important parameters of boiling curve for different kinds of ingredients in cooling water	76
4.4	Summary of experiments for water quality	77
5.1	Detail of experiments for water jet quenching of nickel plate	84
5.2	Geometry & specific properties of nickel	85
5.3	Obtainable range of surface roughness in microns	102
5.4	Summary of results of experiments for surface roughness	103

List of Figures

2.1	(a) Secondary cooling regime during DC casting of aluminum (b) detail of boiling regimes during water film cooling process	6
2.2	Boiling curve for water cooling indicating the different heat transfer regimes	9
2.3	Film flow device [Celata et al. [22]]	10
2.4	Wetting front velocity vs temperature [Celata et al. [22]]	11
2.5	Wetting front velocity vs jet velocity [Celata et al. [22]]	11
2.6	Heat flux vs time [Celata et al. [22]]	11
2.7	Moving aluminum sample quenched by array of water jets [Caron and Wells [23]]	12
2.8	Hydrodynamic phenomena on the surface together with cooling curve and heat flux at $t = 4.8$ s [Monde et al. [24]]	13
2.9	Schematic of cooling process in continuous casting	16
2.10	Orientation of spray inclination angle [Silk et al. [51]]	18
2.11	The effect of dissolved salts on heat transfer during spray cooling with 0.06 mol/l concentration salt solutions with impingement density of $3.0 \text{ kg/m}^2\cdot\text{s}$ [Cui et al. [6]]	20
2.12	The effect of varying salt concentration on heat flux during spray cooling with MgSO_4 solution with with impingement density of $3.0 \text{ kg/m}^2/\text{s}$ [Cui et al. [6]]	20
2.13	The effect of surfactant on spray cooling heat transfer at two different impingement densities [Chandra et al. [5]]	20
3.1	Infra-red camera [Courtesy:FLIR systems]	24
3.2	Optical device for measuring starting surface temperature [Courtesy:optris]	25
3.3	Surface of KS 83 coating after heating into furnace at $600 \text{ }^\circ\text{C}$	25
3.4	Surface of KS 82 coating after heating into furnace at $600 \text{ }^\circ\text{C}$	25
3.5	Set-up for calibration IR camera for emissivity	26
3.6	Relation between emissivity & temperature	27

3.7	Flow diagram of pneumatic atomizing nozzle	28
3.8	Impingement density distribution of pneumatic atomizer	28
3.9	Flow diagram of hydraulic full cone nozzle	29
3.10	Impingement density distribution of hydraulic full cone nozzle	29
3.11	Mold with eight orifices	29
3.12	Mold with seven orifices	29
3.13	Circular disc	30
3.14	Rectangular sheet	30
3.15	Front side of nickel sheet for mold quenching	31
3.16	Back side of nickel sheet for mold quenching	31
3.17	Front side of aluminium sheet for spray quenching	31
3.18	Back side of aluminium sheet for spray quenching	31
3.19	Patternator: A device for measuring impingement density distribution	32
3.20	Experimental set-up	34
3.21	Infrared image of rectangular sheet quenched by array of jets	35
3.22	Infrared image of circular sheet quenched by full cone spray	35
3.23	A run time temperature profiles image for quenching circular disc by full cone spray	35
3.24	High speed camera [Courtesy: La Vision]	43
4.1	Impingement density distribution for pneumatic atomizing nozzle for varying water flow	46
4.2	Impingement density distribution for hydraulic full cone nozzle for varying water flow	46
4.3	Temperature profiles of hydraulic & pneumatic nozzle	47
4.4	Heat transfer coefficient vs temperature for two nozzles	47
4.5	Temperature profiles for two different materials at center point of disc	48
4.6	Heat transfer coefficient vs temperature for two different materials at center point of disc	48
4.7	Heat transfer coefficient in the range of film boiling for spray quenching with water as a function of impingement density [Jeschar et al.]	48
4.8	Temperature profiles with respect to initial surface temperature	49
4.9	HTC VS temperature with respect to initial surface temperature	49
4.10	Temperature distribution along the diameter of the nickel disc for pneumatic nozzle	49

4.11	Temperature distribution along the diameter of the AA2024 disc for pneumatic nozzle	50
4.12	Temperature distribution along the diameter of the nickel disc for hydraulic nozzle	50
4.13	Temperature distribution along the diameter of the AA6082 disc for hydraulic nozzle	51
4.14	Impingement density distribution along radius at air pressure of 2 bar . . .	52
4.15	Temperature profiles for varying impingement densities at two radial positions on circular disc of nickel	53
4.16	Temperature profiles for varying impingement densities at two radial positions on circular disc of AA2024	53
4.17	HTC-Temperature curve for varying impingement densities at center of circular disc of nickel	53
4.18	HTC-Temperature curve for varying impingement densities at radius = 15 mm on circular disc of nickel	53
4.19	HTC-Temperature curve for varying impingement densities at center of circular disc of AA2024	54
4.20	HTC-Temperature curve for varying impingement densities at radius = 15 mm on circular disc of AA2024	54
4.21	Schematic of finite element model	55
4.22	Temperature profiles for three different dates showing repeatability of hydraulic spray at center of spray	56
4.23	Temperature profiles for three different dates showing repeatability of hydraulic spray at radius = 17 mm	56
4.24	Temperature profiles for three different dates showing repeatability of hydraulic spray at radius = 34 mm	56
4.25	Temperature profiles for MgSO ₄ solutions-pneumatic spray	57
4.26	Temperature Profiles for MgSO ₄ solutions at center of the disc-hydraulic spray	57
4.27	Temperature profiles for MgSO ₄ solutions at the radius of 17 mm-hydraulic spray	58
4.28	Relation between heat flux and surface temperature for MgSO ₄ solutions-hydraulic spray	58
4.29	Relation between heat transfer coefficient and surface temperature for MgSO ₄ solutions-hydraulic spray	59

4.30	Temperature profiles of average temperature for salts solution of 0.5 molar concentration-pneumatic spray	60
4.31	Temperature profiles for Borax solutions at center of disc-hydraulic spray	60
4.32	Temperature profiles for Borax solutions at the radius of 17mm-hydraulic spray	61
4.33	Relation between heat flux and surface temperature for borax solutions-hydraulic spray	61
4.34	Relation between heat transfer coefficient and surface temperature for borax solutions-hydraulic spray	62
4.35	Temperature profiles for CaCO ₃ solutions at at center of disc-hydraulic spray	62
4.36	Temperature profiles for CaCO ₃ solutions-hydraulic spray	63
4.37	Relation between heat flux and surface temperature for CaCO ₃ solutions-hydraulic spray	63
4.38	Relation between heat transfer coefficient and surface temperature for CaCO ₃ solutions-hydraulic spray	64
4.39	Heat flux distribution along radius of the disc-pneumatic spray	65
4.40	Propagation of maximum heat flux position for salts' solutions-pneumatic spray	65
4.41	Heat flux distribution at t = 3.3 sec for salts' solutions-pneumatic spray . .	66
4.42	Temperature profiles for various concentrations of surfactant solution-pneumatic spray	67
4.43	Heat Transfer Coefficient vs temperature within film boiling region for various concentrations of surfactant solution-pneumatic nozzle	67
4.44	Temperature profiles for various concentrations of surfactant solution-hydraulic spray	68
4.45	Heat transfer coefficient vs temperature within film boiling region for various concentrations of surfactant solution-hydraulic spray	68
4.46	Relation between heat flux and surface temperature for various concentrations of surfactant solution-hydraulic Spray	69
4.47	Maximum heat flux position propagation for various concentrations of surfactant solution-pneumatic spray	69
4.48	Heat flux distribution at t = 3.3 s for various concentrations of surfactant solution-pneumatic spray	70
4.49	Temperature-time curve for solutions of borax and surfactant-hydraulic spray	71

4.50	Relation between heat flux and surface temperature for solution of borax & surfactant-hydraulic spray	71
4.51	Relation between heat transfer coefficient and surface temperature for solution of borax & surfactant-hydraulic spray	72
4.52	Temperature-time curve for solutions of $MgSO_4$ and surfactant-hydraulic spray	72
4.53	Relation between heat flux and surface temperature for solution of $MgSO_4$ & surfactant-hydraulic spray	73
4.54	Temperature-time relation for different dissolved gases with respect to deionized water-hydraulic spray	73
4.55	Relation between heat transfer coefficient and surface temperature for various gases dissolved in cooling water-hydraulic spray	74
4.56	Influence of oil on temperature profile at the center of the spray	75
4.57	Influence of oil on temperature profile at radius of 17 mm	75
4.58	Influence of basic pH on temperature profile at the center of the spray	75
4.59	Influence of basic pH on temperature profile at radius of 34 mm	75
4.60	Principle of atomized spray cooling	78
4.61	Relation between heat transfer coefficient versus impingement density and air pressure [Jacek Krol [10]]	79
4.62	Relation between heat transfer coefficient of atomized spray quenching and surface temperature within film boiling region during atomized spray quenching [Jacek Krol [10]]	80
4.63	Quenching of an edge: temperature profile (left), picture from infrared camera [F. Puschmann]	80
4.64	Effect of overlapping sprays on impingement density [Jacek Krol [10]]	81
4.65	Time dependent temperature profile of aluminium sheet with three nozzles [Jacek Krol [10]]	82
4.66	Spatial temperature profile aluminium sheet with three nozzles [Jacek Krol [10]]	82
5.1	Schematic of finite element model	84
5.2	Temperature profile for nickel for jet velocity 1 m/s	85
5.3	Temperature profile for nickel for jet velocity 1.5 m/s	85
5.4	Heat flux distribution for nickel for jets' velocity 1 m/s	86
5.5	Heat flux distribution for nickel for jets' velocity 1.5 m/s	86
5.6	Maximum heat flux propagation for nickel for jets' velocity 1 m/s	86

5.7	Maximum heat flux propagation for nickel for jets' velocity 1.5 m/s	86
5.8	MaxHF propagation velocity for nickel for jets' velocity 1 m/s	87
5.9	MaxHF propagation velocity for nickel for jets' velocity 1.5 m/s	87
5.10	Heat flux as a function of surface temperature for two jet velocities	88
5.11	Temperature difference between measured and quenched side	89
5.12	Temperature-time curves for four repeated experiments at different positions for initial temperature $\approx 600^{\circ}\text{C}$	90
5.13	Temperature-time curves for four repeated experiments at different positions for initial temperature $\approx 800^{\circ}\text{C}$	90
5.14	Heat flux-time curves for four repeated experiments at specific position for initial temperature $\approx 600^{\circ}\text{C}$	90
5.15	Heat flux-time curves for four repeated experiments at specific position for initial temperature $\approx 800^{\circ}\text{C}$	90
5.16	Wetting front propagation for four repeated experiments for initial surface temperature $\approx 600^{\circ}\text{C}$	91
5.17	Wetting front propagation for four repeated experiments for initial surface temperature $\approx 800^{\circ}\text{C}$	91
5.18	Temperature profile at a distance of 53 mm from top for AA2024 for four jets' velocities	91
5.19	Temperature profile at a distance of 96 mm from top for AA2024 for four jets' velocities	91
5.20	Heat flux-length curves for AA2024 for four jets' velocities at 3.3 second	92
5.21	Heat flux-Length curves for AA2024 for four jets' velocities at 5.5 second	92
5.22	Maximum heat flux propagation for AA2024 for four jets' velocities . . .	93
5.23	Heat flux as a function of surface temperature for AA2024 for four jets' velocities	93
5.24	Temperature profile at a distance of 53 mm from top for nickel for four jets' velocities	94
5.25	Temperature profile at a distance of 96 mm from top for nickel for four jets' velocities	94
5.26	Heat flux-length curves for nickel for four jets' velocities at 3.3 second . .	94
5.27	Heat flux-length curves for nickel for four jets' velocities at 5.5 second . .	94
5.28	Heat flux-time curves for nickel for four jets' velocities at 3.3 second . . .	94
5.29	Heat flux-time curves for nickel for four jets' velocities at 5.5 second . . .	94
5.30	Maximum heat flux propagation for nickel for four jets' velocities	95

5.31	Heat flux as a function of surface temperature for nickel for four jets' velocities	96
5.32	Visual estimation of wetting front velocity for spray quenching by high speed camera at initial stage	96
5.33	Visual estimation of wetting front velocity for spray quenching by high speed camera at later stage	96
5.34	Visual estimation of wetting front velocity for jet quenching by high speed camera at initial stage	97
5.35	Visual estimation of wetting front velocity for jet quenching by high speed camera at later stage	97
5.36	Wetting front propagation during spray quenching for AA2024 at different impingement densities	98
5.37	Wetting front propagation during spray quenching for nickel at different impingement densities	98
5.38	Wetting front propagation during spray quenching for Inconel 600 at different impingement densities	99
5.39	Wetting front propagation during jets' quenching for AA2024 at different jet velocities	99
5.40	Wetting front propagation during jets' quenching for nickel at different jet velocities	100
5.41	Wetting front propagation during jets' quenching for Inconel 600 at different jet velocities	100
5.42	Variation of wetting front velocity with respect to jet velocity for three materials	101
5.43	Measurement of surface roughness	101

Nomenclature

A	Area [m ²]
At	Atomic weight of surface material [a.m.u.]
c	Specific heat capacity [J/kg/K]
d	Tube diameter [m]
f	Force vector [-]
g	Gravitational acceleration [m/s ²]
h	Latent heat, Enthalpy [J/kg]
i	dissociation constant [-]
k	Boiling point elevation constant [-]
K	Conductance matrix [-]
m	Solution concentration [mol/kg]
ṁ	Impingement density of spray [kg/m ² /sec]
M	Mass/Molar [mole]
M	Capacitance matrix [-]
n	Previous time step [-]
q	Heat flux [W/m ²]
q̃	Heat flux vector [W/m ²]
r	Radius [m]
s	Thickness [m]
S	Instantaneous error norm [-]
t	Time [sec]
T	Temperature [°C]
V	Volume [m ³]
Ẋ	Sensitivity coefficient matrix [-]
Ỹ	Measured temperature vector [°C]
z	Distance between nozzle & metal sheet [m]

Greek Symbol

α	Heat transfer coefficient [W/m ² /K]
β	Heat penetration coefficient $(\lambda_s \rho_s c_{p,s})^{-1}$
ϵ	Emissivity [-]
θ	Temperature [°C]
$\tilde{\Theta}$	Calculated temperature vector [°C]
λ	Thermal conductivity [W/m/K]
μ	Dynamic viscosity [N.s/m ²]
ρ	Density [kg/m ³]

σ Surface tension [N/m]

Subscript

l	Saturated liquid
α	Convection
b	Boiling point
c	Critical point
f	Fluid
λ	Conduction
Leid	Leidenfrost point
ml	Concentration in molality
MFB	Minimum film boiling point
p	Constant pressure
R	Radiation
s	Solid surface
sat	Saturation property
sp	Spray
v	Saturated vapour
w	Wall
∞	Ambient

Abbreviation

AA	Aluminum alloy
ACF	Advanced cooling front
CHF	Critical heat flux
DC	Direct chill
DHCP	Direct heat conduction problem
D.I.	De-ionized(water)
FEM	Finite element method
FLIR	Forward looking infrared radiometer
GDE	Governing differential equation
HF	Heat flux
HTC	Heat transfer coefficient
ID	Impingement density
IDD	Impingement density distribution
IHCP	Inverse heat conduction problem
IR	Infrared
LFP	Leidenfrost point temperature
MaxHF	Maximum heat flux
QWIP	Quantum well infrared photo-detector

Bibliography

- [1] R. Jeschar, E. Specht, and C. Köhler, "Heat transfer during cooling of heated metallic objects with evaporating liquids," *Springer-Verlag Berlin*, pp. 73–92, 1992.
- [2] R. Jeschar, R. Scholz, and U. Reiner, "Heat transfer during one and two-phase water-spray cooling in hot metals," *Sixth Japan-Germany Seminar. Proceedings*, pp. 146–159, 1984.
- [3] U. Reiner, R. Jeschar, D. Zebrowski, and W. Reichelt, "A measuring method for quick determination of local heat transfer coefficients in spray water cooling within the range of stable film boiling," *Steel Research*, vol. 56, pp. 239–246, 1985.
- [4] Q. Cui, S. Chandra, and S. McCahan, "The effect of dissolving salts in water sprays used for quenching a hot surface part 2: Spray cooling," *ASME Journal of Heat Transfer*, vol. 125, pp. 333–338, 2003.
- [5] Q. Cui and S. Chandra, "Spray cooling enhancement by addition of a surfactant," *ASME Journal of Heat Transfer*, vol. 120, pp. 92–98, 1998.
- [6] Q. Cui, S. Chandra, and S. McCahan, "The effect of dissolving gases or solids in water droplets boiling on a hot surface," *ASME Journal of Heat Transfer*, vol. 123, pp. 719–728, 2001.
- [7] C. Oh, J. L. V. H. Younis, R. Dahbura, and D. Michels, "Liquid jet-array cooling modules for high heat fluxes," *AIChE Journal*, vol. 44, p. 4, 1998.
- [8] U. Alam, K. Abdalrahman, and E. Specht, "Experimental investigation of influence of dissolved salts and surfactant on heat transfer in atomized spray quenching of metal," *Proceedings of 14th International Heat Transfer Conference, Washington D.C., USA*, vol. IHTC 14-22873, August 8-13, 2010.
- [9] U. Alam, K. Abdalrahman, and E. Specht, "Influence of quality of water on the heat transfer in secondary cooling zone during continuous casting," *Proceedings of Symposium Strangiessen, Neu Ulm, Germany*, November 15-17, 2010.
- [10] U. Alam, J. Krol, E. Specht, and J. Schmidt, "Enhancement and local regulation of metal quenching using atomized sprays," *Journal of ASTM International*, vol. 5(10), 2008.
- [11] A. Nallathambi, U. Alam, and E. Specht, "Heat flux estimation in direct chill casting using experimental and inverse finite element method," *Proceedings of ASME summer heat transfer conference, Jacksonville Florida, USA*, vol. HT 2008-56500, August 10-14, 2010.
- [12] K. Abdalrahman, U. Alam, and E. Specht, "Wetting front tracking during metal quenching using array of jets," *Proceedings of 14th International Heat Transfer Conference, Washington D.C., USA*, vol. IHTC 14-22080, August 10-14, 2010.
- [13] K. Abdalrahman, U. Alam, A. Nallathambi, and E. Specht, "Aluminum quenching by array of water jets," *Proceedings of 1st Mediterranean conference on heat treatment and surface engineering, Sharm El-Sheikh, Egypt*, December 1-3, 2010.

- [14] J. Sengupta, B. Thomas, and M. Wells, "The use of water cooling during the continuous casting of steel and aluminum alloys," *Metallurgical & Materials Transactions*, vol. 36A, pp. 187–204, 2005.
- [15] K. Ehrke and W. Schneider, *Continuous casting*. WILEY-VCH, 2000.
- [16] J. Bernardin and I. Mudawar, "The leidenfrost point: Experimental study and assessment of existing models," *ASME Journal of Heat Transfer*, vol. 121, pp. 894–903, 1999.
- [17] K. Baumeister and F. Simon, "Leidenfrost temperature: its correlation for liquid metal, cryogenes, hydrocarbons and water," *ASME Journal of Heat Transfer*, vol. 95(2), pp. 166–173, 1973.
- [18] P. Berenson, "Film boiling heat transfer from a horizontal surface," *ASME Journal of Heat Transfer*, vol. 83, pp. 351–358, 1961.
- [19] R. Henry, "A correlation for the minimum film boiling temperature," *Chemical Engineering Program*, vol. 70(138), pp. 81–90, 1974.
- [20] J. Bernardin and I. Mudawar, "A cavity activation and bubble growth model of the leidenfrost point," *ASME Journal of Heat Transfer*, vol. 124, pp. 864–874, 2002.
- [21] J. Bernardin and I. Mudawar, "A leidenfrost point model for impinging droplets and sprays," *ASME Journal of Heat Transfer*, vol. 126, pp. 272–278, 2004.
- [22] G. P. Celata, M. Cumo, and A. Mariani, "A comparison between spray cooling and film flow cooling during the rewetting of a hot surface," *Journal of Heat & Mass Transfer*, vol. 45, pp. 1029–1035, 2007.
- [23] E. J. Caron and M. A. Wells, "Effect of advanced cooling front (AFC) phenomena on film boiling and transition boiling regimes in the secondary cooling zone during the direct-chill casting of aluminum alloys," *Material Science Forum*, vol. 519-521, pp. 1687–1692, 2006.
- [24] J. Hammad, Y. Mitsutake, and M. Monde, "Movement of maximum heat flux and wetting front during quenching of hot cylindrical block," *International Journal for Thermal Science*, vol. 43, pp. 743–752, 2004.
- [25] A. Mozumder, M. Monde, and P. Woodfield, "Delay of wetting propagation during jet impingement quenching for a high temperature surface," *International Journal of Heat & Mass Transfer*, vol. 48, pp. 5395–5407, 2005.
- [26] A. Mozumder, M. Monde, P. Woodfield, and M. Islam, "Maximum heat flux in relation to quenching of a high temperature surface with liquid jet impingement," *International Journal of Heat & Mass Transfer*, vol. 49, pp. 2877–2888, 2006.
- [27] A. Mozumder, P. Woodfield, M. Islam, and M. Monde, "Maximum heat flux propagation velocity during quenching by water jet impingement," *International Journal of Heat & Mass Transfer*, vol. 50, pp. 1559–1568, 2007.
- [28] M. Islam, M. Monde, P. Woodfield, and Y. Mitsutake, "Jet impingement quenching phenomena for hot surfaces well above the limiting temperature for solid-liquid contact," *International Journal of Heat & Mass Transfer*, vol. 51, pp. 1226–1237, 2008.
- [29] M. Monde, "Heat transfer characteristics during quench of high temperature solid," *Journal of Thermal Science & Technology*, vol. 3, 2008.

-
- [30] P. Woodfield, A. Mozumder, and M. Monde, "On the size of the boiling region in jet impingement quenching," *International Journal of Heat & Mass Transfer*, vol. 52, pp. 460–465, 2009.
- [31] Y. Mitsutake and M. Monde, "Heat transfer during transient cooling of high temperature surface with an impinging jet," *Heat & Mass Transfer*, vol. 37, pp. 321–328, 2001.
- [32] M. Meyer, I. Mudawar, C. Boyack, and C. Hale, "Single-phase and two-phase cooling with an array of rectangular jets," *International Journal of Heat & Mass Transfer*, vol. 49, pp. 17–29, 2006.
- [33] A. Fortier, "Menique des suspensions.," *Paris: Masson*, 1967.
- [34] E. R. Morgan, T. Dancy, and M. Korchynski, "Improved steels through hot strip mill controlled cooling," *Journal of Metals*, vol. 8, pp. 829–831, 1965.
- [35] E. R. Morgan, T. Dancy, and M. Korchynski, "Improving high strength low alloy steels through controlled cooling," *Metal Producing Prog.*, vol. 1, pp. 125–130, 1966.
- [36] J. Couvreur, "Calculation of the optimum geometry of a spray cooler for rolled wire rods," *C.R.M. Reports*, vol. 26, pp. 25–30, 1971.
- [37] R. Jeschar, U. Reiner, and R. Scholz, "Heat transfer during water and water-air spray cooling in the secondary cooling zone of continuous casting plant," *Proceedings of 69th Steelmaking Conference in Washington*, vol. 69, pp. 511–521, 1986.
- [38] J. Wendelstorf, K. Spitzer, and R. Wendelstorf, "Spray water cooling heat transfer at high temperatures and liquid mass fluxes," *International Journal of Heat & Mass Transfer*, vol. 52, pp. 4902–4910, 2008.
- [39] F. Puschman and E. Specht, "Atomized spray quenching as an alternative quenching method for defined adjustment of heat transfer," *Steel Research*, vol. 75, pp. 283–288, 2004.
- [40] F. Puschman, E. Specht, and J. Schmidt, "Measurement of spray cooling heat transfer using an infrared-technique in combination with the phase-doppler technique and a patternator," *International Journal of Heat & Technology*, vol. 19, pp. 51–56, 2001.
- [41] J. Bernardin, C. Stebbins, and I. Mudawar, "Mapping of impact and heat transfer regimes of water drops impinging on a polished surface," *International Journal of Heat & Mass Transfer*, vol. 40(2), pp. 247–267, 1997.
- [42] J. Fukai, Y. Shiiba, and O. Miyatake, "Theoretical study of droplet impingement on a solid surface below the leidenfrost temperature," *International Journal of Heat & Mass Transfer*, vol. 40(10), pp. 2490–2492, 1997.
- [43] J. Bernardin and I. Mudawar, "Experimental and statistical investigation of changes in surface roughness associated with spray quenching," *International Journal of Heat & Mass Transfer*, vol. 39(10), pp. 2023–2037, 1996.
- [44] J. Bernardin, C. Stebbins, and I. Mudawar, "Effect of surface roughness on water droplet impact history and heat transfer regimes," *International Journal of Heat & Mass Transfer*, vol. 40(1), pp. 73–88, 1997.
- [45] M. Ciofalo, I. Piyazza, and V. Brucato, "Investigation of the cooling of hot walls by liquid water sprays," *International Journal of Heat & Mass Transfer*, vol. 42, pp. 1157–1175, 1999.

- [46] K. Estes and I. Mudawar, "Correlation of sauter mean diameter and critical heat flux for spray cooling of small surfaces," *International Journal of Heat & Mass Transfer*, vol. 38(16), pp. 2985–2996, 1995.
- [47] R. Chen, L. Chow, and J. Navedo, "Effect of spray characteristics on critical heat flux in subcooled water spray cooling," *International Journal of Heat & Mass Transfer*, vol. 45, pp. 4033–4043, 2002.
- [48] R. Chen, L. Chow, and J. Navedo, "Optimal spray characteristics in water spray cooling," *International Journal of Heat & Mass Transfer*, vol. 47, pp. 5095–5099, 2004.
- [49] A. Pautsch and T. Shedd, "Spray impingement cooling with single- and multiple-nozzle arrays. part 1: Heat transfer data using fc-72," *International Journal of Heat & Mass Transfer*, vol. 48, pp. 3167–3175, 2005.
- [50] J. Rybicki and I. Mudawar, "Single-phase and two-phase cooling characteristics of upward-facing and downward-facing sprays," *International Journal of Heat & Mass Transfer*, vol. 49, pp. 5–16, 2006.
- [51] E. Silk, J. Kim, and K. Kiger, "Spray cooling of enhanced surfaces: Impact of structured surface geometry and spray axis inclination," *International Journal of Heat & Mass Transfer*, vol. 49, pp. 4910–4920, 2006.
- [52] B. Gottfried, C. Lee, and K. Bell, "The leidenfrost phenomenon: film boiling of liquid droplets on a flat plat," *International Journal of Heat & Mass Transfer*, vol. 9(11), pp. 1167–1188, 1966.
- [53] M. Yu, "The effect of cooling water quality on aluminum ingot casting light metal," *AIME*, pp. 1331–1347, 1985.
- [54] Q. Cui., S. Chandra, and S. McCahan, "The effect of dissolving salts in water sprays used for quenching a hot surface. part 1: Boiling of single droplet," *ASME Journal of Heat Transfer*, vol. 125, pp. 326–332, 2003.
- [55] C. Huang and V. Carey, "The effect of dissolved salt on the leidenfrost transition," *International Journal of Heat & Mass Transfer*, vol. 50, pp. 269–282, 2006.
- [56] A. Morgan, L. Broomley, and C. Wilkey, "Effect of surface tension on heat transfer in boiling," *Industrial & Engineering Chemistry*, vol. 41, pp. 2767–2769, 1949.
- [57] A. Lowery and J. Westwater, "Heat transfer to boiling methanol-effect of added agents," *Industrial & Engineering Chemistry*, vol. 49, pp. 1445–1448, 1957.
- [58] P. Jontz and J. Myers, "The effect of dynamic surface tension on nucleat boiling coefficients," *AIChE Journal*, vol. 6, pp. 34–38, 1960.
- [59] B. Shah and R. Darby, "The effect of surfactant on evaporative heat transfer in vertical film flow," *International Journal of Heat & Mass Transfer*, vol. 16(10), pp. 1889–1903, 1973.
- [60] S. Shibayama, T. Kurose, K. Suzuki, M. Katsuta, and Y. Hatano, "A study on boiling heat transfer in thin liquid film. part 1, in the case of pure water and aqueous solution of surface-active agents as working liquid," *Japanese Society of Mechanical Engineers*, vol. 44(383), pp. 2429–2438, 1978.

- [61] P. Kotchaphakdee and M. Williams, "Enhancement of nucleate pool boiling with polymeric additives," *International Journal of Heat & Mass Transfer*, vol. 13(5), pp. 835–840, 1970.
- [62] Y. Yang and J. Maa, "Pool boiling of dilute surfactant solutions," *International Communications in Heat & Mass Transfer*, vol. 17, pp. 190–92, 1983.
- [63] Y. Tzan and Y. Yang, "Experimental study of surfactant effects on pool boiling heat transfer," *ASME Journal of Heat Transfer*, vol. 112, pp. 207–212, 1990.
- [64] Y. Yang, "Dynamic surface effect on boiling of aqueous surfactant solutions," *International Communications in Heat & Mass Transfer*, vol. 17, pp. 711–727, 1990.
- [65] W. Frost and C. Kippenhan, "Bubble growth and heat transfer mechanisms in the forced convection boiling of water containing a surface active agent," *International Journal of Heat & Mass Transfer*, vol. 10, pp. 931–949, 1967.
- [66] C. Ammerman and S. You, "Determination of boiling enhancement mechanism caused by surfactant addition of water," *ASME Journal of Heat Transfer*, vol. 118, pp. 429–435, 1996.
- [67] S. Freund, A. Pautsch, T. Shedd, and S. Kabelac, "Local heat transfer coefficients in spray cooling systems measured with temperature oscillation ir thermography," *International Journal of Heat & Mass Transfer*, vol. 50(9), pp. 1953–1962, 2007.
- [68] J. Schmidt and H. Boye, "Influence of velocity and size of the droplets on the heat transfer in spray cooling," *Chemical Engineering Technology*, vol. 24(3), pp. 255–260, 2001.
- [69] M. Monde, "Analytical method in inverse heat transfer problem using laplace transform technique," *International Journal of Heat & Mass Transfer*, vol. 43, p. 3965–3975, 2000.
- [70] U. Ijaz, A. Khambampati, M. Kim, S. Kim, and K. Y. Kim, "Estimation of time-dependent heat flux and measurement bias in two-dimensional inverse heat conduction problems," *International Journal of Heat & Mass Transfer*, vol. 50, pp. 4117–4130, 2007.
- [71] S. Deng and Y. Hwang, "Applying neural networks to the solution of forward and inverse heat conduction problems," *International Journal of Heat & Mass Transfer*, vol. 49, pp. 4732–4750, 2006.
- [72] C. Huang and H. Wu, "An inverse hyperbolic heat conduction problem in estimating surface heat flux by the conjugate gradient method," *Journal of Physics D: Applied Physics*, vol. 39.
- [73] Q. Xue and H. Yang, "Conjugate gradient method for the hyperbolic inverse heat conduction problem with multivariables," *JisuanWuli / Chinese Journal of Computational Physics*, vol. 22.
- [74] X. Ling, R. Keanini, and H. Cherurkuri, "A non-iterative finite element method for inverse heat conduction problems," *International Journal for Numerical methods in Engineering*, vol. 56, pp. 1315–1334, 2003.
- [75] D. Celentano, E. Orate, and S. Oller, "A temperature-based formulation for finite element analysis for generalized phase-change problems," *International Journal for Numerical Methods in Engineering*, vol. 37(20), pp. 3441–3465, 1994.
- [76] K. J. Bathe, "Finite element procedures in engineering analysis," *Prentice Hall, New Jersey*, 1982.

Umair Alam

W. Rathenau Str. 19, Zim. 408
39106 Magdeburg, Germany
Tel: +49-391-67-12331 (business)
+49-176-64168385 (private)
Email: Umair.Alam@st.ovgu.de
Date of Birth: November 25, 1978
Place of Birth: Karachi, Pakistan



Curriculum Vitae

Academic Qualifications

- | | |
|-----------|---|
| 2007-2011 | PhD, Otto von Guericke University of Magdeburg, Germany
Thesis title: Experimental Study of Local Heat Transfer during Quenching of Metals by Spray and Multiple Jets |
| 2004-2005 | Master (Quality, Safety & Environment), Otto von Guericke University of Magdeburg, Germany
Thesis title: Influence of kind of metal and surface structure on heat transfer for spray quenching |
| 1997-2001 | Bachelor of Engineering (Textile Engg.), NED University of Engineering & Technology, Karachi, Pakistan |

Work Experience

- | | |
|------------|---|
| 2007- 2011 | Research, Faculty Process & System Engineering, Institute of Fluid Dynamics and Thermodynamics University of Magdeburg, Germany |
| 2006-2006 | Compliance Auditor- SGS (Pvt.) Ltd. A swiss company |
| 2003-2004 | Quality Auditor- SGS (Pvt.) Ltd. A swiss company |
| 2001-2003 | Al-karam (Pvt.) Ltd |

Research & Development Projects

- | | |
|-----------|---|
| 2008-2011 | Worked on an industrial project titled as “Experimental Investigation of influence of water quality on heat transfer during quenching of metal in direct chill casting of non-ferrous metals”. This project was sponsored by Industriellen Gemeinschaftsforschung des Bundesministeriums für Wirtschaft, BR#04253/08. |
|-----------|---|

Languages

- Deutsch (Above average, passed B-1 Threshold, GrundStufe 2)
- English (fluent, passed TOEFL computer based with score 213/300)

List of Publications

1. **Alam, U.**, Krol, J., Specht, E., Schmidt, J., “Enhancement and Local Regulation of Metal Quenching using Atomized Sprays” published online on October 22, 2008 in Journal of ASTM International Volume 5, Issue 10, and ISSN: 1546-962X.
<http://www.astm.org/JOURNALS/JAI/PAGES/JAI101805.htm>
2. Nallathambi, A.K, **Alam, U.**, Specht, E., “ Heat Flux Estimation in Direct Chill Casting using Experimental and Inverse Finite Element Method” , proceedings of HT 2008, ASME 2008, Summer Heat Transfer Conference, August 10-14, 2008, Jacksonville, Florida, USA.
3. Abdalraham, Khalid, **Alam, U.**, Nallathambi, A.K., Specht, E., “Aluminum quenching by array of water jets”, 1st Mediterranean conference on heat treatment and surface engineering December 1-3, 2009, Sharm El-Sheikh, Egypt.
4. **Alam, U.**, Abdalraham, Khalid, **Alam, U.**, , “ Experimental investigation of influence of dissolved salts and surfactant on heat transfer in atomized spray quenching of metal” International heat transfer conference (IHTC-14) August 8-13, 2010, Washington, USA.
5. Abdalraham, Khalid, **Alam, U.**, Specht, E.,“ Wetting front tracking during metal quenching using array of jets” International heat transfer conference (IHTC-14) August 8-13, 2010, Washington, USA.
6. Specht, E., **Alam, U.**, Abdalrahman K.H.M.,“ Influence of quality of water on the heat transfer in secondary cooling zone during continuous casting” Symposium Stranggiessen, November 15-17, Neu Ulm Germany.
7. **Alam, U.**, Specht, E., “ Influence of water quality on heat transfer during quenching of metals by pneumatic and hydraulic sprays” (Submitted to International Journal of Thermal Science, Review received , to be corrected and submitted)